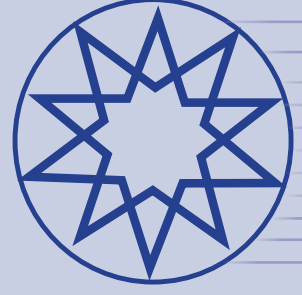


ISSN 2636-8498

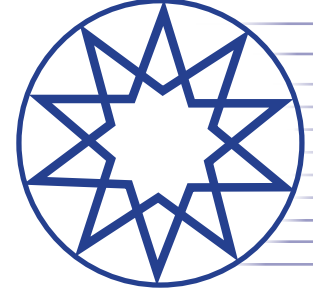


Environmental Research & Technology

Year 2022
Volume 5
Number 2

**YTÜ
PRESS**

www.ert.yildiz.edu.tr



Environmental Research & Technology

Volume 5 Number 2 Year 2022

EDITOR-IN-CHIEF

Ahmet Demir, *Yildiz Technical University, Istanbul, Turkey*

Mehmet Sinan Bilgili, *Yildiz Technical University, Istanbul, Turkey*

ACADEMIC ADVISORY BOARD

Adem Basturk

Mustafa Ozturk

Lutfi Akca

Oktay Tabasaran

Ahmet Demir

SCIENTIFIC DIRECTOR

Ahmet Demir, *Yildiz Technical University, Istanbul, Turkey*

ASSISTANT EDITOR

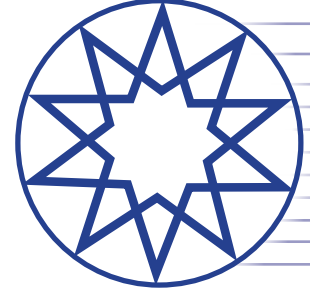
Hanife Sari Erkan, *Yildiz Technical University, Istanbul, Turkey*

LANGUAGE EDITOR

Güleda Engin, *Yildiz Technical University, Istanbul, Turkey*

EDITORIAL BOARD

Andjelka Mihajlov, Serbia; **Artur J. Badyda**, Poland; **Aysegul Pala**, Turkey; **Aysen Erdinler**, Turkey; **Azize Ayol**, Turkey; **Bulent Keskinler**, Turkey; **Didem Ozcimen**, Turkey; **Erwin Binner**, Austria; **Eyup Debik**, Turkey; **F. Dilek Sanin**, Turkey; **Gulsum Yilmaz**, Turkey; **Hamdy Seif**, Lebanon; **Hanife Buyukgungor**, Turkey; **Ilirjan Malollari**, Albania; **Ismail Koyuncu**, Turkey; **Jaakko Puhakka**, Finland; **Lucas Alados Arboledas**, Spain; **Mahmoud A. Alawi**, Jordan; **Marcelo Antunes Nolasco**, Brazil; **Martin Kranert**, Germany; **Mehmet Emin Aydin**, Turkey; **Mesut Akgun**, Turkey; **Mukand S. Babel**, Thailand; **Mustafa Odabasi**, Turkey; **Mufide Banar**, Turkey; **Mustafa Okutan**, Turkey; **Mufit Bahadir**, Germany; **Neslihan Dogan Saglamtimur**, Turkey; **Nihal Bektas**, Turkey; **Nurdan Gamze Turan**, Turkey; **Osman Arikan**, Turkey; **Osman Nuri Agdag**, Turkey; **Omer Akgiray**, Turkey; **Ozer Cinar**, Turkey; **Pier Paolo Manca**, Italy; **Recep Boncukcuoglu**, Turkey; **Saim Özdemir**, Turkey; **Sameer Afifi**, Palestine; **Serdar Aydin**, Turkey; **Timothy O. Randhir**, United States; **Ülkü Yetis**, Turkey; **Victor Alcaraz Gonzalez**, Mexico; **Yaşar Nuhoğlu**, Turkey



Environmental Research & Technology

Volume 5 Number 2 Year 2022

CO-EDITORS (AIR POLLUTION)

Arslan Saral, Turkey; Mohd Talib Latif, Malaysia; Nedim Vardar, Puerto Rico; Sait Cemil Sofuođlu, Turkey; Wina Graus, Netherlands

CO-EDITORS (ENVIRONMENTAL ENGINEERING AND SUSTAINABLE SOLUTIONS)

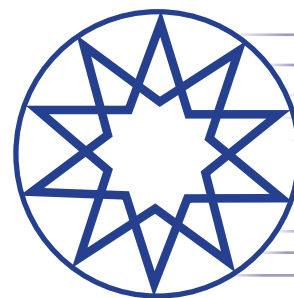
Bulent Inanc, Turkey; Guleda Engin, Turkey; Hossein Kazemian, Canada; Raffaella Pomi, Italy; Yilmaz Yildirim, Turkey; Zenon Hamkalo, Ukraine

CO-EDITORS (WASTE MANAGEMENT)

Bestami Ozkaya, Turkey; Bulent Topkaya, Turkey; Kahraman Unlu, Turkey; Mohamed Osmani, United Kingdom; Pin Jing He, China

CO-EDITORS (WATER AND WASTEWATER MANAGEMENT)

Ayşe FİLİBELİ, Turkey; Baris CALLİ, Turkey; Marina PRİSCIANDARO, Italy; Selvam KALİYAMOORTHY, Japan; Subramanyan VASUDEVAN, India



Environmental Research & Technology

Volume 5 Number 2 Year 2022

CONTENTS

Research Articles

- 111** Production of liquid fuel from co-pyrolysis of jatropha cake with tyre waste
Sulaiman Abubakar BABAJO
- 119** Reverse osmosis treatment system for landfill leachate: Operation conditions, advantages and challenges
Aysun Derya TOPAL, Ayşe Dilek ATASOY
- 128** Investigation of synergetic effect of adsorption and photocatalysis for the removal of tetracycline by BiFeO₃ immobilized on copolymer seeds
Esra BİLGİN ŞİMŞEK, Zeynep BALTA
- 137** Degree of Pb stabilization in MSWI fly ash using size-fractionated natural fishbone hydroxyapatite
Mitali NAG, Amirhomayoun SAFFARZADEH, Takayuki SHIMAOKA, Hirofumi NAKAYAMA
- 148** Characterisation study of solid wastes: A case of districts in Tekirdağ
Elçin GÜNEŞ, Kübra GÜMÜŞ BAYINDIR, Nesli AYDIN, Deniz İzlen ÇİFÇİ
- 155** Assessing the efficiency of drinking water treatment plant and the impact of broken distribution systems on water quality of Wukari-Ibi plant
Ezekiel SAMAILA, Williams Abel GIN, Williams Kwari JOSHUA
- 165** Principal component analysis in long term assessment of total viable plate count of municipal water distribution network system in healthcare facility
Mostafa ESSAM EISSA, Engy REFAAT RASHED, Dalia ESSAM EISSA
- 172** Indoor air CO₂ concentrations and ventilation rates in two residences in İzmir, Turkey
Aybüke TAŞER, Sedef UÇARYILMAZ, Ilgın ÇATAROĞLU, Sait Cemil SOFUOĞLU
- 181** Degradation and mineralization of tetracycline by Fenton process
Engin GÜRTEKİN, Murat ÇELİK, Ekrem AYDIN, Aytekin ÇELİK
- 188** Calculation of rainwater harvest in greenhouses for semi-arid and continental climate zones
Abdullah Nafi BAYTORUN, Zeynep Binnaz ZAIMOĞLU, Fatma Elçin ERKURT, Behzat BALCI, Hasan Kivanç YEŞİLTAŞ



Research Article

Production of liquid fuel from co-pyrolysis of jatropha cake with tyre waste

Sulaiman Abubakar BABAJO*

Department of Mechanical Engineering, Modibbo Adama University, Yola, Adamawa State, Nigeria

ARTICLE INFO

Article history

Received: 17 November 2021

Revised: 15 January 2022

Accepted: 09 March 2022

Key words:

Co-pyrolysis; Feedstock materials; Fixed bed reactor; Jatropha cake and tyre waste

ABSTRACT

This paper introduces the technique that can be used to produce liquid fuel in high quantity, and the technique is called co-pyrolysis technique. Co-pyrolysis is a process which involves two or more materials as feedstock. To the best of my knowledge, there have not been any research about the co-pyrolysis of Jatropha seed cake with tyre waste. The feedstock materials were Jatropha cake and tyre waste. The characterization of the feedstock materials were carried out based on proximate and ultimate analysis. The Jatropha cake with tyre waste were in particle form and were pyrolyzed in an externally heated fixed bed reactor with nitrogen as an inert gas. The reactor was heated by means of electrical furnace. The products of the experiment were: liquid fuel, char and gas. The ratio of jatropha cake to tyre waste materials were 1:1, 1:2 and 1:3 respectively. The parameters that has more influence on the production of liquid fuel yields includes: feed ratio, temperature and reaction time. The maximum liquid yield obtained from the co-pyrolysis of Jatropha cake with tyre waste was 68.0 wt% (that is at the parameters of: feed ratio 1:1, temperature 500°C and reaction time of 45 minutes).

Cite this article as: Babajo SA. Production of liquid fuel from co-pyrolysis of jatropha cake with tyre waste. Environ Res Tec 2022;5:2:111–118.

INTRODUCTION

Fossil fuels such as petroleum and natural gas are predicted to phased out after 2042, and only the coal reserves that will be available until at least 2112 [1]. This effect has made some researchers to put more effort in order to find solutions by utilizing alternative energy. Biomass is very abundant worldwide and can be easily found in diverse forms such as agricultural residues, wood residues, dedicated energy crops, and municipal solid waste [2]. Biomass based on its availability and its status as a waste product is one of the prime sources of renewable energy worldwide.

Biomass receives more attention in the utilization of energy source in Nigeria, contributing about 78% of Nigeria's primary energy supply [1, 3]. Biomass originates from plants or their by-products that are produced completely or partly by photosynthesis such as forestry residues, agricultural bi products or animal wastes that can be used as a source of energy [4]. The use of biomass as an energy fuel source also helps the environment because it has been recognized as a carbon neutral energy source. The conversion of biomass sources into energy fuels was achieved in several ways, such as thermal, biological, and physical methods. In thermal conversion, pyrolysis is the most

*Corresponding author.

*E-mail address: bbjosul@gmail.com



promising processes that can convert biomass to various types of products such as liquid, char and gas. This technique is widely recognized as an environmentally friendly method, because no wastes are produced during the process. The process has also received more attention because it can produce liquid yield of up to 75 wt% with conditions of moderate temperature (500°C) and short hot vapor residence time [2]. The liquid fuel obtained from the pyrolysis process has the potential to be used as fuels or feedstock for many commodity chemicals. The research to produce liquid fuel via the pyrolysis of biomass has been conducted since the last four decades. In 1972, the energy crisis has pushed researchers to put more attention to maximize the production of pyrolysis oil by minimizing the byproducts of char and gases [5]. One of the best use of pyrolysis was achieved in the 1980s [6]. This co-pyrolysis technique has successfully led to several improvements, such as the high yield of liquid fuel production. Although the issue associated with liquid fuel quantity has been addressed, the improvement in liquid fuel quality still requires further research. Currently, many researchers put efforts in finding the suitable technique to produce high-grade pyrolysis oil and to explore more new variations of biomass that can be used as feedstock in the pyrolysis process. The liquid fuel produced from the pyrolysis of biomass contain high level of oxygen content and can cause many problems, such as low calorific value, high viscosity and corrosion problems. The current research finding showed that the technologies to eliminate the oxygen content are still expensive and can cost more than the oil itself [7]. Therefore, the sustainability of this research seems necessary to overcome this cost and to improve the quality of pyrolysis oil that is expected to compete with fossil-based liquid fuel.

Around 1.5 billion tires are produced worldwide every year, which will eventually be categorized or interpreted as waste tires [8, 9]. Waste or scrap tires are known to have a significant impact on the increasing the urban waste stream and it has become a major threat to the environment. Approximately 64% of waste tires are sent to landfill or illegally dumped or stockpiled, with only 13% of them being recycled [10]. In landfills, the waste or scrap tires are not easily degraded, but tend to float to the top over time due to the trapped gases contained, thus breaking landfill covers. The incineration of waste or scrap tires requires the more expensive control system of air emissions because this process produces toxic gases, which contain carcinogenic and mutagenic chemicals. More attention and treatment were needed to tackle waste or scrap tires, and pyrolysis has been found to be a technically feasible way to treat tires and recover valuable products. According to Abnisa et al. [11], palm shell and tyre waste materials were mixed in a ratio of 1:1. The palm shell material alone was heated at a temperature of 500°C, the liquid fuel and calorific value obtained from the palm shell alone was 46.13 wt% and 11.94MJ/Kg.

The second experiment was conducted by mixing the two materials and heated at same temperature of 500°C, the liquid fuel yield and calorific value obtained were 61.63 wt% and 38.01MJ/Kg respectively.

Alias et al. [12] carried out an experiment on pinewood and tyre waste materials, the pinewood material alone was heated at a temperature of 500°C. The liquid fuel and the calorific value obtained from the pinewood alone was 32.00 wt% and 21MJ/Kg respectively. While the mixture of pinewood and tyre waste materials were mixed in a ratio of 1:1 and were also heated at same temperature, the liquid fuel yield and the calorific value obtained were 53 wt% and 45MJ/Kg respectively.

According to Cao et al. [13], Waste tyres without wire steel were mixed with empty fruit bunches with a ratio of 1:1. The experiment was performed using a fixed bed reactor. Co-pyrolysis was carried out under a nitrogen atmosphere at a temperature of 500°C. Pyrolysis oils were collected in a condenser. The products of liquid obtained was 42.80 wt%. The liquid product was significantly decreased when the empty fruit bunches were pyrolyzed alone without being mixed with waste tyre. These showed that an increase of tyre waste in biomass during pyrolysis increases the liquid fuel yield and the calorific value of the fuel.

Wastes of tires are considered to be potential sources to use as a co-feed in co-pyrolysis to produce liquid fuel [14–16]. The materials having much energy content, the sources were specifically easy to find and readily available in huge amounts in all countries around the world. Pyrolysis of tire waste with other biomass (Jatropha cake) wastes will encourage the creation of innovative new concepts in waste management, energy security enhancement, and environmental concerns. Therefore, it is significant to note that, the development of the co-pyrolysis technique to produce liquid fuel is applicable in most countries of the world.

There is growing interest among researchers in the use of waste tyres as a fuel source through the process of pyrolysis. As a research output, several comprehensive reviews on various aspects of waste tyres pyrolysis for liquid production have been published [17]. In co-pyrolysis, many studies of pyrolysis of waste tyres mixed with other materials have been carried out. However, studies which focused on the pyrolysis of waste tyre/woodbased biomass blends are currently still limited. Therefore, some effort should be made to examine the existence of synergistic effects when employing various pyrolysis conditions for the pyrolysis of waste tyre/biomass.

The aim of this study is to produce liquid fuel from jatropha cake with tyre waste via co-pyrolysis technique. Jatropha normally grows in an arid land that means it can grow in area where there is no sufficient or lack of availability of water. Many researchers tried to find alternative fuels by converting jatropha oil to biodiesel for several purposes.

Jatropha cake is non edible materials which are produced in large quantities while producing biodiesel. The jatropha cakes were dumped as a waste after producing the biodiesel.

MATERIALS AND METHODS

Materials

The materials used in this research study includes;

- i. Jatropha Curcas Seed Cake: Jatropha curcas seed cake was selected for this study. It was obtained at Technology Business Incubation Center (TBIC), Kano, in Kano state. It was used as one of the feed stock in this research.
- ii. Shredded rubber tire was selected as tire waste in this study. It was used as one of the feed stocks in the co-pyrolysis process because of its availability, and are not easily degraded, which may become a major threat to the environment. It was obtained at Kofar Wambai, Kano market, Kano state. The waste or scrap tire was shredded into smaller sizes using an iron saw and the iron reinforcement content in the tire was removed. The sample was allowed to dry. The passenger car tire was used as scrap tire in this study.
- iii. Thermocouple: This is a sensor that is used to measure temperature of a sample. The thermocouple is a sensing device that detects the temperature inside the reactor produced by the electric heater. The thermocouple used for this research study was for measuring the temperature inside the reactor. The thermocouple comprises of a wire which was placed in the fixed bed reactor in order to detect the temperature inside the reactor. The model of the thermocouple used was PSI-TTM 1 model.
- iv. Temperature Controller: A temperature controller is a device that controls the temperature of the electric heater. It was used to control the temperature inside the fixed bed reactor. The model of the temperature controller used in this research was TEC201 Model.
- v. Test Sieves: The test sieve that was used for this study was a standard sieve that will sieve the particle of the material or feed stock of not more than 2 mm. It was used for sieving the feed stocks to a desired particle size.
- vi. Weight Balance: This is a device to measure weight. The type of weight balance that was used for this study was Digital of (TCS-100-ZE11) model. It was used for determining the weight of the material or feedstock.
- vii. Stop Watch: The type of stop watch that was used for this research was Digital Stop watch of N1280 model. The stop watch was used for measuring or determining the time that will take a feedstock materials to pyrolyzed.

Methods

Jatropha seed cake and tyre waste were sorted, sun dried and shredded into smaller size. Proximate and ultimate

analysis of a sample of the prepared feedstock was undertaken based on American Society for Testing and Materials (ASTM).

Proximate Analysis of the Feedstock Materials

The proximate analysis is defined as the loss in weight of the feedstock materials (Jatropha curcas seed cake and tyre waste) in terms of moisture content, ash content, volatile matter and fixed carbon. The proximate analysis was carried out in accordance with ASTM D3172–73 [18].

Determination of Ash Content (ASTM D 2939–07)

The samples (Jatropha curcas seed cake and tyre waste) were weighed and burnt in a furnace at 350°C and was left for some time in the furnace and the ash was later weighed. The ash content was determined on dried basis as follows:

$$\text{Ash content (wt \%)} = \left(\frac{W_3 - W_1}{W_2 - W_1} \right) \times 100 \quad \dots \quad (1)$$

Where W_1 =weight of empty crucible, W_2 =weight of crucible and sample and W_3 =weight of crucible and sample after heating.

Determination of Moisture Content (ASTM D 4643–18)

Percentage of moisture content (MC) of the samples was determined by calculating the loss in weight of sample using oven drying at temperature of 105°C–115°C until the weight of the sample was constant, after 60 minutes oven dried weight was obtained. Moisture content was then determined as thus;

Calculation;

$$\text{Moisture content (wt \%)} = \left(\frac{W_5 - W_6}{W_5 - W_4} \right) \times 100 \quad \dots \quad (2)$$

Where W_4 =weight of empty crucible, W_5 =weight of crucible and liquid fuel, and W_6 =weight of crucible and liquid fuel after heating.

Determination of Volatile Matter (ASTM E897–88)

Percentage of volatile matter (VM) of the samples was determined by calculating the loss in weight of sample using electrical furnace at temperature of 500°C–550°C, until the weight of the sample was constant, after 10 minutes to obtain dry weight, by weighing the dried sample after been cooled. Volatile matter was then calculated as thus;

$$\% \text{ VM} = \left(\frac{W_8 - W_9}{W_5 - W_7} \right) \times 100 \quad \dots \quad (3)$$

Where W_7 =weight of empty crucible, W_8 =weight of crucible and sample and W_9 =weight of crucible and sample after heating.

Determination of Fixed Carbon (ASTM E–870)

This was calculated by subtracting the sum of % of moisture content, volatile matter (VM) and % of ash content (AC) of the samples from 100.

$$\%FC = 100 - (\%MC + \%AC + \%VM) \quad \dots \quad (4)$$

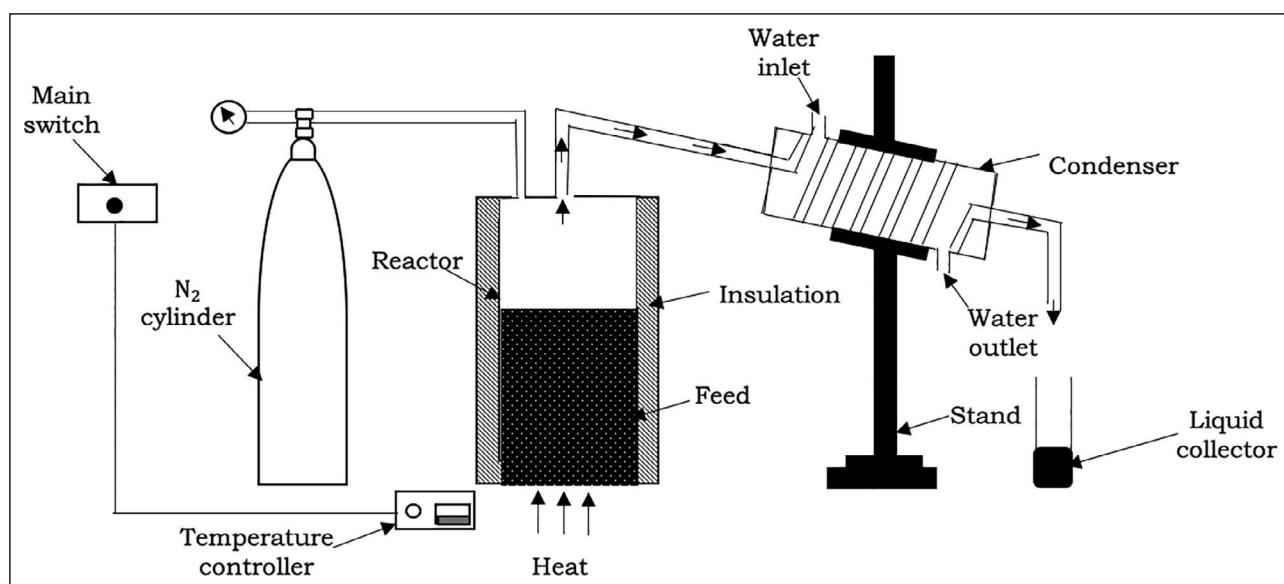


Figure 1. Conceptual representation of co-pyrolysis system.

Ultimate Analysis of the Feedstock Materials

The purpose of the test was to determine element percent of carbon, hydrogen, nitrogen, oxygen and sulphur content in the feedstock materials. The ultimate analysis was conducted according to ASTM standards E777–17a, E–778–15 and E–711–15. This is the estimation of the important chemical elements present in the feed stock materials of this study. The composition of the elements are percentage of carbon (C), hydrogen (H), Nitrogen (N₂), Sulphur (S).

Determination of Oxygen Content (ASTM D 7607)

Oxygen was determined by calculation

$$\text{Oxygen (\%)} = 100 - (\%C + \%H + \%N + \%S) \quad \dots \quad (5)$$

Where C=Carbon, H=Hydrogen, N=Nitrogen and S=Sulphur

Determination of Calorific Value (ASTM D2015–96)

The gross calorific value was determined using a bomb calorimeter model (CAB 101). Approximately 0.8 g fuel sample was weighed in a bomb crucible. The bomb cup was placed on its stand provided with the outfit. Firing nickel wire piece was stretched between the electrodes of the bomb (ASTM E–711). A wicking cotton thread, 9 cm long was tied to the stretched wire and the end dipped into the sample in the crucible. The crucible was then placed on a support ring. Exactly 1 ml of distilled water was pipetted out into the body of the bomb and then filled with $3.0 \times 10^6 \text{ N/m}^2$ of oxygen gas. Calorimeter was filled with distilled water until a weight of 3 kg (water plus the can) was obtained to submerge the bomb completely. The bomb was placed on the three supports in the calorimeter vessel and checked for leakage (it was confirmed by absence of bubbles). Cooling water was adjusted to flow at rate of 300 ml per minute. The water jacket was covered

with thermometers and stirrer was lowered and circuit completeness tested by firing circuit test plug. The temperature of the calorimeter vessel was allowed to stabilize and the initial temperature taken at $\pm 0.001^\circ\text{C}$, the fire switch was then pressed for 2 seconds to ignite the sample. The final temperature of the apparatus was taken after 10 minutes at $\pm 0.001^\circ\text{C}$. Readings were taken after sequential 3 minutes until the reading was found to be within a range of $\pm 0.002^\circ\text{C}$. The final temperature was recorded. Rise in temperature was calculated as a difference from initial to final temperature reading. Each sample was tested three times and the average values of weight of sample and temperature rise taken for the final determination of total heat released from the sample. The gross heat released was calculated using the equation 6:

$$\text{Calorific Value} = \frac{cv\Delta T - 0.12600}{M} \quad \dots \quad (6)$$

Where;

H=Calorific value, C_v =Heat capacity of apparatus (10.380 J/°C) and 0.12600 J=Constant heat gain. ΔT =Change in Temperature in °C, M=mass of the sample in (g).

The Co-pyrolysis System

Pyrolysis can be defined as the thermal decomposition of feedstock materials at higher temperatures in an inert atmosphere (absence of oxygen). The byproducts of pyrolysis process includes; liquid, gas and char. The main objective of this co-pyrolysis system is to produce liquid fuel. The main components of the system are the reactor and the condenser.

Figure 1 shows the conceptual representation of the pyrolysis system and Figure 2 depicts the co-pyrolysis system for the production of liquid fuel.



Figure 2. Co-pyrolysis system.

Experimental Procedure

Dried and weighted *Jatropha curcas* seed cake with tyre waste of (1:1) of particle size of 1.5 mm was fed into the fixed bed reactor for pyrolysis. The sample was taken in the stainless steel reactor for each run and placed in an electrically heated furnace. The experiments were conducted at various temperatures of 450°C, 500°C and 550°C with a heating rate of 20°C min⁻¹ and kept at constant till the reaction completes in 30 minutes. A nitrogen flow rate of 2 L/min was employed in other to purge air out of the system which prevent it from secondary cracking. The volatiles contents emanating from the reactor were channeled to the water cooled condenser and the non-condensable gases were flared into the atmosphere. The condensed oil was collected in a liquid collector, and weighted. The remaining residue (char) and the gases that escaped to the atmosphere were regarded as byproduct in this study. The experiments were conducted three times and the average values were recorded and reported. The liquid fuel yield was collected after it was condensed and was recorded carefully kept (separately) in well-sealed containers under room temperature. This procedure was repeated for the following feed ratios of 1:2 and 1:3 (i.e *Jatropha* cake with tyre waste) and the temperatures of 500°C and 550°C, with the reaction time of 45 and 60 minutes.

Optimization Using Taguchi Design of Experiment

The Taguchi method is a structured approach for determining the best combination of inputs to produce a product or service. Design of experiment is an important tool for designing processes and products. It is a method for quantitatively identifying the right inputs and parameters levels for making a high quality product or service. It is also a statistical or engineering methodology that aim at reducing the performance “variation” of a system [19]. In this study contains 3 parameters which are feed ratio, temperature and reaction time, and three levels for each. Meaning the feed ratio levels of 1:1, 1:2 and 1:3, the temperature has levels of 450°C, 500°C, and 550°C, and the reaction time has levels of 30 min, 45 mins and 60 min. By inputting the parameters and levels on taguchi design of experiment, Table 1 would be generated automatically.

Table 1. Co-pyrolysis of *jatropha* cake with tyre waste

Experiment no	Parameters			Liquid fuel (% wt)
	Feed ratio	Temp (°C)	Reaction time (min)	
1	1:1	450	30	63.0
2	1:1	500	45	68.0
3	1:1	550	60	60.0
4	1:2	450	45	57.3
5	1:2	500	60	58.2
6	1:2	550	30	53.0
7	1:3	450	60	52.0
8	1:3	500	30	53.0
9	1:3	550	45	50.3

Table 2. Proximate and ultimate analysis of *jatropha* cake

Proximate analysis (% wt)	
Moisture content	0.76
Volatile matter	78.30
Ash content	1.80
Fixed carbon	19.14
Ultimate analysis (% wt)	
Carbon	57.20
Hydrogen	8.30
Nitrogen	6.10
Sulphur	0.5
Oxygen	27.90
Calorific value (MJ/Kg)	25.47

¹Calorific value = $\frac{C_p \Delta T - 0.12600}{M}$, Where; C_v = Heat capacity of apparatus, ΔT = Change in temperature in °C, M = mass of the sample in (g).

It would come up with the minimum number of experiment to be conducted/performed. Both the means and delta values are automatically generated from the minitab version 18 software, and the delta is calculated as the difference between the maximum and the minimum of each column.

RESULTS AND DISCUSSION

Results

Table 2 shows the results of proximate and ultimate analysis of *Jatropha* Cake.

Proximate analysis (Table 2) shows that the sample (*Jatropha* cake) had high concentration of volatile matter (78.30%). The inherent moisture content of the sample was 0.76%. The ash and fixed carbon content contains 1.8% and 19.14% respectively.

Table 3. Proximate and ultimate analysis of tyre waste

Proximate analysis (% wt)	
Moisture content	0.76
Volatile matter	78.30
Ash content	1.80
Fixed carbon	19.14
Ultimate analysis (% wt)	
Carbon	83.20
Hydrogen	5.52
Nitrogen	1.50
Sulphur	0.20
Oxygen	9.78
Calorific value (MJ/Kg)	30.47

²Calorific value = $\frac{cv\Delta T - 0.12600}{M}$, Where; C_v = Heat capacity of apparatus, ΔT = Change in temperature in °C, M = mass of the sample in (g).

Ultimate analysis data (Table 2) indicates that the sample contains high proportion of carbon of 57.20%, with relatively low concentrations of sulphur (0.5%), nitrogen (6.10%), and hydrogen (8.30%). The oxygen content of the sample was found by calculation (27.90%). The calorific value or energy content of the sample was determined to be 25.47 MJ/kg.

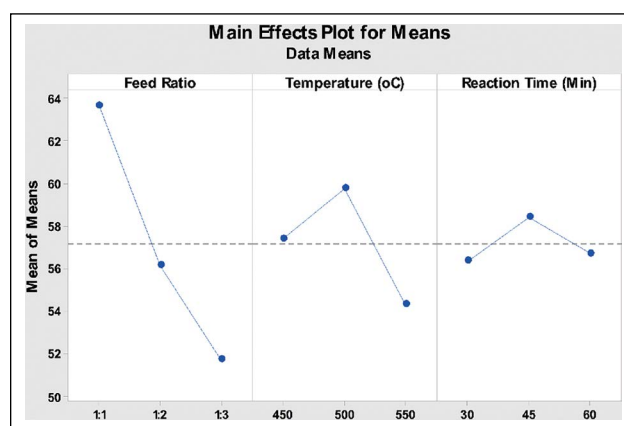
The Table 3 depicts the results of proximate and ultimate analysis of tyre waste.

Proximate analysis (Table 3) shows that the sample (tyre waste) has high content of volatile matter (55.95%). The inherent moisture content of the sample was 0.57%, however, the sample contains 15.30% of ash content. The fixed carbon obtained from the sample by calculation was 28.18%.

Ultimate analysis data (Table 3) indicates that the tyre waste contains high proportion of carbon of 83.0%, with low sulphur contents of (0.2%), nitrogen (1.50%), and hydrogen (5.52%). The oxygen content of the sample was found by calculation (9.78%). The calorific value or energy content of the sample determined was 30.47 MJ/kg.

The Table 1 depicts the results of liquid fuel produced via co-pyrolysis of Jatropa cake with tyre waste operating under various conditions using Taguchi's design of experiment.

It can be observed that from Table 1, at constant feed ratio of 1:1, as the temperature and the reaction time increases, the liquid yield produced decreases with the exception of the reaction temperature of 500°C and reaction time of 45 minutes, which had liquid yield of 68.0 wt%. It can also be observed that, at constant feed ratio of 1:2, as the temperature increases and the reaction time decreases, the liquid yield produced also decreases with the exception of the reaction temperature of 500°C and reaction time of 60 minutes, which had liquid yield of 58.2 wt%. It can also note that,

**Figure 3.** The graph of mean of means versus feed ratio, temperature and reaction time.**Table 4.** Response table for means

Level	Feed ratio (A)	Temperature (°C)	Reaction time (min)
1	63.67	57.43	56.33
2	56.17	59.73	58.53
3	51.77	54.43	56.73
Δ	11.94	5.30	2.20
Rank	1	2	3

at constant feed ratio of 1:3, as the temperature increases and the reaction time decreases, the liquid yield produced also decreases with the exception of the reaction temperature of 500°C and reaction time of 30 minutes, which had liquid yield of 53.0 wt%. The percentage weight of the liquid fuel obtained from pure jatropa cake and pure tyre waste were 22.6 wt% and 38.4 wt% respectively which are in consonance with the study of [1, 16–18]. As the waste tyre was added to the biomass as feedstock material, the liquid fuel yield increases so also the calorific value of the liquid fuel compared to that of pure jatropa cake or pure tyre waste.

Maximum Process for the Co-pyrolysis of Jatropa Cake with Tyre Waste

The Figure 3 shows the results of the optimization process for the co-pyrolysis of Jatropa cake with tyre waste.

It can be observed that from Figure 3, as the feed ratio of the samples decreases the liquid yield increases, and the liquid fuel yield was optimum at the feed ratio of 1:1. Furthermore, the reaction temperature and the reaction time that produces high liquid fuel yield was at 500°C and 45 minutes respectively. So the parameters that can yield maximum liquid fuel was at a feed ratio of 1:1, reaction temperature of 500°C and reaction time of 45 minutes. The result (liquid fuel) obtained at that conditions was 68.0 wt%. The Table 4 demonstrates the results of response table for means.

The results from the Table 4 shows the effect of each parameter or factor in the liquid fuel production. It showed that the feed ratio has the greatest effect on the production of liquid fuel, followed by temperature, and then reaction time.

CONCLUSION AND RECOMMENDATION

Conclusion

The findings of the characterization study using proximate and ultimate analysis indicate that, the *Jatropha* cake and tyre waste has a potential source of liquid fuel production. It was inferred from the Taguchi analysis that the combination of feed ratio of 1:1, reaction temperature of 500°C and the reaction time of 45 minutes was the optimal setting for obtaining maximum liquid fuel for the co-pyrolysis of *Jatropha* cake with tyre waste. The maximum liquid yield obtained from the co-pyrolysis of *Jatropha* cake with tyre waste was 68.0 wt%. It can also concluded that, the ratio of feed stock material has greatest influence on the production of the liquid fuel compared to reaction temperature and reaction time.

Recommendations

- i. Proximate and ultimate analyses showed that, the *jatropha* cake and the tyre waste materials has high content of carbon and hydrogen with low oxygen content and has potentials for the production of qualitative liquid fuel. Considering the results obtained, the liquid fuel from *Jatropha* cake and tyre waste can be used as an alternative fuel.
- ii. Other materials like HPDE (High density Polyethylene) and LDPE (Low density Polyethylene) and biomass mixtures should be researched upon to determine the synergy effect between them via co-pyrolysis technique. Because these materials has high carbon and hydrogen content. When mixed together with biomass will produce more content of pyrolytic liquid fuel.

DATA AVAILABILITY STATEMENT

The author confirm that the data that supports the findings of this study are available within the article. Raw data that support the finding of this study are available from the corresponding author, upon reasonable request.

CONFLICT OF INTEREST

The author declared no potential conflicts of interest with respect to the research, authorship, and/or publication of this article.

ETHICS

There are no ethical issues with the publication of this manuscript.

REFERENCES

- [1] S.A Babajo, J. S. Enaburekhan, and I. A. Rufa'i, "Design, fabrication and performance study of co-pyrolysis system for production of liquid fuel from *jatropha* cake with polystyrene waste," *Journal of Applied Sciences and Environmental Management*, Vol. 25, pp. 407–414, 2021. [\[CrossRef\]](#)
- [2] T. Bridgewater, "Biomass for energy," *Journal of the Science of Food and Agriculture*, pp.1755–1768, 2006. [\[CrossRef\]](#)
- [3] B. Sulaiman, and A. Abdullahi, "A optimum conditions for maximizing pyrolysis liquid of oil palms empty fruit bunches," *Energy*, Vol. 36(5), pp. 2352–2359, 2011. [\[CrossRef\]](#)
- [4] F. G. Hasan, "The production and evaluation of bio-oils from the pyrolysis of sunflower -oil cake," *Biomass and Bioenergy*, Vol. 23, pp. 307–314, 2002. [\[CrossRef\]](#)
- [5] B. Antal, and G. Gronli, "The art, science and technology of charcoal production," *Industrial and Engineering Chemistry Research*, pp. 1619–1640, 2003.
- [6] G. Vamvuka, "Bio-oil, solid and gaseous biofuels from biomass pyrolysis processes; An overview," *International Journal of Energy Research*, Vol. 35(10), pp. 835–862, 2011. [\[CrossRef\]](#)
- [7] D. M. Zheng, M. Liu, and Y.-X. Chen, "Study on the catalytic cracking of waste plastics and waste lubricating oil for producing fuel oil," *Modern Chemical Industry*. Vol. 31(8), pp. 47–49, 2011.
- [8] P. T. Williams, "Pyrolysis of waste tyres: A review," *Waste Management*. Vol. 33, pp. 1714–1728, 2013. [\[CrossRef\]](#)
- [9] M. Hita, M. Arabiourrutia, J. Olazar, J. M. Bilbao, P. Arandes, and A. Castano, "Opportunities and barriers for producing high quality fuels from the py-rolysis of scrap," *Renewable and Sustainable Energy Reviews*, Vol. 56, 745–759, 2016. [\[CrossRef\]](#)
- [10] W. C. Wang, C. J Bai, C.T.S. Lin, and S. Prakash, "Alternative fuel produced from thermal pyrolysis of waste tires and its use in a DI diesel engine," *Applied Thermal Engineering*, Vol. 93, pp. 330–338, 2016. [\[CrossRef\]](#)
- [11] F. Abnisa, W. Wan-Daud, M. Ramalingam, S. Azemi, and J. Sahu, "Co-pyrolysis of palm shell and tyre waste mixtures to synthesis liquid fuel," *Fuel*, Vol. 108, pp. 311–318, 2013. [\[CrossRef\]](#)
- [12] R. Alias, K. Hamid, and K Ismail, "Co-pyrolysis and catalytic copyrolysis of waste tyres with oil palm empty fruit bunches," *Journal of Applied Sciences*, Vol. 11(13), pp. 2448–2451, 2011. [\[CrossRef\]](#)
- [13] Q. Cao, L. Jin, W. Bao, and Y. Lv, "Investigations into the characteristics of oils produced from co-pyroly-sis of biomass and tire," *Fuel Processing Technology*, Vol. 90(3), pp. 337–342, 2009. [\[CrossRef\]](#)

- [14] D. Demirbas, "Pyrolysis mechanism of biomass materials," *Energy Sources, Part A: Recovery Utilization and Environmental Effects*, Vol. 31(13), pp. 1186–1193, 2009. [\[CrossRef\]](#)
- [15] S. A Babajo, "Effect of pressure variation on performance characteristics of jatropha biodiesel - kerosene blends used for cooking application," *African Journal of Renewable and Alternative Energy*, Vol 5(1), pp. 20–33, 2020.
- [16] B. Zhang, and E. Mei, "Upgrading of bio-oil from biomass pyrolysis in China: A Review," *Renewable and Sustainable Energy Reviews*, pp. 66–72, 2013. [\[CrossRef\]](#)
- [17] S. A. Babajo, J. S. Enaburekhan, and I. A. Rufa'i, "Review on production of liquid fuel from co-pyrolysis of biomass with scrap/waste tire," *Journal of Applied Sciences and Environmental Management*, Vol. 23(8), pp. 1475–1482, 2019. [\[CrossRef\]](#)
- [18] AOAC Association of Official Analytical Chemists. "Official Methods of Analysis of Association of Official Analytical Chemists," 19th ed. Washinfon D.C.: Association of Official Analytical Chemists, 2010.
- [19] K. Senthilkumar and PS. Sirinivasan, "Application for taguchi method for the optimization of system parameters of centrifugal evaporative air cooler," *Journal of Thermal Science* Vol. 19(5), pp. 473–479, 2010. [\[CrossRef\]](#)



Research Article

Reverse osmosis treatment system for landfill leachate: Operation conditions, advantages and challenges

Aysun Derya TOPAL¹, Ayşe Dilek ATASOY^{1*}

Department of Environmental Engineering, Harran University Engineering Faculty, Şanlıurfa, Türkiye

ARTICLE INFO

Article history

Received: 24 November 2021

Revised: 25 January 2022

Accepted: 02 April 2022

Key words:

Contamination; Membrane filtration; Solid waste; Waste management

ABSTRACT

Landfill leachate treatment by Reverse Osmosis (RO) system was evaluated in this study. Operational conditions of sand filters, sulfuric acid dosing and pH adjustment, cartridge filters and cat pumps, and membrane modules were discussed in detail. Advantages and challenges of RO for leachate treatment in developing countries handled with sustainability logic. The system has been successfully applied in leachate treatment with high removal rates as 98% of COD, 99% of total Nitrogen and suspended solids and substantial heavy metal removal. However, high costly operating expenses, dependency on the manufacturers for membranes, chemicals and other materials indicated the system unsustainable. Especially high-strength characteristic of leachate, high energy consumption of RO process, difficulty to struggle with scaling problems, limited lifetime of membranes and management/treatment of concentrate were expressed as the constraints of the system.

Cite this article as: Topal AD, Atasoy AD. Reverse osmosis treatment system for landfill leachate: Operation conditions, advantages and challenges. Environ Res Tec 2022;5:2:119–127.

INTRODUCTION

Landfilling with the feature of being a short-term solution alternative is preferred widely by the municipalities for disposing the industrial and municipal solid wastes (MSW) owing to its low capital costs and minimum technology being practiced. A major issue arising from solid waste landfilling is intense impact of landfill leachates on the environment [1–3]. Leachates are high-strength wastewaters formed as a result of percolation of rainwater and moisture through waste in landfills [4, 5]. MSW landfill leachate varies widely in composition and needs to be treated effectively before being discharged into the environment. To maximise resources recycling with the least negative environmental

impacts, regulations on both landfill management and leachate discharge are becoming more stringent throughout the world [6].

Landfill leachate must be appropriately treated and managed, maximizing the recovery and minimizing the waste disposals. In particular, standalone on-site treatments are more effective on unstable characteristics of leachate. Raw leachate from young landfills contains most of organic substances in biodegradable form thus can be easily treated by biological processes. For old landfills, most of the leached organic compounds are hardly or non-biodegradable forms and they should be treated by physico-chemical processes or a combination of biological and physico-chemical pro-

*Corresponding author.

*E-mail address: adilek@harran.edu.tr



Table 1. Specific parameters of leachate

Parameters	Quantity
Flowrate of leachate	180 m ³ /day
Chemical oxygen demand (COD)	35.000 mg/L
Suspended solid	1.000 mg/L
Conductivity	30.0/cm

cesses [7]. On the other hand, the use of membrane technologies allows stable quality of the permeate that can be locally reused or discharged in water bodies. Reverse Osmosis (RO), as single post-treatment step has shown to be an indispensable means of achieving high purification, removal of hazardous metals and potential water recovery [8]. RO process was studied for treatment of landfill leachate within two decades from its discovery and was reported to be the most effective method for treating leachates [9–14]. By the mid-1980s, RO systems had already penetrated significantly into the market of leachate treatment [15]. However, RO concentrate is difficult to deal, the specific energy consumption of RO process is much higher than other treatments and it is difficult to struggle with significant scaling problems. Additionally, the frequent cleaning and strong demand of acid and alkali limits the continuous operation of the system and dramatically increases the running costs [6]. It is a controversial issue that the reverse osmosis system is a sustainable method in leachate treatment.

Table 2. RO treatment design criteria for max and average annual flow rates

Rate (%)		Max annual value			Average annual value		
		L/h	m ³ /day	m ³ /year	L/h	m ³ /day	m ³ /year
Raw leachate	100.00	11.57	277.80	101.39	10.42	250.00	91.25
Concentrate	34.30	3.97	95.40	34.81	3.58	85.80	31.33
Permeate	65.70	7.60	182.40	66.70	6.84	164.20	59.92

**Figure 1.** RO treatment plant membrane design and disc membranes.

In this context, our study aims to evaluate the operational conditions of reverse osmosis system with interpreting its advantages and challenges for a landfill leachate treatment.

MATERIALS AND METHODS

Landfill Leachate

The amount of leachate is directly related to precipitation, population, features of the landfill and the waste source of the city where it is located. The amount of leachate is calculated by Equation 1.

$$C = Pr \times (1-R) - \Delta S - Ev \quad (1)$$

C is total amount of leachate (mm/year), Pr is precipitation (mm/year), R is runoff coefficient, ΔS is amount of accumulated water in landfill area and Ev is Evaporation from landfill surface (mm/year). Although the amount of leachate in landfills depends on many factors such as the rainfall in the region, the moisture content of the solid waste and the age of the landfill area, the daily amount of leachate from unit area of the landfill is generally considered to be 8.6 m³/ha.day. Specific leachate parameters for study area are presented in Table 1.

Reverse Osmosis System

Design criteria of RO system for the treatment of landfill leachate located in Gaziantep, Turkey was presented in Table 2. In the facility designed using reverse osmosis system,

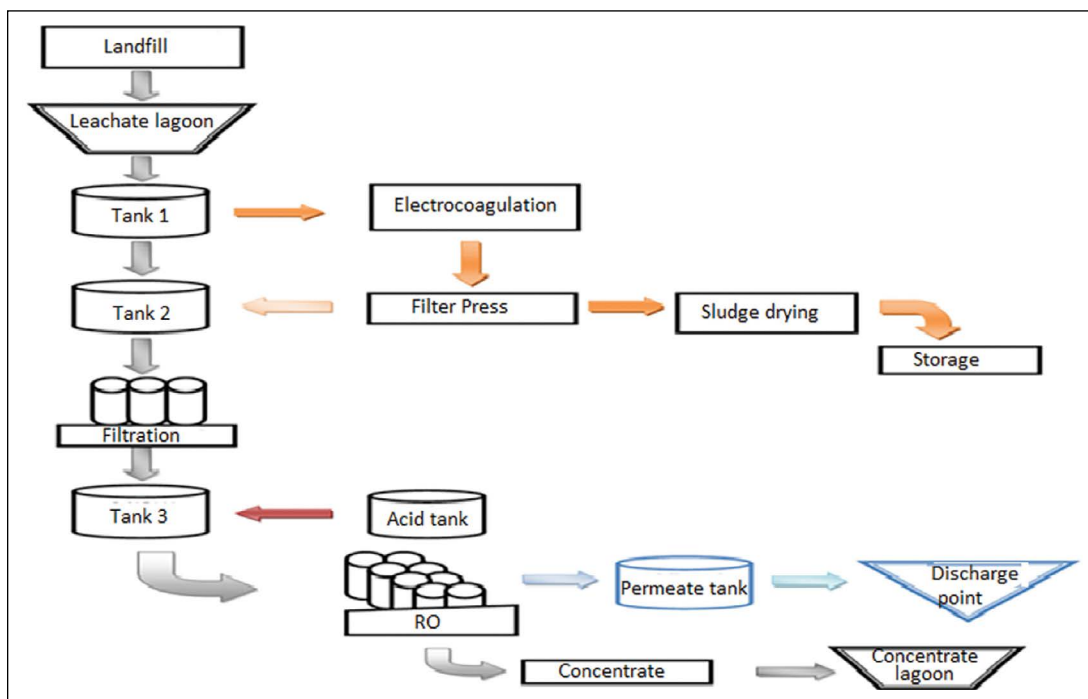


Figure 2. RO process flow chart.



Figure 3. Inlet unit-tank 1.

vertical modeling system and disc membranes were used. The manufacturer is PALL Company and it is located in Germany. The reverse osmosis is a 2-stage system operating for an average pressure of 75 bar. Disc membrane technology was preferred for the treatment (Fig. 1). The facility used 100 modules 21.000 disc membranes in the 1st stage, and 18

modules 3.780 disc membranes in the 2nd one. The system is completely assembled on a portable base. It can be easily commissioned with water and energy connections. The system is fully equipped with pH, conductivity, antiscalant dosage control and chemical cleaning equipment.

Analysis of Leachate Parameters

The leachate flow was measured continuously by the Burket brand flow meter at the entrance of the facility. Monitoring of conductivity and pH value was made with LTH conductivity/pH meter. Oil and grease were measured by the method of SM 5520 D. Total Cyanide and Fluoride (F) were analyzed by the methods of SM 4500 CN C E and SM 4500 F B D, respectively. Total Kjeldahl N, Total P, chemical oxygen demand (COD), and suspended solids (SS) were measured using SM 4500 Norg B, SM 4500 P B E, SM 5220 B, SM 2540 D, respectively. Cr, Cu, Zn, Fe, Cd, Pb were analyzed by EPA Method 200.7.

RESULTS AND DISCUSSION

Operation of RO Treatment System

The schematic figure for process flow chart is represented in Figure 2. A cartridge filtration is applied at the inlet of the system and pH adjusted pre-treated water is fed to the system with antiscalant dosage. The concentrate is taken to a lagoon to be used in order to humidify the landfill area. Excess water is transferred to lagoon 1. Permeate is taken to a tank with a volume of 15.000 L to be used for water utilization for afforestation and similar purposes (Fig. 2).



Figure 4. Sand filters in the system.



Figure 5. Tank 3 for pH adjustment.

Sand Filters

Leachate from the solid waste landfill enters the lagoon with its own attraction and passes to water intake structure to be stored in tanks. The leachate transmitted to the tank 1 must be delivered to the electrocoagulation (EC) unit positioned in the project. Due to the failure of the EC unit the tank 2 is used as a backup of the tank 1 (Fig. 3). The system has three sand filters (fiberglass reinforced PE filter) in series with 2.7 m³. Average capacity is 13 m³/h. Sand filters alleviate the load of leachate before the reverse osmosis and increase the

membrane lifetime (Fig. 4). Since the system works continuously, both blower and backwash are applied to the sand filters in each shift to protect the sand filter environment life. However low pH in the concentrate due to returning of diluted leachate to the system with recirculating shortens the sand filter media life and causes encrustation problem.

Sulfuric Acid Dosing and pH Adjustment

Leachate after sand filters is taken into tank 3 for pH adjustment before its transferring to membranes. 98% pure

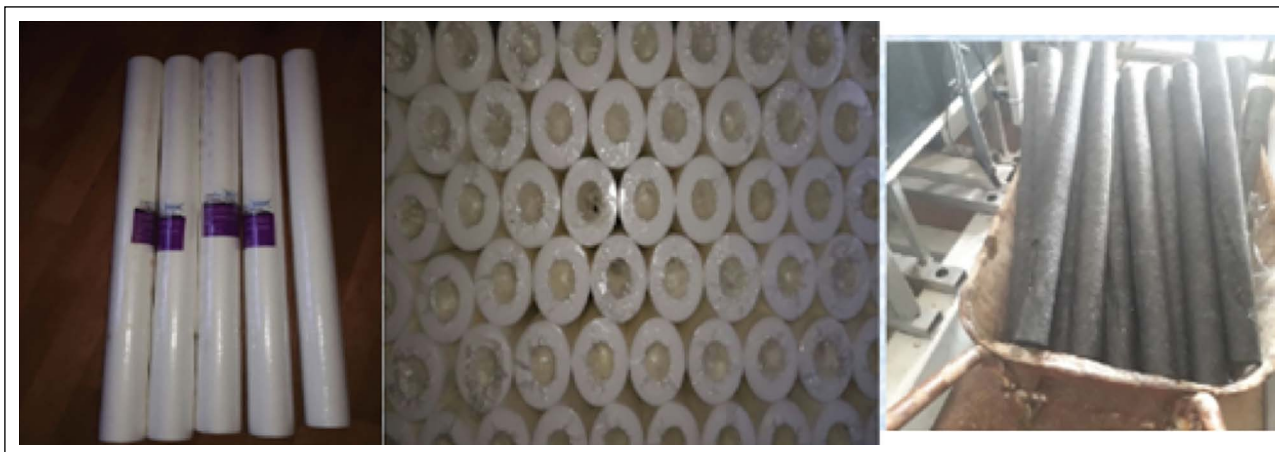


Figure 6. Cartridge filters for >10 µm particulates.



Figure 7. Pump center.

sulfuric acid is circulated with leachate in tank 3 to set pH as 6.4 (Fig. 5). Thus, desired pH value in membranes is achieved. The water that comes out of the tank 3 is delivered to the cartridge filters.

Cartridge Filters and Cat Pumps

Total of 21 cartridge filters consist of 3 modules and 7 in each module (Fig. 6). Cartridge filters prevent the entrance of >10 µm particulates to membrane filter. Andiscalant dosing is applied into the system to prevent any silica formation which causes calcification in the lines. Dydo et al. [16], have declared a similar problem on the examined leachate. They indicated that the wastewater was almost saturated with calcium sulfate, thus causing serious scaling problem. Furthermore, there was a large extent of sulfate ions over stoichiometric CaSO₄ composition. Also, they claimed that the large amount of magnesium ions could not be ignored for high pH conditions.

Pre-treated leachate from cartridges is transmitted to piston pumps called cat pump. Piston pumps raise the water to pressure of 65 bar. Since the basic logic of reverse osmosis is the pressure purification method, these pumps constitute

the most important part of the system. In addition, these pumps require the most serious investment in maintenance and repair costs.

There are 3 cat pumps on the system. Two of them transmit the water to the 1st stage and one to the 2nd stage. Leachate pressurized by cat pump is transmitted to horizontal pumps ensuring the water access to modules (Fig. 7).

Membrane modules

Facility is operated as 2-stage system. 1st stage consists of 100 modules and 21.000 (100x210) disc membranes and it is divided into 4 sections as unit 11/1, 11/2, 11/3 and 11/4 (Fig. 8). The leachate is first taken to the membranes in unit 11/1. The water treated in unit 11/1 is transferred to unit 21 (Fig. 9), and the untreated part to unit 11/2 and this process continues until the 1st stage is completed. The treated leachate in 1st stage is filtered again in unit 21 to get a better-quality effluent (Fig. 10). Unit 21 contains 18 modules and 3.780 (18x210) disc membranes. In this way, permeate and concentrate are produced as a result of the treatment process. Membrane-based treatment processes, including reverse osmosis generate a large volume of membrane con-

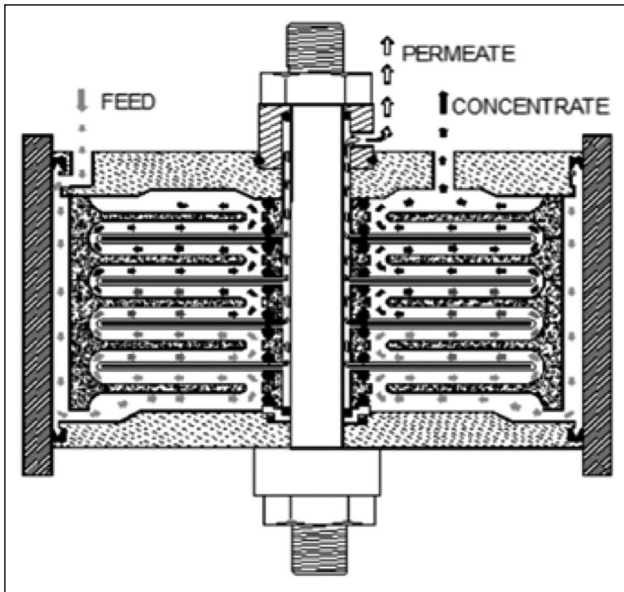


Figure 8. Schematic representation of modules and disc membranes.

concentrate (MC) [17]. The concentrate that can no longer be treated in unit 11/4 is sent to concentrate lagoon. Leachate from lagoon is transferred back to the landfill through the pipes and the pumps to distribute the water with jets over the field as ensuring its evaporation and to dilute it by mixing with fresh leachate. The treated leachate from unit 21 is stored in permeate tanks. Caustic is dosed to permeate for a further pH adjustment as 6.9-7.0 and it is discharged into a stream bed by its own attraction.

Operating Problems/Challenges of Reverse Osmosis System for Leachate Treatment

The leachate has the potential to cause serious harm to human health and the environment. High removal of contaminants such as COD, SS, Total N, color, oil/grease, and heavy metal has been achieved using reverse osmosis process (Table 3). It is seen that the effluent discharge parameters are comply with the receiving environment discharge criteria. However, reverse osmosis is difficult process in terms of both operating cost and operating conditions.

Alkaline and acidic cleaning to protect the disc membranes increases the operating costs. Cartridge filter is a consumable with a certain lifetime. Time to change cartridge filter is monitored when the pressure difference reaches 1 bar in the scada system. In addition, an-discalant is dosed to prevent any silica formation in the system. Dydo et al. [16], concluded that the most reasonable method to mitigate scaling problem during reverse osmosis of the examined leachate is chemical softening pretreatment with sodium carbonate and sodium hydroxide mixture. Sodium carbonate will behave as the calcium while sodium hydroxide as magnesium precipitants. At



Figure 9. Unit 21 Disc membranes.



Figure 10. Raw leachate (on the left) and permeate (on the right).

the same time these precipitants will shift the examined leachate pH to the level desired for further treatment.

Before the raw leachate is taken into the membranes, sulfuric acid is added to provide the desired pH value in the media. In order to meet the pH discharge criterion, caustic dosing is applied in permeate tank to increase the pH which is reduced at the beginning of the system. The disc membranes used in the system have also a limited lifetime and the membranes constitute approximately 50% of the

Table 3. 3-years (2016–2018 years) averages of influent and effluent parameters of leachate and removal rates by reverse osmosis system

Parameters	Influent water (mg/L)	Effluent water (mg/L)	Removal rate (%)
Chemical oxygen demand (COD)	6464.17	153.17	97.63
Suspended solids (SS)	429.43	<6	98.84
Total kjeldahl nitrogen	1495.90	17.87	98.81
Total phosphorus	10.71	6.00	43.98
Oil and grease	561.83	35.70	93.65
Color (Pt–Co)*	3355.04	142.09	95.76
Total chromium (Cr)	1.05	0.01	98.92
Chromium (Cr+6)	0.39	0.03	91.72
Fluoride (F)	3.04	0.48	84.20
Copper (Cu)	0.03	0.02	46.00
Zinc (Zn)	0.27	0.06	78.75
Iron (Fe)	2.33	0.25	89.43

*Unit of color is (Pt–Co).

Table 4. Consumable quantities reflected in operating expenses

Consumption during the operation	Consumable amount
Sulfuric acid	1872 kg/day
Andiscalant	3.12 L/day
Caustic	156 L/day
Alkaline cleaning chemical	125 L/per cleaning
Acidic cleaning chemical	75 L/per cleaning
Used cartridge filters	21 cartridges/per change

plant investment cost. Due to the sensitivity of the membrane structure and in case of insufficient pre-treatment processes, the membrane life will be completed in a short time. Renou et al. [18], argued that there were important limitations to this process. They stated that high salinities of the leachates caused high osmotic pressures, which required working at high pressures and low conversion rates. Chemical consumption is presented in Table 4 considering the facility as operating at full capacity for 312 m³/day. The RO process is also strongly limited by the irreversible membrane fouling, which requires frequent chemical cleaning of the membranes [18].

Among the constant problems encountered in the system, there is also the corrosion problem of electronic equipment caused by the H₂S in the leachate content. To prevent corrosion, the facility should be located away from lagoons. In this case, the pump and the electricity cost of the equipment will also create a disadvantage for the system. While making cost calculations at the project stage of the reverse osmosis system, operating expenses should also be taken into account in this direction. Operation of more costly filtration technologies is more complex and requires the experienced

teams. That's why problems occur in the leachate treatment plants due to the lack of trained personnel and an efficient treatment process cannot be provided.

The most important factors affecting the feasibility of membrane applications are formation, management, and treatment of the concentrate. Li et al. [11], Liu et al. [12], Renou et al. [18, 19], and Talalaj and Biedka [20], expressed the recirculation of concentrated leachate as one of the most debated options for RO treatment. Especially concentrate removal expenses constitute a significant part of the operating cost of the membrane processes. The rejection of the membrane processes generates a significant volume of membrane concentrate (MC) [21]. The MC is enriched with large quantities of refractory organics and salinity from leachate and is a particularly problematic issue in waste management. Therefore, there is a clear need to explore a scientific and rational route for MC, preventing it from severe environmental contamination.

Although good quality effluent is obtained in the leachate treatment; high costly operating expenses suggest the system is unsustainable. Once the reverse osmosis system is established, municipalities are financially dependent on the manufacturers for membranes, chemicals and other materials that are consumable during operation. Therefore, it is not an acceptable way for developed countries to exploit the financial resources of developing countries to sell their technologies with high operating costs. Similar approaches should be avoided in order to consider the savings and to offer more scientific solutions. For sustainable leachate treatment solutions, methods with lower initial investment and operating costs and, processes requiring a small number of technical staff support should be investigated in developing countries.

CONCLUSIONS

Leachate treatment is one of the most crucial tasks in municipal solid waste management. Reverse osmosis was assigned as an effective method for treating leachate in this study. The RO system has been successfully applied in leachate treatment with high removal rates as 98% of COD, 99% of total Nitrogen, 99% of suspended solids, 94% of oil/grease, 96% of color and substantial heavy metal removal, respectively. The system has sand filters which reduced the load of leachate before the reverse osmosis and increased the membrane lifetime. pH adjustment on leachate was performed before its transferring to membranes. A cartridge filtration was applied at the inlet of the system and pH adjusted pre-treated water was fed to the system with antiscalant dosage. The leachate was taken to the membranes that was operated as 2-stage system. 1st and 2nd stages consisted of 100 modules and 21.000 and 18 modules and 3.780 disc membranes, respectively. Permeate and concentrate were taken to a lagoon to be used in order to humidify the landfill area and for afforestation, respectively. Despite the advantages of system, challenges such as high costly operating expenses, dependency on the manufacturers for membranes, difficulty to struggle with scaling problems, high energy consumption, limited lifetime of membranes and management/treatment of concentrate were clarified as the constraints of reverse osmosis.

ACKNOWLEDGMENT

The authors are grateful to Gaziantep local government and city and county municipalities for their support and guidance.

DATA AVAILABILITY STATEMENT

The authors confirm that the data that supports the findings of this study are available within the article. Raw data that support the finding of this study are available from the corresponding author, upon reasonable request.

CONFLICT OF INTEREST

The authors declared no potential conflicts of interest with respect to the research, authorship, and/or publication of this article.

ETHICS

There are no ethical issues with the publication of this manuscript.

REFERENCES

- [1] P. Kjeldsen, M.A. Barlaz, A.P. Rooker, A. Baun, A. Ledin, and T.H. Christensen, "Present and long-term composition of MSW landfill leachate: A review," *Critical Reviews in Environmental Science and Technology*, Vol. 32, pp. 297–336, 2002. [\[CrossRef\]](#)
- [2] K. Xiao, Y. Chen, X. Jiang, W.Y. Seow, C. He, Y. Yin, and Y. Zhou, "Comparison of different treatment methods for protein solubilisation from waste activated sludge," *Water Research*, Vol. 122, pp. 492–502, 2017. [\[CrossRef\]](#)
- [3] M. Zolfaghari, K. Jardak, P. Drogui, S.K. Brar, G. Buelna, and R. Dubé, "Landfill leachate treatment by sequential membrane bioreactor and electro-oxidation processes," *Journal of Environmental Economics and Management*, Vol. 184, pp. 318–326, 2016. [\[CrossRef\]](#)
- [4] H. Hasar, S.A. Unsal, U. Ipek, S. Karatas, O. Cinar, C. Yaman, and C. Kınacı, "Stripping/foccculation/membrane bioreactor/reverse osmosis treatment of municipal landfill leachate," *Journal of Hazardous Materials*, Vol. 17, pp. 309–317, 2009. [\[CrossRef\]](#)
- [5] I.A. Talalaj, P. Biedka, and I. Bartkowska, "Treatment of landfill leachates with biological pretreatments and reverse osmosis," *Environmental Chemistry Letters* Vol. 17, pp. 1177–1193, 2019. [\[CrossRef\]](#)
- [6] L. Zhang, M.C. Lavagnolo, H. Bai, A. Pivato, R. Raga, and D. Yue, "Environmental and economic assessment of leachate concentrate treatment technologies using analytic hierarchy process," *Resources Conservation and Recycling* Vol. 141, pp. 474–480, 2019. [\[CrossRef\]](#)
- [7] W. Rukapan, B. Khananthai, C. Chiemchaisri, W. Chiemchaisri, and T. Srisukphun, "Short- and long-term fouling characteristics of reverse osmosis membrane at full scale leachate treatment plant," *Water Science and Technology*, Vol. 65(1), pp. 127–134, 2012. [\[CrossRef\]](#)
- [8] D. Cingolani, F. Fatone, N. Frison, M. Spinelli, and A.L. Eusebi, "Pilot-scale multi-stage reverse osmosis (DT-RO) for water recovery from landfill leachate," *Waste Management*, Vol. 76, pp. 566–574, 2018. [\[CrossRef\]](#)
- [9] M. Bodzek, E. Lobos-Moysa, and M. Zamorowska, "Removal of organic compounds from municipal landfill leachate in membrane bioreactor," *Desalination*, Vol. 198, pp. 16–23, 2006. [\[CrossRef\]](#)
- [10] G. Chan, J. Chang, T.A. Kurniawan, C.X. Fu, H. Jiang, and Y. Je, "Removal of non-biodegradable compounds from stabilized leachate using VSEPRO membrane filtration," *Desalination*, Vol. 202(1-3), pp. 445–453, 2006. [\[CrossRef\]](#)
- [11] F. Li, K. Wichmann, and W. Heine, "Treatment of the methanogenic landfillleachate with thin open channel reverse osmosis membrane modules," *Waste Management*, Vol. 29, pp. 960–964, 2009. [\[CrossRef\]](#)
- [12] Y. Liu, X Li, B. Wang, and S. Liu, "Performance of landfill leachate treatment system with disc-tube reverse osmosis unit," *Frontiers of Environmental Science & Engineering*, Vol. 2(1), pp. 24–31, 2008. [\[CrossRef\]](#)

- [13] M. Smol, M. Włodarczyk-Makula, K. Mielczarek, J. Bohdziewicz, and D. Włoka, “The use of reverse osmosis in the removal of PAHs from municipal landfill leachate,” *Polycyclic Aromatic Compounds* Vol. 36, pp. 20–39, 2016. [\[CrossRef\]](#)
- [14] S. Theepharaksapan, C. Chiemchaisri, W. Chiemchairi, and K. Yamamoto, “Removal of pollutants and reduction of bio-toxicity in a full scale chemical coagulation and reverse osmosis leachate treatment system,” *Bioresource Technology* Vol. 102, pp. 5381–5388, 2011. [\[CrossRef\]](#)
- [15] S. Ramaswami, J. Behrendt, R. Otterpohl, “Comparison of NF-RO and RO-NF for the treatment of mature landfill leachates: A guide for landfill operators,” *Membrane*, Vol. 8(17), pp. 1–13, 2018. [\[CrossRef\]](#)
- [16] P. Dydo, M. Turek, J. Ciba, J. Trojanowska, and J. Kluczka, “Boron removal from landfill leachate by means of nanofiltration and reverse osmosis,” *Desalination*, Vol. 185, pp. 131–137, 2005. [\[CrossRef\]](#)
- [17] R. He, X.M. Wei, B.H. Tian, Y. Su, and Y.L. Lu, “Characterization of a joint recirculation of concentrated leachate and leachate to landfills with a microaerobic bioreactor for leachate treatment,” *Waste Management*, Vol. 46, pp. 380–388, 2015. [\[CrossRef\]](#)
- [18] S. Renou, J.G. Givaudan, F. Dirassouyan, and P. Moulin, “Landfill leachate treatment: review and opportunity,” *Journal of Hazardous Materials*, Vol. 150(3), pp. 468–493, 2008. [\[CrossRef\]](#)
- [19] S. Renou, S. Poulain, J.G. Givaudan, and P. Moulin, “Treatment process adapted to stabilized leachates: lime precipitation–prefiltration–reverse osmosis,” *Journal of Membrane Science*, Vol. 313, pp. 9–22, 2008. [\[CrossRef\]](#)
- [20] I.A. Talalaj, and P. Biedka, “Impact of concentrated leachate recirculation on effectiveness of leachate treatment by reverse osmosis,” *Ecological Engineering*, Vol. 85, pp. 185–192, 2015. [\[CrossRef\]](#)
- [21] C. Hou, G. Lu, L. Zhao, P. Yin, and L. Zhu, “Estrogenicity assessment of membrane concentrates from landfill leachate treated by the UV-Fenton process using a human breast carcinoma cell line,” *Chemosphere* Vol. 180, pp. 192–200, 2017. [\[CrossRef\]](#)



Research Article

Investigation of synergetic effect of adsorption and photocatalysis for the removal of tetracycline by BiFeO₃ immobilized on copolymer seeds

Esra BİLGİN ŞİMŞEK^{*}, Zeynep BALTA^{id}

Department of Chemical Engineering, Yalova University, Yalova, Türkiye

ARTICLE INFO

Article history

Received: 02 November 2021

Revised: 06 February 2022

Accepted: 09 March 2022

Key words:

Adsorption; Antibiotic; BiFeO₃;
Perovskite; Photocatalysis

ABSTRACT

The utilization of powdered photocatalysts can cause problems such as agglomeration and difficulty in separation in conventional applications. In this work, deposition of photocatalyst particles on a co-polymeric network was suggested to solve this issue. For this purpose, ferrite type perovskite BiFeO₃ particles were immobilized on the sulphonated polystyrene-divinyl benzene seeds via a facile impregnation process and the heterostructured catalyst (BFO@co-STR/DVB) exhibited boosted removal performance towards tetracycline antibiotic. The co-polymer itself showed attractive adsorption (93% removal) towards tetracycline due to the robust π - π stacking or hydrophobic relationship. The photocatalytic performance of optimal BFO@co-STR/DVB catalyst had the greatest value of apparent rate constant (0.037 min⁻¹), which was 6.16 times higher than that for bare BiFeO₃ (0.006 min⁻¹). Moreover, the heterostructured photocatalyst displayed the highest catalytic efficiency as 98.5% which was mainly assigned to the synergetic effect of adsorption and photocatalysis. Therefore, detailed adsorption mechanism was examined by applying three kinetic models and the pseudo-second order model ($q_e=88.9$ mg/g; $R^2=0.993$) was fitted well describing well the adsorption. The impact of perovskite amount on the polymer structure was also investigated. Apart from tetracycline molecule, the photocatalytic activity of the heterostructured catalyst with respect to different pharmaceutical (isoniazid) was also investigated and the adsorptive removal of isoniazid over the co-STR/DVB polymer was calculated as 80.0% while it significantly increased to 98.2% in the BFO@co-STR/DVB photocatalytic system. This study demonstrated the effective utilization of the perovskite deposited co-polymeric network in the field of “photocatalysis”.

Cite this article as: Bilgin Şimşek E, Balta Z. Investigation of synergetic effect of adsorption and photocatalysis for the removal of tetracycline by BiFeO₃ immobilized on copolymer seeds. Environ Res Tec 2022;5:2:128–136.

INTRODUCTION

In recent years, ferrite type perovskite materials have attracted great attentions due to their excellent characteristics in the field of photocatalysis. Among these perovskites,

bismuth ferrite (BiFeO₃) has been a great interest, because of its high chemical stability, magnetoelectric and optical properties [1]. The rhombohedral distorted BiFeO₃ structure has been investigated as multiferroic material which have ferroelectric ($T_c=1103$ K) and antiferromagnetic

^{*}Corresponding author.

^{*}E-mail address: esrabilgin622@gmail.com



($T_N=643$ K) characteristics over a wide temperature range [2]. The band gap of BiFeO_3 (2.1–2.6 eV) lying in the visible region of the solar spectrum enables it to be applied as photovoltaic cell and photocatalyst [3]. Additionally, BiFeO_3 has been also used as Fenton-catalyst which can effectively catalyze the decomposition of H_2O_2 into $\bullet\text{OH}$ for the degradation of organic pollutants in heterogeneous processes [4].

However, the powder forms of the perovskites can bring some drawbacks such as agglomeration and difficulty in separation which strongly restricts their catalytic activities as well as industrial utilizations. In addition, the bulk perovskites show relatively low surface areas, limiting their interaction with the target molecules. To address these problems, the usage of supporting materials for perovskite oxides has been concerned as an effective strategy. The selection of support is essential as the physicochemical features and catalytic activities of the photocatalysts are closely associated with the type and nature of the matrix. For example, Wu et al. [5] investigated the effect of various supports (Al_2O_3 , TiO_2 , CeO_2 , and SiO_2) for the LaFeO_3 particles and applied for the degradation of Acid Orange 7. Authors stated that the perovskite supported on Al_2O_3 exhibited the highest catalytic activity ascribed to its large surface area, oxygen vacancies, suitable redox property, and fast electron mobility. Li et al. [6] tested different mesoporous silica supports for LaFeO_3 for the catalytic oxidation of rhodamine B and concluded as the roles of the support were absorbing dye molecules from solution to the pores (i) and then transferring them from the pores to the active site (ii). Alpay et al. [7] demonstrated that the commercial polystyrene based resin (DiaionTM HP21) served as a well matrix for the deposition of LaFeO_3 perovskites and the composite catalyst displayed improved visible light absorption as well as high photocatalytic, degradation activity towards many dyes and antibiotics.

Porous polymeric materials with tunable pore size and controllable morphology have been effectively used as matrices for the deposition of fine particles [8, 9]. It is well known that the styrene-divinylbenzene co-polymers are mechanically and chemically stable as well as they have high adsorption abilities towards many organics [10, 11]. Also, their distinct features of including abundant surface functional groups enable them to be applied as efficient adsorbents for binding organic molecules [12]. Besides, the sulphonated aromatic polymers have higher ion exchange capacity and water absorption features, and they can be effectively utilized in wastewater treatment owing to their abundant sulphonic acid groups [13, 14]. The cross-linked polystyrene co-divinyl benzene has many phenyl rings which can be easily functionalized with sulfonated groups [15]. Therefore, it was hypothesized that the sulfonated styrene-divinylbenzene co-polymers can be a good candidate for the adsorption of the organics and can serve as a matrix for the immobilization of perovskite particles.

Inspired by these perspectives, in this work, BiFeO_3 perovskite particles were immobilized over the co-polymer surface through wet impregnation method. To the best of our knowledge, there has been no study reported yet about deposition of BiFeO_3 particles over polymeric substances which might be ideal support for powdered photocatalysts. The as-prepared heterostructure catalyst was applied to the photocatalytic degradation of tetracycline antibiotic under visible light illumination. The enhancement of the photocatalytic activity was attributed to the synergistic effect of adsorption and photocatalysis. In addition, the loading amount of BiFeO_3 over the resin was investigated. Besides, the photoactivity was tested towards another pharmaceutical namely isoniazid which is known as a persistent drug. We report for the first time on the facile fabrication of co-polymer supported BiFeO_3 perovskites, integrating both adsorption and photodegradation to simultaneously improve elimination of pharmaceuticals from water media.

MATERIALS AND METHODS

Materials

Bismuth (III) nitrate pentahydrate ($\text{Bi}(\text{NO}_3)_3 \cdot 5\text{H}_2\text{O}$, 98%) and iron (III) chloride ($\text{FeCl}_3 \cdot 6\text{H}_2\text{O}$, 99%) were purchased from Sigma-Aldrich and Lab-Scan Analytical Sciences, respectively. Styrene (Fluka), divinyl benzene (Aldrich), chlorosulfonic acid (99%, Fluka) were purified before use. All other chemicals used in the studies were of analytical reagent grade.

Preparation of Raw BiFeO_3 Perovskite

Perovskite type BiFeO_3 particles were prepared by using precipitation method. First, defined amount of $\text{Bi}(\text{NO}_3)_3 \cdot 5\text{H}_2\text{O}$ was dissolved in 2.5 M HNO_3 solution. Meanwhile, equal molar amount of $\text{FeCl}_3 \cdot 6\text{H}_2\text{O}$ was prepared in deionized water. Then, both solutions were mixed and magnetically stirred for 30 min. The solution pH was adjusted to 10 by adding NaOH (6 M) and kept stirring for 24 h at room temperature. At the end of the period, the precipitate was filtered and dried 90 °C for 4 h. Finally, the powder was calcined at 600 °C for 3 h. Final product was coded as BFO.

Preparation of co-Polymer

Styrene-divinyl benzene (STR/DVB) co-polymer beads were synthesized with 50% of cross-linking divinyl benzene. In a typical synthesis, styrene and divinyl benzene were first dissolved in toluene. Alumina and gum arabic emulsifier were prepared in a three-necked round-bottomed flask under nitrogen gas. Then, the mixture of styrene-divinyl benzene was added to the above solution. The polymerization reaction was allowed to continue for 4 h under continuous stirring at 75 °C. The obtained seeds were washed with excess water and dried at 60 °C for overnight. The sulphonation procedure was followed according to the

procedure described in the literature [16]. 10 mL of chlorosulfonic acid was poured into a solution of formamide under constant stirring at 0 °C and the cross-linked polymer beads (2 g) was added to the mixture and kept stirred under reflux conditions for 5 h. The resultant resins were filtered and washed with cold water and acetone. The final seeds were labelled as co-STR/DVB.

Immobilization of BiFeO₃ Over co-Polymer Structure

The immobilizing of BiFeO₃ particles on co-STR/DVB structure was performed via impregnation method. Briefly, 5 mg BFO particles mixed with 50 mg of co-STR/DVB seeds (0.2 g). The suspension was mixed at orbital shaker for 48 h. Then, the brown seeds were collected, washed with de-ionized water and subsequently dried at 60 °C overnight. The product was coded as BFO@co-STR/DVB (1:10). In order to examine effect of perovskite ratio, the amount of BFO particles were changed as 10 and 25 mg; the resultant samples were coded as BFO@co-STR/DVB (2:10) and BFO@co-STR/DVB (5:10), respectively.

Characterization Tests

The surface morphology and elemental analysis were investigated by scanning electron microscopy (FEI Inc., Inspect S50 SEM, EDAX Octane Prime). The Fourier transfer infrared (FTIR) spectra were obtained on Perkin Elmer Spectrum One using attenuated total reflectance method. X-ray powder diffraction (XRD) data were collected using CuK α radiation (Panalytical X'Pert PRO Model).

Adsorption and Photocatalytic Degradation Studies

In order to examine the adsorptive removal of TC-HCl over co-STR/DVB seeds, the adsorption kinetic tests were performed with initial concentration of 10 mg/L at 298 K and pH 6.5. Photocatalytic decomposition of tetracycline (TC-HCl) was investigated under visible light irradiation by using a square-shaped photochemical reactor coupled with two visible metal halide lamps (λ : 400–800 nm). The fan at the bottom of the system was used to decrease the temperature to ambient conditions. For each test, 0.01 g of catalyst was dispersed with 50 mL TC-HCl solution with an initial concentration of 10 mg/L. After 30 min of dark adsorption period, the mixture was exposed to light, and aliquots were taken at time intervals. The residual TC-HCl concentration was analyzed by UV-vis spectrophotometer at the wavelength of 360 nm. The degradation efficiency was calculated by Eq.(1):

$$\text{Degradation\%} = \left[\frac{(C_0 - C)}{C_0} \right] \times 100 \quad (1)$$

In order to examine the photocatalytic performance of the as-synthesized catalyst towards different pharmaceutical, the degradation of isoniazid was also investigated under similar conditions and the equilibrium isoniazid concentration was determined by UV-Vis spectrophotometer at 262 nm.

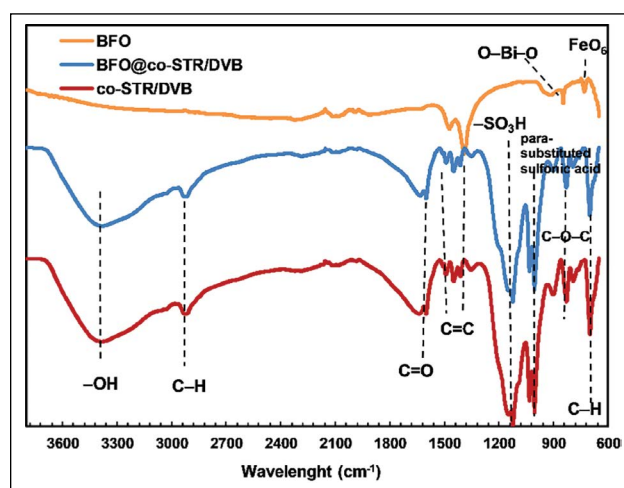


Figure 1. FTIR spectra of BFO, BFO@co-STR/DVB and co-STR/DVB samples.

RESULTS AND DISCUSSION

Characterization

In order to examine the surface functional groups after immobilization, FTIR spectra of BFO, BFO@co-STR/DVB and co-STR/DVB samples were obtained, and the results were shown in Figure 1. In the spectrum of bare BFO perovskite, the presence of nitrate ions was observed at nearly 1450 cm⁻¹ [17] while the absorption bands at 800–900 cm⁻¹ were assigned to the symmetric stretching vibrations of O–Bi–O in the BiFeO₃ structure [18]. The FTIR spectra of as-synthesized co-polymers confirmed the presence of aromatic ring features of skeletal C=O and C=C in plate-stretching vibrations at 1601 and 1450 cm⁻¹, respectively. The peak at 701 cm⁻¹ was assigned to the bending vibration of the substituted benzene ring (C–H) [19]. The sulfonation was verified from the peaks in the range of 1000–1130 cm⁻¹. The band at 1126 cm⁻¹ was ascribed to the presence of -SO₃H groups while the band at 1006 cm⁻¹ indicated the vibrations of the aromatic ring released from the para-substituted sulfonic acid [19, 20]. The O–H stretching vibration of water was observed at about 2900–3400 cm⁻¹. The peaks at 700 and 831 cm⁻¹ were assigned to the aromatic ring C–H bend and stretching vibration of C–O–C bonds, respectively. After immobilization of BiFeO₃ particles on co-STR/DVB surface, the peak intensities slightly decreased but the characteristic peaks were still observed confirming that the incorporation of perovskites did not alter the functional groups of bare co-STR/DVB.

X-ray diffraction (XRD) was employed to detect the crystallinity of bare BiFeO₃ perovskite. As shown in Figure 2b, the diffraction peak was well indexed to the standard XRD data of rhombohedral BiFeO₃ (JSPDS file No. 86-1518), indicating successful synthesis of crystal perovskite. Regarding the peak intensities, the sharp peaks at $2\theta=23.2, 30.2, 32.2, 40.9, 45.0, 50.0, 51.0, 54.2, 55.0$ and 67.3° were related

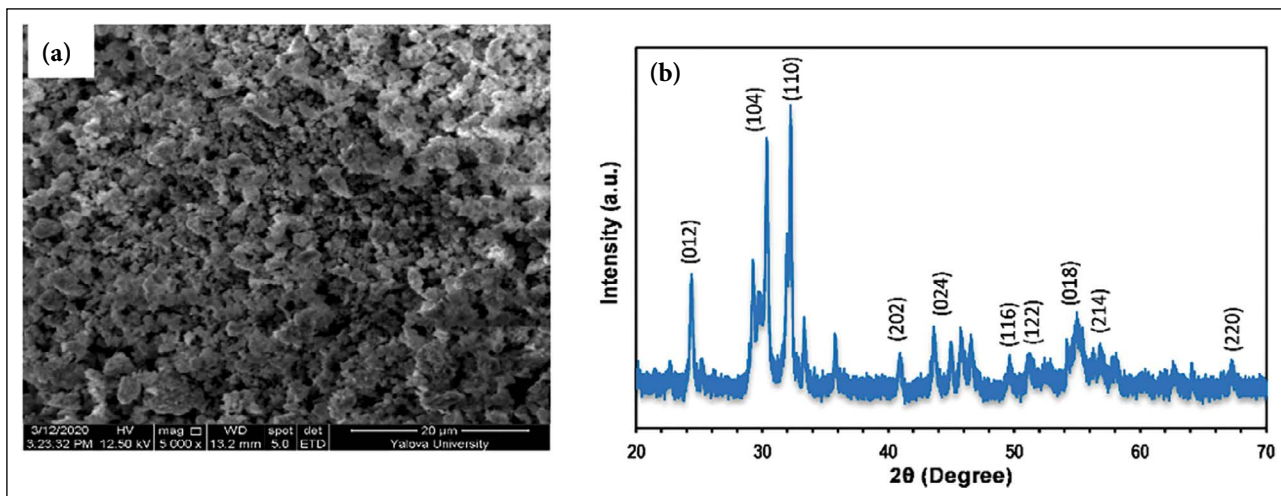


Figure 2. (a) SEM image (a) and XRD spectrum of raw BFO.

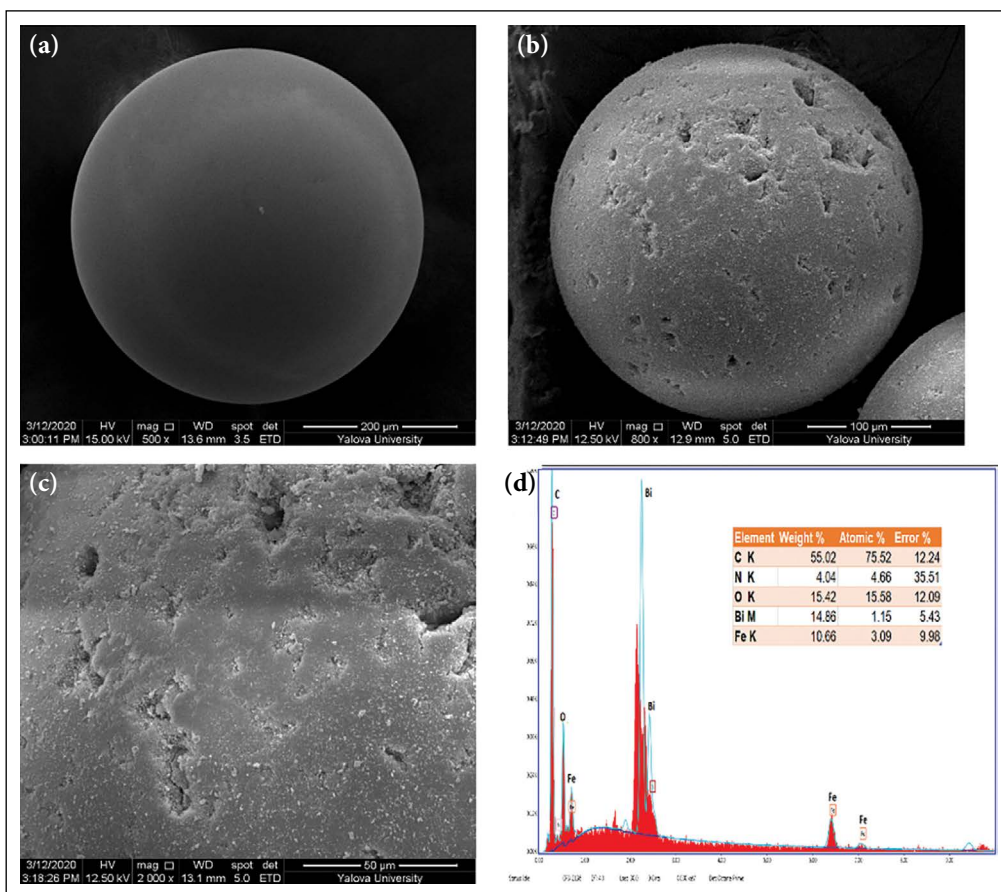


Figure 3. SEM images of raw co-STR/DVB (a), BFO@co-STR/DVB (b, c) and EDS spectrum of BFO@co-STR/DVB composite catalyst.

to their Miller indices (0 1 2), (1 0 4), (1 1 0), (2 0 2), (0 2 4), (1 1 6), (1 2 2), (0 1 8), (2 1 4), (2 2 0), respectively.

Scanning electron microscope (SEM) images of bare BFO, co-STR/DVB and BFO@co-STR/DVB catalysts were presented in Figure 2a, Figure 3. It could be seen that bare BFO

perovskite exhibited irregular polyhedral structure which was in accordance with previous studies [21]. The raw co-STR/DVB sample indicated smooth spherical shape (Fig. 3a) enabling active surface sites to promote the adsorption and degradation towards the tetracycline molecule. After

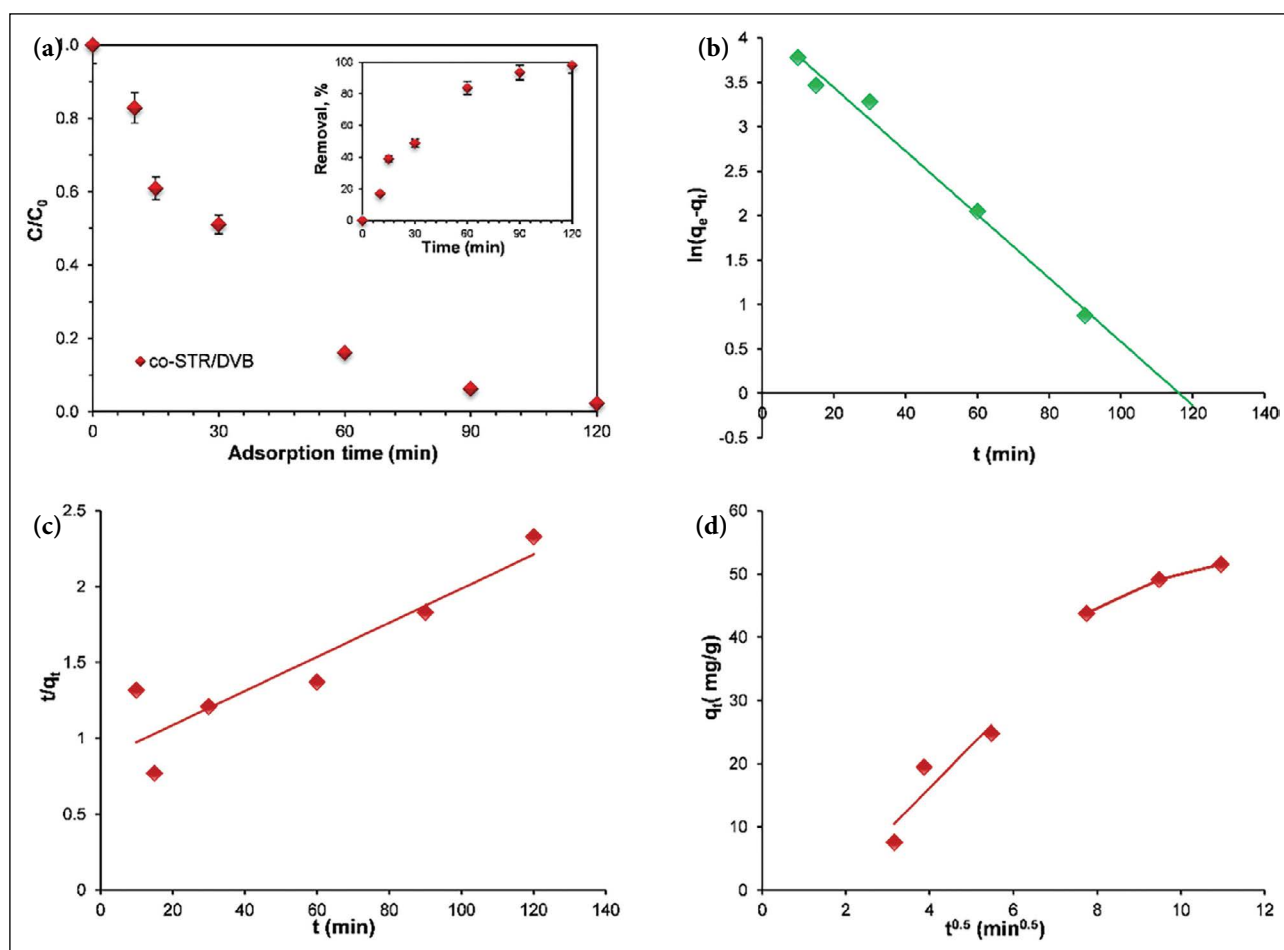


Figure 4. (a) TC-HCl adsorption kinetics, Pseudo-first order (b), Pseudo-second order (c) and Intra-particle diffusion kinetic modelling over co-STR/DVB.

immobilization of BiFeO_3 perovskites over the co-polymer structure, the spherical shapes morphology of the polymer was not altered (Fig. 3b, c). It was clearly observed that the surface was fully covered with BiFeO_3 perovskite particles. The particle diameter of the heterostructured catalyst was nearly 100 μm , which was decreased from 200 μm revealing that the impregnation route might impact the particle size of the polymer seeds. The EDX elemental distribution demonstrated the presence of Bi, Fe, O, C and N elements in the composite catalyst verifying effective immobilization of BNQDs into the perovskite framework. The weight ratio of Bi, Fe and O elements were estimated as 14.8%, 10.6% and 15.4%, respectively.

Adsorption Kinetics Over co-STR-DVB

The kinetics of adsorption over co-STR/DVB seeds were studied to ensure the required time for equilibrium as well as to find the rate limiting steps of the process. As seen in Figure 4a, at the end of 90 and 120 min, the TC-HCl removal percentages of raw co-STR/DVB were achieved as 93% and 98%, respectively. This robust interaction could

be attributed to the predominant π - π stacking or hydrophobic relationship between tetracycline and the co-polymeric structure [11]. The adsorption kinetic data were applied to three kinetic models namely, pseudo-first order, pseudo-second order and Weber-Morris intra-particle diffusion. Table 1 shows the kinetic model parameters with their related correlation coefficients (R^2).

The pseudo-first-order kinetic equation is based on the surface physisorption mechanism, and it is defined as:

$$\log(q_e - q_t) = \log q_e - \left(\frac{k_1}{2.303}\right)t \quad (2)$$

where q_e and q_t are the amounts of adsorbed TC-HCl (mg/g) at equilibrium and at time t (min), respectively, and k_1 is the rate constant of pseudo-first-order model (min^{-1}) which was determined from the plots of $\log(q_e - q_t)$ vs. time (Fig. 4b). From Table 1, the correlation coefficients (R^2) for the pseudo-first model were found slightly lower indicating the model is not fitted well the adsorption kinetics of TC-HCl over co-STR/DVB seeds, revealing physical forces were not involved in the adsorption process.

Table 1. Adsorption kinetic model constants of co-STR/DVB

q_e (mg/g)	78.54
Pseudo-first order	
q_e (mg/g)	64.01
k_1 (min^{-1})	0.082
R^2	0.988
Pseudo-second order	
q_e (mg/g)	88.92
k_2 (g/mg min)	0.00014
h (mg/g min)	1.160
R^2	0.993
Weber–Morris intra-particle diffusion	
k_{id-1} ($\text{mg/g min}^{0.5}$)	6.749
R^2	0.822
k_{id-2} ($\text{mg/g min}^{0.5}$)	2.434
R^2	0.972

The pseudo-second-order kinetic model is generally utilized to explain the adsorption mechanisms driven by surface chemisorption process and the model is shown as Eq. (3):

$$\frac{t}{q_t} = \frac{1}{k_2 q_e^2} + \frac{1}{q_e} \quad (3)$$

where k_2 is the second-order rate constant (g/mg min). The k_2 and q_e values are evaluated from the intercept and the slope of the plot t/q_t versus t . Initial adsorption rate (h , mg/g min) is calculated from Eq. (4):

$$h = k_2 q_e^2 \quad (4)$$

According to the obtained R^2 value and second order rate constant, the second-order model displayed high correlation coefficients ($R^2=0.993$) for of TC-HCl adsorption over co-STR/DVB sample (Fig. 4c). Moreover, the theoretical and experimental adsorption capacities of the pseudo-second-order model were found nearly identical, indicating that this model was more proper for describing that the TC-HCl adsorption was mainly occurred through on π - π stacking interactions. Similar observation was reported by Yang et al. [22] and they underlined the fact that electrostatic interactions played minor role in the tetracycline adsorption.

The intra-particle diffusion model was also applied to determine the rate determining step. The model is shown as:

$$q_t = k_{id} t^{0.5} + C \quad (5)$$

where q_t is the amount of adsorbed TC-HCl at the time (mg/g); k_{id} ($\text{mg/g min}^{0.5}$) is the Weber-Morris intra-particle-diffusion rate constant; t is the time (t); C is intercept (mg/g). The intra-particle-diffusion model parameters including k_{id-1} , k_{id-2} and R^2 were listed in Table 1, and the plots were shown in Figure 4d. The plot of this model exhibited two linearity, verifying the existence of two adsorption

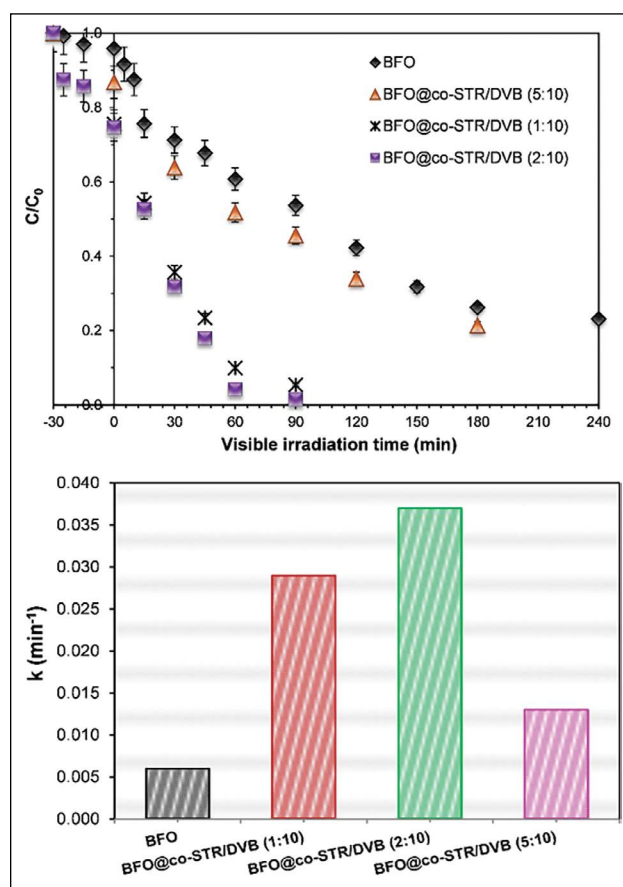


Figure 5. Photocatalytic degradation curves and related kinetic constants of BFO and BFO@co-STR/DVB catalysts.

states (phase I-fast adsorption and phase II-slow adsorption) of mass transfer. The first linearity is related with macropore/mesopore diffusion while the second line deals with the micropore diffusion [23]. In the first step, approximately 48% TC-HCl was removed by co-STR/DVB within 30 min which was attributed to the fast utilization of the most active adsorptive areas on the co-polymer surface. Then, 83% of TC-HCl was eliminated within 60 min. The kinetic rate constant of first step ($k_{id-1}=6.749 \text{ mg/g min}^{0.5}$) was found much higher than the second step of adsorption ($k_{id-2}=2.434 \text{ mg/g min}^{0.5}$). Furthermore, R^2 values of the phase I were higher than the phase II suggesting that the external mass transfer could be the rate-limiting step in the adsorption process.

Photocatalytic Performance Tests of BFO@co-STR/DVB Heterostructure Catalyst

The photocatalytic activities of the BFO@co-STR/DVB heterostructured catalysts were evaluated towards tetracycline degradation from 50 mL of 10 mg/L aqueous solution. Figure 5 revealed the TC-HCL elimination over the photocatalysts, in which the degradation degree of bare BFO was found low (76.9%) even after 240 min of visible irra-

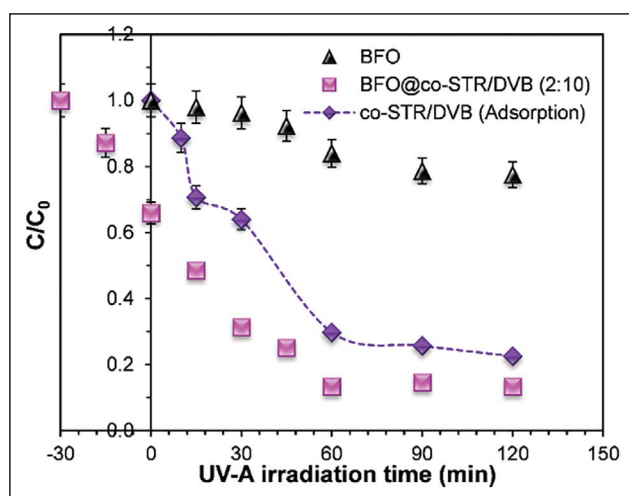


Figure 6. Photocatalytic degradation and adsorption curves of towards isoniazid molecule.

diation. This could be owing to its limited light absorption and high recombination of electrons and holes. Moreover, the photodegradation rates over the BFO@co-STR/DVB catalysts increased for the increasing BiFeO₃: co-STR/DVB ratios of (1:10) and (2:10). Notably, the BFO@co-STR/DVB (2:10) photocatalyst displayed the highest catalytic efficiency as 98.5% while that of for BFO@co-STR/DVB (1:10) was determined as 94.5% at the end of 90 min of irradiation. However, the increasing perovskite content over the heterostructure led to decrease in the removal efficiency and 78.6% photodegradation was calculated for BFO@co-STR/DVB (5:10) catalyst. This could be explained as the increment of the perovskite particles on the surface significantly inhibited the interaction and adsorption of target antibiotic molecules with the co-polymer surface, resulting decrease in the adsorption performance. To confirm this theory, the adsorption performances were also compared. At the end of dark period of 30 min, 24.4%, 25.3% and 13.2% adsorptive removal percentages were observed for BFO@co-STR/DVB (1:10), (2:10) and (5:10) catalysts, respectively, verifying the fact that the interaction of antibiotic molecules was restricted by increased BiFeO₃ particles on the co-polymer surface. Similar phenomenon was observed by Phan et al. [24] who deposited LaFeO₃ particles on acid-modified natural zeolite for the Rhodamine B degradation.

To further elucidate the photodegradation efficiency of the composite catalysts, the degradation kinetic data were applied to the pseudo-first order kinetic equation $\ln(C/C_0) = -k_{app} \cdot t$, where k_{app} shows the apparent first-order reaction rate constant (Fig. 5). The photodegradation performances of the as-prepared samples were quantitatively compared according to the k_{app} values. It was observed that the BFO@co-STR/DVB (2:10) catalyst had the greatest value of k_{app} (0.037 min⁻¹); in contrast, the rate constants for bare BiFeO₃ was calculated as 0.006

min⁻¹, implying that the photodegradation activity of the heterostructured catalyst was 6.16 times higher than that for bare BiFeO₃, demonstrating that the as-prepared heterostructure can be effectively used as a high-efficiency photocatalyst for antibiotic elimination.

Investigation of Photocatalytic Activity Towards Different Pharmaceutical: Isoniazid Degradation

The synergetic adsorption and photocatalytic removal efficiency of the as-prepared composite catalyst was investigated towards another pharmaceutical isoniazid (C₆H₇N₃O) which is often used as a first-line drug in the prevention and treatment of tuberculosis disease [25]. In literature, few studies showed that this persistent drug could be degraded by using TiO₂, ZnO, Bi₂O₃ type catalysts under light illumination [26]. Therefore, it is essential to examine the removal of these kinds of pharmaceuticals from aqueous media. In this work, the adsorptive removal of isoniazid by the raw co-polymer seeds was also examined under dark conditions. According to the obtained results shown in Figure 6, the adsorptive removal of isoniazid over the co-STR/DVB polymer was calculated as 80.0% at the of 120 min. The high adsorptive behavior could be related with the interaction of carbonyl groups of isoniazid molecule with the sulfonated aromatic co-polymer structure. It was reported that the hydrogen bonding interactions through the ring nitrogen, the amino nitrogen, and the carbonyl oxygen groups of isoniazid played a dominant role in its adsorption mechanism [27]. Moreover, the isoniazid molecule might be adsorbed on co-STR/DVB through π - π stacking effects. On the other hand, raw BFO perovskite showed low degradation efficiency towards isoniazid molecule and only 26% degradation was occurred after 120 min of UV-A light irradiation. Interestingly, the BFO@co-STR/DVB (2:10) catalyst exhibited relatively higher removal rate as 98.2% thanks to the synergetic effect of adsorption and photocatalysis.

Cost Estimation of TC Removal in BFO@co-STR/DVB Photocatalytic System

Since cost of the wastewater treatment is a significant factor for photocatalytic and adsorption processes, an economic estimation of applied BFO@co-STR/DVB catalytic system was developed for the tetracycline elimination by considering industrial grade prices of reagents used in the preparation of photocatalyst. The optimum degradation percentage as 98% over BFO@co-STR/DVB was selected with the volume of 50 mL. Table 2 represents the total cost of the reagent consumptions of BFO@co-STR/DVB system which was calculated as \$12.87/m³. The cost of the wastewater treatment in this system was calculated much lower than treatment of pharmaceutical wastewater with Fe-TiO₂ system (\$71/m³) [28] and caffeine degradation with fenton oxidation process on zeolite supported iron particles (\$23.2m³) [29].

Table 2. Cost of wastewater treatment per cubic water with BFO@co-STR/DVB system

	Quantity consumed for 1 m ³ (kg/m ³)	Unit cost (\$/kg)	Total cost (\$/m ³)
Bi(NO ₃) ₃ ·5H ₂ O	0.22	35	7.7
FeCl ₃ ·6H ₂ O	0.154	20	3.08
NaOH	2.64	0.15	0.39
co-STR/DVB	0.17	10	1.7
Total	12.87		

CONCLUSION

In this study, perovskite type BiFeO₃ particles were successfully immobilized over copolymer styrene-divinyl benzene surface through simple impregnation method. SEM images with EDX spectrum demonstrated the presence of BiFeO₃ particles on the copolymer surface. FTIR analysis indicated that the deposition did not alter the surface functional groups of co-polymer network. The adsorption abilities of the raw co-polymer were investigated in dark conditions by performing kinetic tests and the results revealed that the robust adsorption occurred between the antibiotic and functional groups of co-STR/DVB structure. The as-prepared composite catalyst showed outstanding removal performance towards tetracycline molecule via synergetic effect of adsorption and photocatalysis. The increasing perovskite ratio on the polymer first increased the removal rate while after certain amount the removal was decreased due to the hindered interaction and adsorption of antibiotic molecules with the co-polymer surface. The composite catalyst was also utilized in another pharmaceutical namely isoniazid and effective adsorptive and photocatalytic behavior was assigned to the mutual effect of carbonyl groups of isoniazid molecule with the sulfonated aromatic co-polymer. This study showed efficient utilization of highly adsorptive co-polymer structure in heterogeneous catalytic processes.

DATA AVAILABILITY STATEMENT

The authors confirm that the data that supports the findings of this study are available within the article. Raw data that support the finding of this study are available from the corresponding author, upon reasonable request.

CONFLICT OF INTEREST

The authors declared no potential conflicts of interest with respect to the research, authorship, and/or publication of this article.

ETHICS

There are no ethical issues with the publication of this manuscript.

REFERENCES

- [1] V. Dutta, S. Sharma, P. Raizada, A. Hosseini-Bandegharai, J. Kaushal, and P. Singh, "Fabrication of visible light active BiFeO₃/CuS/SiO₂ Z-scheme photocatalyst for efficient dye degradation," *Materials Letters*, Vol. 270, pp. 2–5, 2020. [\[CrossRef\]](#)
- [2] J. Ćirković, A. Radojković, D. Luković Golić, N. Tasić, M. Čizmić, G. Branković, and Z. Branković, "Visible-light photocatalytic degradation of Mordant Blue 9 by single-phase BiFeO₃ nanoparticles," *Journal of Environmental Chemical Engineering*, Article 104587, 2020. [\[CrossRef\]](#)
- [3] C. Ponraj, G. Vinitha, and J. Daniel, "A review on the visible light active BiFeO₃ nanostructures as suitable photocatalyst in the degradation of different textile dyes," *Environmental Nanotechnology, Monitoring & Management*, Vol. 7, pp. 110–120, 2017. [\[CrossRef\]](#)
- [4] H. Iboukhoulef, R. Douani, A. Amrane, A. Chaouchi, and A. Elias, "Heterogeneous Fenton like degradation of olive Mill wastewater using ozone in the presence of BiFeO₃ photocatalyst," *Journal of Photochemistry and Photobiology A: Chemistry*, Vol. 383, Article 112012, 2019. [\[CrossRef\]](#)
- [5] S. Wu, Y. Lin, C. Yang, C. Du, Q. Teng, Y. Ma, D. Zhang, L. Nie, and Y. Zhong, Enhanced activation of peroxymonosulfate by LaFeO₃ perovskite supported on Al₂O₃ for degradation of organic pollutants. *Chemosphere* Vol. 237, Article 124478, 2019. [\[CrossRef\]](#)
- [6] H. Li, J. Zhu, P. Xiao, Y. Zhan, K. Lv, L. Wu, and M. Li, "On the mechanism of oxidative degradation of rhodamine B over LaFeO₃ catalysts supported on silica materials: Role of support," *Microporous and Mesoporous Materials*, Vol. 221, pp. 159–166, 2015. [\[CrossRef\]](#)
- [7] A. Alpay, Ö. Tuna, and E.B. Simsek, "Deposition of perovskite-type LaFeO₃ particles on spherical commercial polystyrene resin: A new platform for enhanced photo-Fenton-catalyzed degradation and simultaneous wastewater purification," *Environmental Technology Innovation*, Vol. 20, pp. 101175, 2020. [\[CrossRef\]](#)
- [8] O. Suarez, J.J. Olaya, and S.E. Rodil, "Structural and electrochemical characterization of sulfonated styrene-divinyl benzene/Bismuth-Tin electrodes," *Colloids and Surfaces A: Physicochemical and Engineering Aspects*, Vol. 627, Article 126975. [\[CrossRef\]](#)
- [9] A. Gouthaman, R.S. Azarudeen, A. Gnanaprakasam, V.M. Sivakumar, and M. Thirumarimurugan, "Polymeric nanocomposites for the removal of Acid red 52 dye from aqueous solutions: Synthesis, characterization, kinetic and isotherm studies," *Ecotoxicology and Environmental Safety*, Vol. 160, pp. 42–51, 2018. [\[CrossRef\]](#)

- [10] L. Mohammadi, A. Rahdar, R. Khaksefidi, A. Ghamkhari, G. Fytianos, and G. Z. Kyzas, "Polystyrene magnetic nanocomposites as antibiotic adsorbents," Vol. 12, pp. 1313, 2020. [\[CrossRef\]](#)
- [11] M. Akbulut Söylemez, and B.Ö. Kemaloğulları, "Surface modification of magnetic nanoparticles via admicellar polymerization for selective removal of tetracycline from real water samples, New Journal of Chemistry, Vol. 45, pp. 6415–6423, 2021. [\[CrossRef\]](#)
- [12] M. Qiao, M.M. Wang, M.L. Chen, and J.H. Wang, "A novel porous polymeric microsphere for the selective adsorption and isolation of conalbumin," Analytica Chimica Acta, Vol. 1148, Article 238176, 2021. [\[CrossRef\]](#)
- [13] P. Ergenekon, E. Gürbulak, and B. Keskinler, "Polyol derived sulfonated solvothermal carbon for efficient dye removal from aqueous solutions," Journal of Molecular Liquids, Vol. 50, pp. 16–21, 2011.
- [14] Y. Zhang, K. Chen, B. Gong, Y. Yin, S. Zhou, and K. Xiao, "Scalable synthesis of monodisperse and recyclable sulphonated polystyrene microspheres for sustainable elimination of heavy metals in wastewater," Environmental Technology (United Kingdom), pp. 1–13, 2021. [\[CrossRef\]](#)
- [15] E. Córdova-Mateo, O. Bertran, C.A. Ferreira, and C. Alemán, Transport of hydronium ions inside poly(styrene-co-divinyl benzene) cation exchange membranes, Journal of Membrane Science, Vol. 428, pp. 393–402, 2013.
- [16] T.A. Rauf, and T.S. Anirudhan, "Synthesis and characterization of sulphonic acid ligand immobilized Aminopropyl silanetriol copolymer and evaluation of its Bovine serum albumin adsorption efficiency," Materials Today: Proceedings, Vol. 41, pp. 728–735, 2020. [\[CrossRef\]](#)
- [17] L. Wang, J.B. Xu, B. Gao, A.M. Chang, J. Chen, L. Bian, and C.Y. Song, "Synthesis of BiFeO₃ nanoparticles by a low-heating temperature solid-state precursor method," Materials Research Bulletin, Vol. 48, pp. 383–388, 2013. [\[CrossRef\]](#)
- [18] N.S. Abdul Satar, R. Adnan, H.L. Lee, S.R. Hall, T. Kobayashi, M.H. Mohamad Kassim, and N.H. Mohd Kaus, "Facile green synthesis of yttrium-doped BiFeO₃ with highly efficient photocatalytic degradation towards methylene blue," Ceramics International, Vol. 45, pp. 15964–15973, 2019. [\[CrossRef\]](#)
- [19] M. Mahmoud Nasef, H. Saidi, and K.Z. Mohd Dahlan, "Kinetic investigations of graft copolymerization of sodium styrene sulfonate onto electron beam irradiated poly(vinylidene fluoride) films," Radiation Physics and Chemistry, Vol. 80, pp. 66–75, 2011. [\[CrossRef\]](#)
- [20] L. Melo, R. Benavides, G. Martínez, L. Da Silva, and M.M.S. Paula, "Degradation reactions during sulphonation of poly(styrene-co-acrylic acid) used as membranes," Polymer Degradation Stability, Vol. 109, pp. 343–352, 2014. [\[CrossRef\]](#)
- [21] Z. Balta, E.B. and Simsek, "Uncovering the systematical charge separation effect of boron nitride quantum dots on photocatalytic performance of BiFeO₃ perovskite towards degradation of tetracycline antibiotic," Journal of Environmental Chemical Engineering, Vol. 9, Article 106567, 2021. [\[CrossRef\]](#)
- [22] J. Yang, L. Han, W. Yang, Q. Liu, Z. Fei, X. Chen, Z. Zhang, J. Tang, M. Cui, X. Qiao, "In situ synthetic hierarchical porous MIL-53(Cr) as an efficient adsorbent for mesopores-controlled adsorption of tetracycline," Microporous and Mesoporous Materials, Vol. 332, Article 111667, 2022. [\[CrossRef\]](#)
- [23] M. Sharma, J. Singh, S. Hazra, and S. Basu, Adsorption of heavy metal ions by mesoporous ZnO and TiO₂@ZnO monoliths: Adsorption and kinetic studies, Microchemical Journal, Vol. 145, pp. 105–112, 2019. [\[CrossRef\]](#)
- [24] T.T.N. Phan, A.N. Nikoloski, P.A. Bahri, and D. Li, "Enhanced removal of organic using LaFeO₃-integrated modified natural zeolites via heterogeneous visible light photo-Fenton degradation," Journal of Environmental Management, Vol. 233, pp. 471–480, 2019. [\[CrossRef\]](#)
- [25] E. Carazo, A. Borrego-Sánchez, F. García-Villén, R. Sánchez-Espejo, C. Viseras, P. Cerezo, and C. Aguzzi, "Adsorption and characterization of palygorskite-isoniazid nanohybrids," Applied Clay Science, Vol. 160, pp. 180–185, 2018. [\[CrossRef\]](#)
- [26] R.R.S. Coronado-Castañeda, M.L. Maya-Treviño, E. Garza-González, J. Peral, M. Villanueva-Rodríguez, and A. Hernández-Ramírez, "Photocatalytic degradation and toxicity reduction of isoniazid using β -Bi₂O₃ in real wastewater," Catal Today, vol. 341, pp. 82–89, 2020. [\[CrossRef\]](#)
- [27] S. Akyuz, T. Akyuz, and E. Akalin, "Adsorption of isoniazid onto sepiolite-palygorskite group of clays: An IR study," Spectrochimica Acta Part A-molecular and Biomolecular Spectroscopy, Vol. 75, pp. 1304–1307, 2010. [\[CrossRef\]](#)
- [28] P. Bansal, A. Verma, and S. Talwar, "Detoxification of real pharmaceutical wastewater by integrating photocatalysis and photo-Fenton in fixed-mode," Chemical Engineering Journal, Vol. 349, pp. 838–848, 2018. [\[CrossRef\]](#)
- [29] M. Anis, and S. Haydar, "Heterogeneous fenton oxidation of caffeine using zeolite-supported iron nanoparticles," Arabian Journal for Science and Engineering, Vol. 44, pp. 315–328, 2019. [\[CrossRef\]](#)



Research Article

Degree of Pb stabilization in MSWI fly ash using size-fractionated natural fishbone hydroxyapatite

Mitali NAG^{*}, Amirhomayoun SAFFARZADEH, Takayuki SHIMAOKA, Hirofumi NAKAYAMA

Department of Urban and Environmental Engineering, Faculty of Engineering, Kyushu University, Fukuoka, Japan

ARTICLE INFO

Article history

Received: 25 September 2021

Revised: 13 February 2022

Accepted: 09 March 2022

Key words:

Fishbone hydroxyapatite;
Fly ash; Heavy metal;
Size-fractionation; Stabilization

ABSTRACT

Incineration is a common technique worldwide for treating Municipal Solid Waste (MSW). However, incineration residues (e.g., bottom and fly ash) require special treatment to prevent environmental risks due to the high content of heavy metals. The present study evaluated the stabilization degree of Pb, a toxic heavy metal in MSW incineration fly ash (IFA) treating by size-fractionated natural fishbone (FB) hydroxyapatite (HA). Bones from various fish species were used at different size fractions (<600 µm, 600 µm–2 mm, and 0–2 mm). The effect of different fishbone hydroxyapatite (FB-HA) sizes was studied by batch tests under the FB/IFA ratios of 0.0 and 1:10 (wt.), the contact or settling time of 6, 12, 24, and 672 hours, and the fixed W/S ratio of 1.5 mL/g. Using only 10% FB, Pb stabilization efficiency after 672 hours obtained 95.55% and 94.24% for FB sizes <600 µm and 600 µm–2 mm, respectively, and about 86.1% for non-fractionated FB (0–2 mm). The results indicated that contact time was the most critical factor for enhanced Pb stabilization. The FB particle size of 0–2 mm was deemed appropriate for Pb immobilization in short and long time settling periods. The adsorption isotherms were fitted well with the Langmuir and Freundlich models. The R_L values of the Langmuir model were less than one and the n values of the Freundlich isotherm lie between 3 and 5, conferring the favorable adsorption of Pb to FB-HA for all size fractions.

Cite this article as: Nag M, Saffarzadeh A, Shimaoka T, Nakayama H. Degree of Pb stabilization in MSWI fly ash using size-fractionated natural fishbone hydroxyapatite. Environ Res Tec 2022;5:2:137–147.

INTRODUCTION

Incineration is a common technique worldwide for treating municipal solid waste (MSW), because it shrinks the volume and weight of waste by about 90% and 70%, respectively [1]. In Japan, the solid waste incineration percentage was almost 75% in 2013 [2]. However, producing markedly huge amounts of solid remnants (e.g., bottom ash and fly ash) is one of the limitations of incineration technology.

Furthermore, because of the high content of heavy metals (Zn, Pb, Cd, Cu, Cr, Sb, etc.), chlorine, soluble salts, organic compounds, and particles fineness, the incineration fly ash (IFA) is classified as a hazardous waste [3]. Therefore, IFA requires appropriate treatment to prevent environmental risks before utilization or landfilling [4]. MSWI fly ash is treated through various methods, such as chemical stabilization by reagents (i.e., chelate compounds), cement or geopolymer solidification, advanced separation, thermal

*Corresponding author.

*E-mail address: nag-m@doc.kyushu-u.ac.jp



treatment via melting, treatment by synthetic phosphate (phosphoric acid), and hydrothermal techniques [5, 6].

Soluble phosphate has been widely used as a chemical treatment to convert heavy metals into insoluble compounds. Usually, phosphoric acid, potassium phosphates, sodium, and ammonium react with multivalent cations to comprise insoluble orthophosphates [7]. An insoluble metal phosphate produced through the reaction between soluble phosphate and the metal ions resembles a naturally growing mineral, which is geologically stable. In addition, various hydrogen and dihydrogen phosphates have also been explored for removing soluble heavy metals from toxic environments [7].

One of the typical examples of lead phosphate with a very low solubility ($K_{sp}=5\times 10^{-119}$) in a wide pH range, is pyromorphite, $Pb_5(PO_4)_3Cl$ [8]. Another frequently used phosphate is the apatite family, with hydroxyapatite (HA), which forms the principal member $[Ca_{10}(PO_4)_6(OH)_2]$ of a large category of substituted compounds with resembling compositions. Solid compounds may be formed with an extensive range of divalent or trivalent metals substituting fluorine, calcium or chlorine for hydroxyl ions, carbonates, vanadates, or arsenates found in place of phosphate [7].

Fishbones and mammal's skeletons contain calcium phosphate that highly resembles to HA. HA, such as synthetic HA, bones, and bone char have been explored for their high absorption capacity for removing heavy metals from aqueous solutions [9]. Therefore, HA can also be effectively used for the stabilization of heavy metals in contaminated waste materials. Compared to other phosphate sources, biogenic apatite (e.g., fishbones) has less initial contamination with heavy metals than processed or mined phosphate rocks and fertilizers. In addition, its high solubility allows it to trap metals easily and release phosphate slowly, thus allowing for long-term stabilization [10]. Many studies have been performed on the efficiency of phosphates and particularly apatites $[M_{10}(PO_4)_6(OH)_2]$, M: Metal], and the mechanisms involved in immobilizing heavy metals in contaminated soil, wastewater, groundwater, and dredged sludge [7, 11, 12].

Phosphation or phosphate treatment is also a promising remediation technique applied to IFA, BA and scrubber residues for heavy metal stabilization [13]. Assessing the effects of the fishbone (a natural phosphate) on heavy metal stabilization in MSW IFA is one of the principal objectives of the present study. Previous researches [14–16] have shown that the fishbone hydroxyapatite (FB-HA) is an effective stabilizer of heavy metals in IFA by considering various parameters such as modified fishbone, varied fishbone species, reaction time, fishbone dosage, and W/S ratio. In this study, size-fractionated natural FB-HA was used to enhance the degree of Pb stabilization in IFA. Therefore, three different sizes of FB-HA were used, and the effect of each size on Pb stabilization was investigated. The mechanism of Pb adsorption by FB-

HA and relevant adsorption isotherms were also studied. FB-HA can help reduce the need for disposal of fishbone waste, increase its recycling, reduce secondary contamination, and provide a low-cost and environmentally friendly technology for stabilizing heavy metals in MSWI fly ash.

MATERIALS AND METHODS

Collection and Preparation of Fishbone and Fly Ash

Waste fishbone from miscellaneous species of fishes (salmon, fly fish sea bream, horse mackerel, mackerel, yellowtail, lizardfish, and Japanese amberjack) was collected from local fish markets in Japan. Fishbones except heads and tails were boiled for about 40 minutes. Upon completion of boiling, the flesh, spinal cords, and soft tissues were cautiously dispelled from bones and rinsed. Afterward, the bones were dipped in a detergent solution and boiled for 1 hour on low heat. The water to detergent ratio was 5:1. Again the bones were rinsed and dipped for 24 h in a hydrogen peroxide (30% H_2O_2) solution. The water to H_2O_2 ratio was maintained at 5:1. Next, the bones were thoroughly rinsed and dried for 24 hours at room temperature (under the dry mode of the air-conditioning system). Finally the dried bones were ground by a kitchen blender. The sieving method was used to separate the ground fishbone into three particle size fractions ($<600\ \mu m$, $600\ \mu m-2\ mm$, and $0-2\ mm$). The details of the fishbone processing have been explained elsewhere [17].

Untreated IFA sample was collected from a WtE facility (S) in Fukuoka, Japan, and stored in hermetically sealed containers. Here "untreated" IFA means that the IFA was not stabilized with any stabilizing agents (such as chelate) in the facility before collection. The IFA sample was directly used for conducting metal stabilization and leaching experiments in the laboratory without any pretreatment. For bulk mineralogical and compositional analyses, IFA was manually ground in an agate mortar.

Characterization of Fishbone and Fly Ash

The chemical composition of the bulk IFA sample was measured with the technique of X-ray fluorescence (XRF). Elemental concentration in the leachate from batch leaching tests was analyzed with the inductively coupled plasma optical emission spectroscopy (ICP-OES). The mineral phases of IFA ash and FB-HA were analyzed with X-ray diffractometry (XRD). Before and after the experiments, the compositions of both IFA and fishbone were measured by the scanning electron microscope coupled with an energy dispersive X-ray (SEM-EDX) detector in the mode of backscattered electron (BSE). Fourier Transform Infrared (FT-IR) Spectroscopy tests were performed on IFA samples (with and without FB-HA treatment) with an instrument of Infrared Spectrophotometer JASCO FT/IR-4200. Details of QA/QC for instrumental analysis has been provided in Supplementary Materials (Appendix 1, 2).

Table 1. Chemical composition of MSWI fly ash

Components (%)	CaO	Cl	Na ₂ O	SiO ₂	K ₂ O	Al ₂ O ₃	MgO	Zn	S	P ₂ O ₅
	35.70	21.07	9.31	9.39	4.06	3.52	2.93	0.06	2.73	2.08
Components (%)	Fe ₂ O ₃	TiO ₂	Pb	Sb	Cu	Ba	Cr	Cd	Others	LOI
	1.40	0.14	0.06	0.07	0.04	0.096	0.02	0.01	7.03	6.50

Pb Stabilization Experimental Method

Two different size ranges of FB (<600 μm and 600 μm–2 mm) and bulk (0–2 mm) were selected to stabilize Pb in IFA. Tests were conducted by batch experiments with 250 ml polypropylene bottles at room temperature. In each bottle, 20.0 g of IFA, 2.0 g of FB (10% of IFA weight), and de-ionized water were added to maintain the initial W/S ratio at 1.5 mL/g. Bottles were settled for 6, 12, 24, and 672 h (28 days) in the ambient condition. Deionized water was added to each bottle to increase the total leachant to 200 mL after each settlement period and the admixtures were subjected to a standard Japanese leaching test (JLT-46). Bottles were centrifuged for 20 min at 3000 rpm to obtain the leachate. The liquid and solid parts were separated by vacuum filtration through the 0.45 μm pore-size membrane. Every test was done in duplicate, and the results were conferred as mean values with standard errors.

The removal efficiency of Pb was calculated using Equation 1:

$$Pb_{ref.}(\%) = \left(1 - \frac{C_t}{C_c}\right) \times 100 \tag{1}$$

where $Pb_{ref.}$ =Pb removal efficiency; C_t =Pb concentration in the test group; and C_c =Pb concentration in the control group.

The competency of using FB-HA for stabilizing a target heavy metal (here Pb) was calculated using Equation 2 as the amount of metal stabilized by the unit mass of FB-HA.

$$Stabilization\ capacity\ of\ Pb\ \left(\frac{mg}{g}\right) = (C_c - C_t) \times v / mass\ (FB-HA) \tag{2}$$

where C_c and C_t are the concentrations of Pb in the control and test groups, respectively, and v is the volume of leachant (i.e., 100 mL).

Calculation of Adsorption Isotherm Constants

The sorption data were applied in two widely used sorption isotherm models such as the Langmuir and the Freundlich isotherms. The equilibrium data for Pb cation over the concentration of 48.5 mg/L at room temperature has been correlated with the Langmuir isotherm, following Equation 3.

$$1/q_e = 1/Q_{max} + 1/b \cdot Q \cdot 1/C_e \tag{3}$$

where C_e =equilibrium concentration, q_e =number of metal ions sorbed onto FB-HA, Q and b are Langmuir constants related to the sorption capacity and energy, respectively. The linear plot is obtained when $1/C_e$ is plotted against $1/q_e$. The Freundlich adsorption isotherms were also applied to

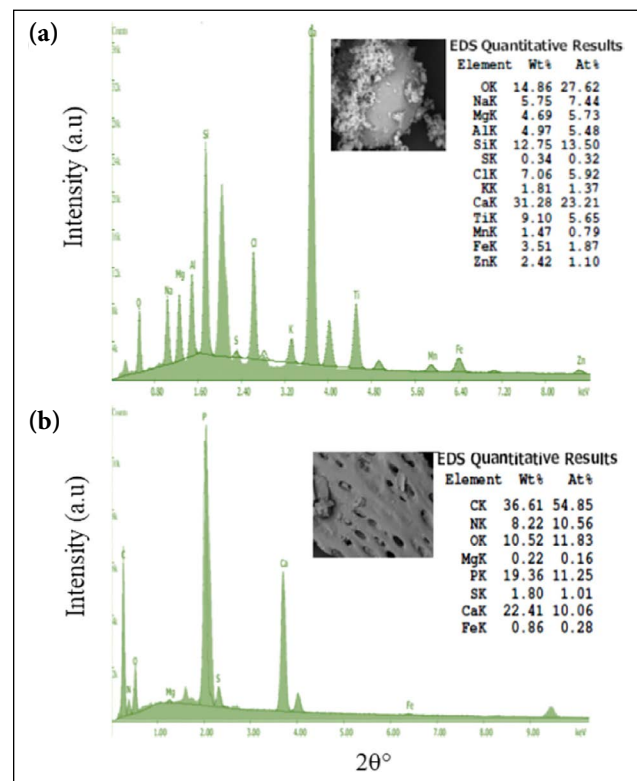


Figure 1. The BSE images and detailed composition of (a) fly ash S and (b) yellowtail fishbone.

investigate the removal of Pb by the size-fractionated natural fishbone, FB-HA using Equation 4.

$$\log q_e = \log K_f + 1/n \log C_e \tag{4}$$

K_f and n are the Freundlich adsorption equation constants, where K_f is the adsorption capacity. The constants K_f and n were determined by plotting $\log q_e$ vs $\log C_e$.

RESULTS AND DISCUSSIONS

Chemical Composition of Fly Ash and Fishbone

The major elements of the IFA sample analyzed by XRF were Ca, Cl, Al, Zn, K, Mg, Na, Si, Ti, P, and S. Among all heavy metals, Pb and Zn were found remarkably higher than other elements as shown in Table 1. Detailed phase analysis was done by SEM-EDX technique. Figure 1a and 1b exhibit the BSE images and detailed composition of an IFA particle (from source S) and the FB-HA, respectively. As shown in Figure 1b, FB-HA presents a coarse and porous texture.

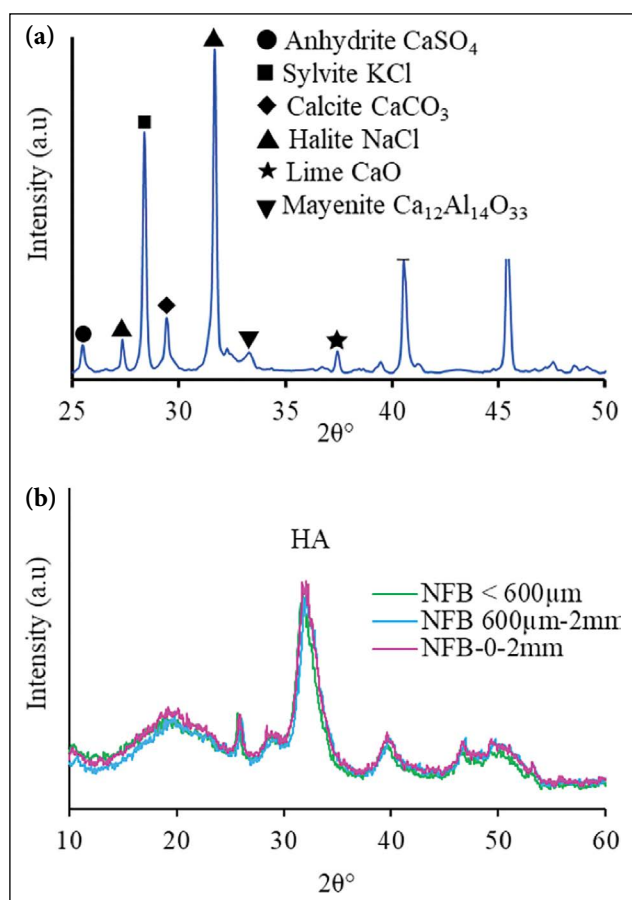


Figure 2. The XRD patterns of (a) fly ash (S) and (b) size-fractionated fishbones.

Mineralogy of Fly Ash and Fishbone

The existing mineral phases in the IFA sample (S) are shown in Figure 2a. Sylvite (KCl) and Halite (NaCl) have found the major mineral phases, since the main sources of Cl is notably high in the IFA (Table 1). A series of Ca-rich minerals such as calcite (CaCO_3), lime (CaO), anhydrite (calcium sulfate: CaSO_4), and mayenite ($\text{Ca}_{12}\text{Al}_{14}\text{O}_{33}$) were identified, which can elucidate the high concentration of Ca in IFA. It should be noted that IFA is not a completely crystalline material, but contains amorphous phases that cannot be detected directly using XRD technique.

The mixed fishbone meal consisting of various fish species was divided into three different size fractions (<600 μm , 600 μm –2 mm, and 0–2 mm) and analyzed by XRD pattern, which showed similar patterns. As shown in Figure 2b, hydroxyapatite (HA) with the chemical formula of $\text{Ca}_{10}(\text{PO}_4)_6(\text{OH})_2$ is the only typical crystalline phase detected in all fishbone fractions.

Effects of Fishbone Hydroxyapatite on Pb Stabilization

Pb stabilization in MSWI fly ash was primarily pursued at few selected settling periods and a fixed W/S ratio. The tests

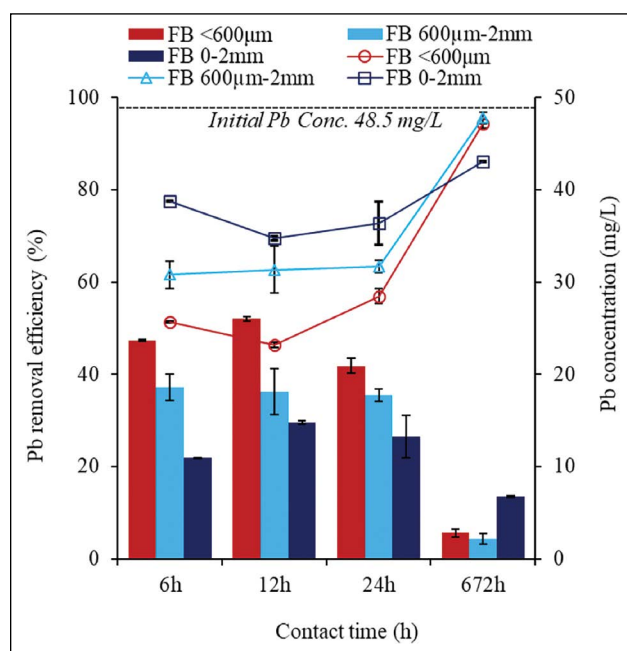


Figure 3. The removal efficiency and the concentration of Pb with different FB-HA sizes.

were conducted on the batch-scale with fishbone/fly ash ratios of 0 (control group) and 1:10 (test groups), settling times of 6, 12, 24, and 672 h (28 days), and a W/S ratio of 1.5 mL/g. The effects of FB-HA on Pb stabilization were characterized by the decrease of Pb concentration in the leachate with contact time and removal efficiency.

The results in Figure 3 show that the decreasing trend is similar for Pb with different size-fractions of FB from the initial Pb concentration (48.5 mg/L) in IFA. Up to 24 h of contact time, the concentration of Pb in the separated samples was higher than the mixed fishbone meal (0–2 mm). However, the Pb concentration in the size-fractionated samples (<600 μm and 600 μm –2 mm) decreased significantly after 28 days, and the removal efficiency exceeded 95%. It was observed that even at the shortest contact time (6 h), the mixed FB (0–2 mm) achieved about 77.5% Pb stabilization, reaching a maximum value of about 86.08% after 28 days when only 10% (w/w) of FB was used.

The results show that FB immobilized a significant amount of Pb leached from fly ash within the first few hours. After adding FB to fly ash, hydroxyapatite can stabilize Pb and control its stability over time. Although Pb in IFA can be stabilized with a shorter settling time, the highest Pb stabilization was achieved at a longer period (28 days) in all cases. This implies that in addition to the dissolution–precipitation mechanism, reaction time is a crucial factor in reaching equilibrium during the settling stage.

A slight decrease in removal efficiency was observed between 6 to 12 hours of settling. Therefore, desorption mechanism may have occurred following the initial 6-h

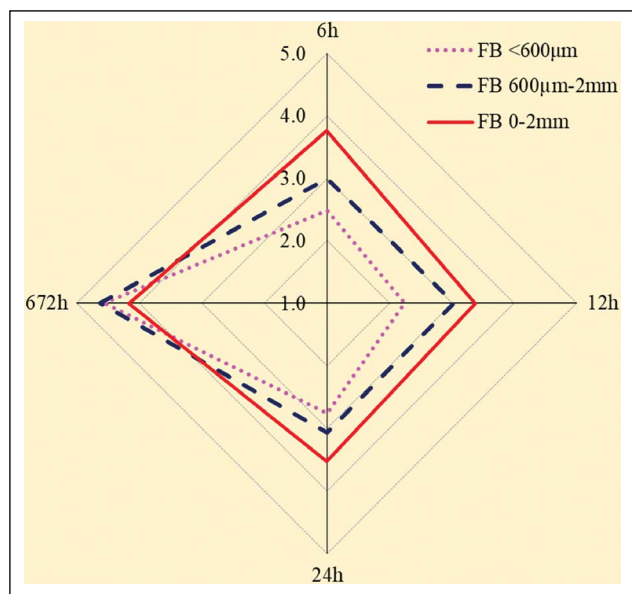


Figure 4. Pb stabilization competency with different sizes of FB-HA.

adsorption. High sorption of Pb onto FB-HA was achieved in the first 6 hours. However, shortly after that, the desorption process likely enhanced the amount of soluble Pb in the process.

It was presumed that sufficient time was needed to reach equilibrium. The results suggested that fishbone particles size in the range of 0–2 mm, there is no significant change in Pb stabilization, even with short or long settling periods. However, if the variation in fishbone particle size is relatively small, i.e., <600 μm or 600 μm–2 mm, Pb can be stabilized significantly (>95%).

Competency of Fishbone Hydroxyapatite for Pb Stabilization in Fly Ash

As shown in Figure 4, the mixed particle size of FB (0–2 mm) was about 1.5 times more competent than fractionated FB-HA (<600 μm and 600 μm–2 mm) for stabilizing Pb with a settling time of 6 hours. However, the size-fractionated FB (<600 μm and 600 μm–2 mm) competitively promoted Pb stabilization after 28 days. Pb stabilization capacity obtained 4.57 and 4.63 mg/g in <600 μm and 600 μm–2 mm FB sizes, respectively, while 0–2 mm reached 4.18 mg/g.

Table 2. Adsorption isotherm constants

FB sample Sizes	Langmuir isotherm				Freundlich isotherm		
	Q	b	R ²	R _L	K _f	n	R ²
<600 μm	5.50	19.76	0.97	0.001	6.20	3.45	0.96
600 μm–2 mm	4.99	28.21	0.99	0.001	5.40	5.03	0.99
0–2 mm	5.24	27.29	0.99	0.001	6.97	3.77	0.98

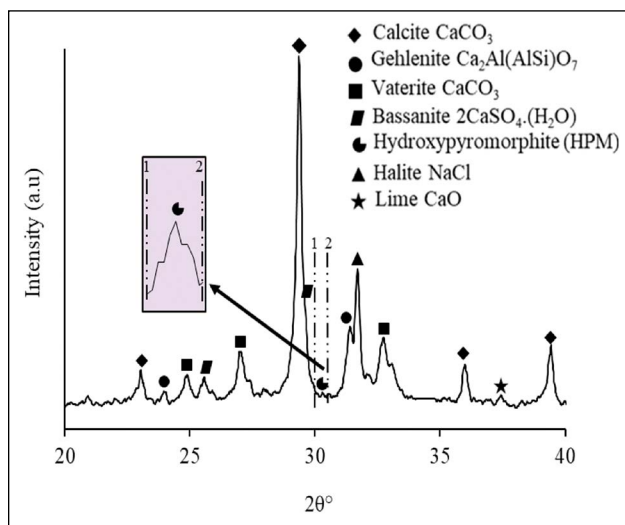


Figure 5. The XRD pattern of fly ash after treatment with FB-HA (0–2 mm).

Adsorption Isotherms

The Langmuir model was effectively narrated the sorption data with all higher values of R², and the R_L values lie in 0 < R_L < 1. This indicates that the isotherm is favorable according to Table 2. The R_L values are calculated by following Equation 5:

$$R_L = \frac{C_0}{1 + K_L C_0} \tag{5}$$

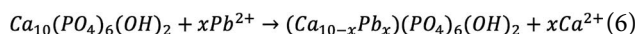
where C₀ (mg/L) is the initial metal concentration and K_L (L/mg) is the Langmuir constant related to adsorption energy. The R_L value indicates that the shape of the isotherm is unfavorable (R_L > 1), linear (R_L = 1), favorable (0 < R_L < 1), or irreversible (R_L = 0).

One of the most extensively used mathematical descriptions is the Freundlich isotherm. This isotherm can be applied to experimental data for a wide range of metal concentrations. The Freundlich isotherm provides an expression that encompasses the surface heterogeneity and the exponential distribution of active sites, and their energies.

Table 2 shows the Freundlich adsorption equation constants (k_f and n) for metal cations at different fishbone sizes. An n -value in the range of 2–10 exhibits good adsorption, but n < 1 slightly inhibits the adsorption capacity at lower equilibrium concentrations. In case of different fishbone sizes, the calculated n values between 3 and 5, indicate favorable

adsorption of Pb on to FB-HA. According to literature [18], illimitable surface coverage is reckoned mathematically, which specifies the multilayer sorption on the surface as because this isotherm cannot predict any saturation of the sorbent by the sorbate. Apatite in fishbone is comparable to hydroxyapatite based on Ca content and is therefore suitable for removing heavy metal ions from IFA. In addition to synthetic hydroxyapatite, bones from fish waste have been studied as a potential source of calcium phosphate for heavy metal stabilization [19–22]. Hydroxyapatite is superior to apatite ore because of its purity and much less unwanted metal substitution.

The ion-exchange and dissolution-precipitation processes are the two most common mechanisms proposed in capturing heavy metals with HA [23]. Through an ion-exchange mechanism, the metal adsorbs to the surface of HA or diffuses inward, releasing Ca by expelling more insoluble endogenic Ca ions. The low solubility of heavy metal phosphates drives the exchange reaction towards the release of Ca ions. In the dissolution-precipitation mechanism, Ca is first dissolved with phosphate ions, and heavy metal ions precipitate by uniform (in solution) or non-uniform (on the remaining solid HA) nucleation [24, 25]. Both mechanisms can explain that the certainty of the sorption reaction is notably retarded since the initiatory HA surface is covered with less soluble phosphate. Following the ion exchange, a new sparingly soluble metal phosphate builds a casing that confines the subsequent dissolution of the underlying Ca ions and interrupts the exchange reaction. It resembles the effect of heavy metal phosphate casing of HA particles due to non-uniform precipitation [26]. Depending on the degree of crystallinity, specific surface area, density, and composition of hydroxyapatite certain amounts of heavy metal ions removed in each mechanism [27]. The parameters, such as pH, initial metal concentration, rate of addition, and temperature, also play a substantial role [28–32]. In general, both of the above mechanisms are strong evidence of Pb precipitation and the formation of hydroxypyromorphite (HPM), a very stable Pb compound in the environment as shown in Equation 6.



The sorption mechanism on this topic has been reviewed details in elsewhere [17, 33].

Cheung et al. [22] used bone char to absorb heavy metals in solutions. Bone char is mainly comprised of HA and also contains 9–11% (by weight) carbon, accounting 50% of the total specific surface area of 100 m² g⁻¹. The sorption mechanism could be imposed to at least three pathways that found by their observations: i) ion exchange of divalent metal ions with HA; ii) sorption of metal ions onto HA surface trellis; and iii) sorption of metal ions onto the surface of carbon.

Calcium compounds in fishbone are mainly in the form of hydroxyapatite with low solubility. Furthermore, hydroxyapatite is embedded in the collagen matrix [34], making contact with the solution very difficult. Therefore, calcium in fishbone is very difficult to dissolve in water or acidic solutions. Calcium solubility in the solution increases as the particle size of the fishbone decreases. This may be due to the increased specific surface area and destruction of the collagen matrix. Therefore, it was suggested that reduced particle size in fishbone might promote metal absorption. Similar results were also obtained in this study with an FB particle size of less than 600 μm.

Figure 5 shows the mineral composition of a fly ash sample treated with mixed particle size FB-HA (0–2 mm). After treatment with FB-HA, the XRD pattern confirmed the occurrence of primitive HPM. However, since IFA has various principal mineral phases, the HPM peaks were not clear. Calcite (CaCO₃) and halite (NaCl) as major phases were confirmed in the IFA treated with FB-HA. Other minor or trace mineral phases, such as basanite (2CaSO₄·H₂O), vaterite (CaCO₃), and lime (CaO), were also detected. Sylvite (KCl) disappeared in the treated fly ash (Fig. 5), due to its high solubility, and new phases, such as bassanite [2CaSO₄·H₂O], vaterite (CaCO₃), and HPM, were developed in the system. Gehlenite [Ca₂Al(AlSi)O₇], a common Ca-rich mineral in incineration residues, was also detected.

The distribution of major elements in the fly ash treated with FB-HA (28 days) was determined using the elemental mapping technique. Ca, Si, and P (infer to bound with O) are the major elements extensively exist in the IFA particles. Despite the presence of hydrate phases in fly ash, light elements like hydrogen (H) cannot be directly measured by the EDX technique. Pb and Zn (Fig. 6) were found to be homogeneously distributed in the treated IFA particles. It is difficult to detect the newly-constituted compounds in the host medium, particularly the immensely scattered or as ultrafine aggregates [17].

Figure 7 shows the FT-IR spectrums of selected sample of fly ash S, before and after treatment with FB-HA (28 days) in the 400–4000 cm⁻¹ scanning range. Compared to the original fly ash sample S, the IR spectra suggested that no other phases developed after heavy metal stabilization. Stretching and bending vibrations of silicates were observed around 910–1020 and 400 cm⁻¹, sulfate anions around 1100–1150 and 600–650 cm⁻¹ and carbonate anions around 870 cm⁻¹ and 1420 cm⁻¹. The variation peaks of phosphate (PO₄³⁻) were prominent around 541 cm⁻¹, 592 cm⁻¹, and 1100 cm⁻¹. The bands of resembling intensities were ascribed to anhydrite (CaSO₄) at 596, 617, 675, 1118, and 1157 cm⁻¹ of wavelengths. Formation of anhydrite caused by the dehydration of gypsum, basanite, or both [35]. The IR spectra also confirmed the existence of gehlenite (485, 815, 860, 980, 880, and 922 cm⁻¹), basanite (1154 cm⁻¹), and calcite (1442 cm⁻¹ and 874 cm⁻¹) in fly ash sample (S).

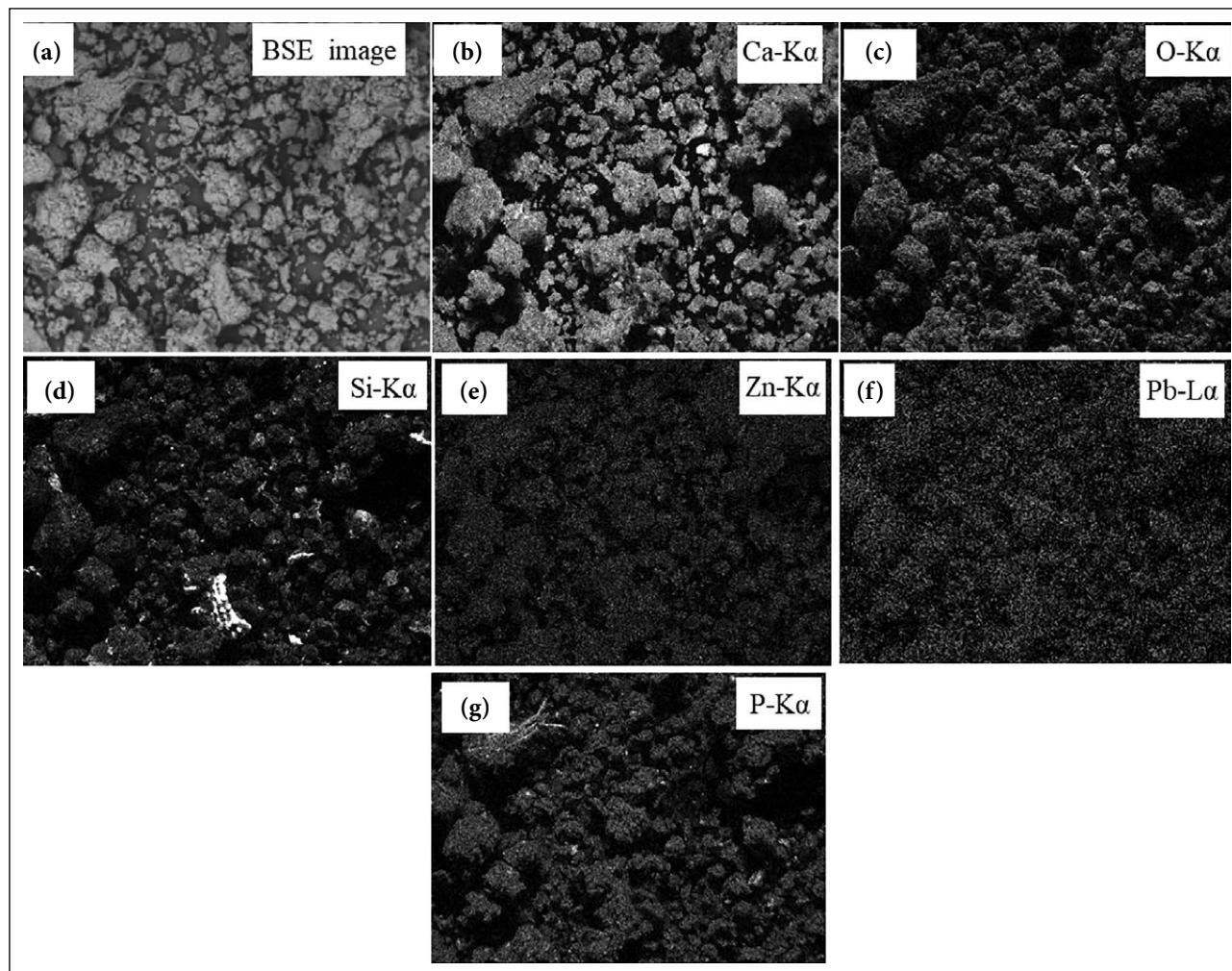


Figure 6. The BSE image (a) and characteristic X-ray images (b to g) of different elements in fly ash treated with FB-HA (0–2 mm).

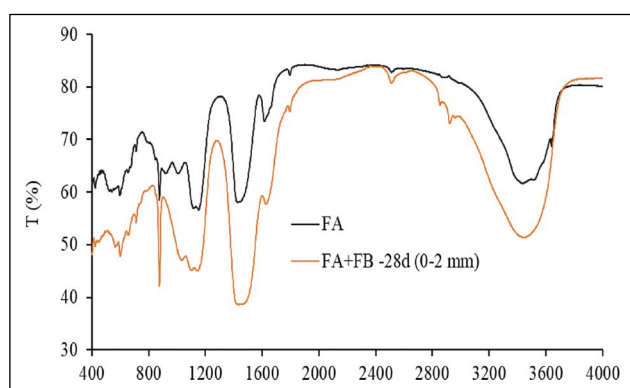


Figure 7. FT-IR spectra of fly ash before and after treatment with FB-HA (0–2 mm size) (28 days).

Utilizing waste fishbone for metal stabilization from in fly ash can reduce the use of chelate, a complex and expensive chemical [36]. Thus, the technique has prospects as a cheap and environmentally friendly approach. In this study, a low dosage of FB-HA was used. Therefore, the amount of ul-

mate mixture (fishbone and fly ash) would be lower than the amount of cement-treated fly ash, which can decelerate the occupation of landfill space. Furthermore, this study demonstrated that fishbone stabilized heavy metals such as Pb as one of the main hazardous heavy metals in fly ash, though the application is case-dependent. Additionally, the reuse or recycling of waste fishbone will be enhanced and therefore reduce the need for its disposal.

There are several advantages to using fishbone HA. Hydroxyapatite can sequester heavy metals and precipitate as minerals that are not biological. HA is considered the ideal non-specific surface sorbents for species that do not precipitate separately and the most economical reactionary medium for many metals [7].

CONCLUSIONS

This study revealed that size-fractionated fishbone (<600 μm and 600 μm–2 mm) was individually more efficient in Pb stabilization than non-fractionated FB (0–2 mm)

over longer contact periods. The finer fishbone fraction achieved the highest Pb removal efficiency (94–96%) over long settling periods due to the uniformity of the fishbone particles and possibly the extensive surface area. Fishbone particles in the size range of 0–2 mm are considered suitable for stabilizing Pb in both short (78%) and long (86%) settling periods. Under any circumstances, Pb stabilization was achieved using only 10% FB-HA. In addition, the use of waste fishbone can increase its recycling rate and reduce the need for disposal. Thus, this technique is expected to be a cheap and environmentally friendly approach. Instead of using a wide size range of FB (0–2 mm), size-fractionated FBs (<600 μm and 600 μm –2 mm) can be used to achieve significant Pb immobilization (>95%) at longer contact time between IFA and FB. Equilibrium adsorption data were best fitted with both Langmuir and Freundlich isotherm models. The R_L values of Langmuir isotherm in the present investigation were less than one and the n values of Freundlich isotherm lie between 3 and 5, suggesting the favorable adsorption of Pb onto FB-HA. The findings also suggest that fishbone meal, a locally attainable and an inexpensive adsorbent, is technically feasible for stabilizing heavy metals in MSWI fly ash.

ACKNOWLEDGMENT

The authors offer sincere gratitude to the Japan Society for the Promotion of Science (JSPS), Grant-in-Aid for Scientific Research (C) no. 18K11697, for the financial support.

DATA AVAILABILITY STATEMENT

The authors confirm that the data that supports the findings of this study are available within the article. Raw data that support the finding of this study are available from the corresponding author, upon reasonable request.

CONFLICT OF INTEREST

The authors declared no potential conflicts of interest with respect to the research, authorship, and/or publication of this article.

ETHICS

There are no ethical issues with the publication of this manuscript.

REFERENCES

- [1] C. Ferreira, and A. Ribeiro, and L. Ottosen, "Possible applications for municipal solid waste fly ash," *Journal of Hazardous Materials*, Vol. 96, pp. 201–216, 2003. [\[CrossRef\]](#)
- [2] Ministry of the Environment of Japan, "The outline of waste treatment in Japan: results of fiscal year," Ministry of the Environment of Japan, 2013.
- [3] Z. Zhang, A. Li, X. Wang, and L. Zhang, "Stabilization/solidification of municipal solid waste incineration fly ash via co-sintering with waste-derived vitrified amorphous slag," *Waste Management*, Vol. 56, pp. 238–245, 2016. [\[CrossRef\]](#)
- [4] I. Garcia-Lodeiro, V. Carcelen-Taboada, A. Fernández-Jiménez, and A. Palomo, "Manufacture of hybrid cements with fly ash and bottom ash from a municipal solid waste incinerator," *Construction and Building Materials*, Vol. 105, pp. 218–226, 2016. [\[CrossRef\]](#)
- [5] F. Wang, F. Zhang, Y. Chen, J. Gao, and B. Zhao. "A comparative study on the heavy metal solidification/stabilization performance of four chemical solidifying agents in municipal solid waste incineration fly ash," *Journal of Hazardous Materials*, Vol. 300, pp. 451–458, 2015. [\[CrossRef\]](#)
- [6] L. Chen, L. Wang, D. W. Cho, D. C. W. Tsang, L. Tong, Y. Zhou, J. Yang, Q. Hu, and C. S. Poon, "Sustainable stabilization/solidification of municipal solid waste incinerator fly ash by incorporation of green materials," *Journal of Cleaner Production*, Vol. 222, pp. 335–343, 2019. [\[CrossRef\]](#)
- [7] A. Nzihou, and P. Sharrock, "Role of phosphate in the remediation and reuse of heavy metal polluted wastes and sites. waste and biomass valorization," Vol. 1, pp. 163–174, 2010. [\[CrossRef\]](#)
- [8] J.O. Nriagu, "Formation and stability of base metal phosphates in soils and sediments," In: J.O. Nriagu, P.B. Moore, (eds). *Phosphate Minerals*. Springer-Verlag, 1984. [\[CrossRef\]](#)
- [9] S.K. Amerkhanova, A.S. Uali, and R.M. Shlyapov, "Sorption of heavy metal ions from water by natural apatite ore," *Journal of Water Chemical Technology*, Vol. 40, pp. 70–76, 2018. [\[CrossRef\]](#)
- [10] A. S. Knox, D.I. Kaplan, and M. H Paller, "Phosphate sources and their suitability for remediation of contaminated soils," *Science of Total Environment*, Vol. 357, pp. 271–279, 2006. [\[CrossRef\]](#)
- [11] G. Dermont, M. Bergeron, and G. Mercier, "Metal-contaminated soils: remediation practices and treatment technologies," *Practice Periodical Hazardous Toxic, and Radioactive Waste Management*, Vol. 12, pp. 188–209, 2008. [\[CrossRef\]](#)
- [12] D. A. C Manning, "Phosphate minerals, environmental pollution and sustainable agriculture," *Elements* Vol. 4, pp. 105–108, 2008. [\[CrossRef\]](#)
- [13] A. Nzihou, and P. Sharrock, "Calcium phosphate stabilization of fly ash with chloride extraction," *Waste Management*, Vol. 22, pp. 235–239, 2002. [\[CrossRef\]](#)
- [14] Y. Mu, A. Saffarzadeh, and T. Shimaoka, "Influence of ignition of waste fishbone on enhancing heavy metal stabilization in municipal solid waste incineration (MSWI) fly ash," *Journal of Cleaner Production*

- tion, Vol. 189, pp. 396–405, 2018. [CrossRef]
- [15] Y. Mu, A. Saffarzadeh, and T. Shimaoka, “Utilization of waste natural fishbone for heavy metal stabilization in municipal solid waste incineration fly ash,” *Journal of Cleaner Production*, Vol. 172, pp. 3111–3118, 2018. [CrossRef]
- [16] A. Saffarzadeh, M. Nag, T. Nomichi, T. Shimaoka, H. Nakayama, and T. Komiya, “A novel approach for stabilizing heavy metals in municipal solid waste incineration (MSWI) fly ash using waste fishbone hydroxyapatite (FB-HAP),” *Proceedings of 2nd Euro-Mediterranean conference for Environmental Integration*, 10-13 October, Sousse, Tunisia, 2019. [CrossRef]
- [17] M. Nag, A. Saffarzadeh, T. Nomichi, T. Shimaoka, and H. Nakayama, “Enhanced Pb and Zn stabilization in municipal solid waste incineration fly ash using waste fishbone hydroxyapatite,” *Waste Management*, Vol. 118, pp. 281–290, 2020. [CrossRef]
- [18] S. M. Hasany, M. M. Saeed, and M. Ahmed, “Sorption and thermodynamic behavior of zinc (II)-thiocyanate complexes onto polyurethane foam from acidic solutions,” *Journal of Radioanalytical and Nuclear Chemistry*, Vol. 252, pp. 477–484, 2002. [CrossRef]
- [19] I.L. Shashkova, A.I. Rat’ko, and N.V. Kitikova, “Removal of heavy metal ions from aqueous solutions by alkaline-earth metal phosphates,” *Colloids and Surfaces A*, Vol. 160, pp. 207–215, 1999. [CrossRef]
- [20] S. Sugiyama, M. Fujisawa, T. Koizumi, S. Tanimoto, K. Kawashiro, T. Tomida, and H. Hayashi, “Immobilization of aqueous heavy metal cations with phosphates and sulfates. *Bulletin of the Chemical Society of Japan*, Vol. 76, pp. 2419–2422, 2003. [CrossRef]
- [21] E. Deydier, R. Guilet, S. Cren, V. Pereas, F. Mouchet, and L. Gauthier, “Evaluation of meat and bone meal combustion residue as lead immobilizing material for in situ remediation of polluted aqueous solutions and soils: chemical and ecotoxicological studies,” *Journal of Hazardous Materials*, Vol. 146, pp. 227–236, 1999. [CrossRef]
- [22] C. W. Cheung, J. F. Porter, and G. McKay, “Removal of Cu (II) and Zn(II) ions by sorption onto bone char using batch agitation,” *Langmuir* Vol. 18, pp. 650–656, 2002. [CrossRef]
- [23] Y. Suzuki, and Y. Takeuchi, “Uptake of a few divalent heavy metal ionic species by a fixed bed of hydroxyapatite particles,” *Journal of Chemical Engineering Japan* Vol. 27, pp. 571–576, 1994. [CrossRef]
- [24] M. Manecki, P. A. Maurice, and S. J. Traina, “Kinetics of aqueous Pb reaction with apatites,” *Soil Science*, Vol. 165, 920–933, 2000. [CrossRef]
- [25] M. Manecki, P.A. Maurice, and S.J. Traina, “Uptake of aqueous Pb by Cl-, F-, and OH- apatites: mineralogic evidence for nucleation mechanisms,” *American Mineralogist*, Vol. 85, pp. 932–942, 2000. [CrossRef]
- [26] S. K. Lower, P. A. Maurice, S. J. Traina, and E.H. Carlson, “Aqueous Pb sorption by hydroxylapatite: applications of atomic forcemicroscopy to dissolution, nucleation, and growth studies,” *American Mineralogist*, Vol. 83, pp. 147–158, 1998. [CrossRef]
- [27] C. Stötzel, F. A. Müller, F. Reinert, F. Niederdraenk, J. E. Barralet, and U. Gbureck, “Ion adsorption behaviour of hydroxyapatite with different crystallinities,” *Colloids Surfaces B Biointerfaces*, Vol. 74, 91–95, 2009. [CrossRef]
- [28] Y. Takeuchi, and H. Arai, “Hironori Removal of coexisting Pb²⁺, Cu²⁺ and Cd²⁺ ions from water by addition of hydroxyapatite powder,” *Journal of Chemical Engineering Japan* Vol. 23, pp. 75–80, 1990. [CrossRef]
- [29] Y. Hashimoto, and T. Sato, “Removal of aqueous lead by poorly-crystalline hydroxyapatites,” *Chemosphere*, Vol. 69, pp. 1775–1782, 2007. [CrossRef]
- [30] Y. Xu, and F.W. Schwartz, “Lead immobilization by hydroxyapatite in aqueous solutions. *Journal of Contaminant Hydrology*, Vol. 15, pp. 187–206, 1994. [CrossRef]
- [31] S. Sugiyama, T. Ichii, H. Hayashi, and T. Tomida, “Lead immobilization by non-apatite-type calcium phosphates in aqueous solutions,” *Inorganic Chemistry Communications*, Vol. 5, pp. 156–158, 2002. [CrossRef]
- [32] G. Lusvardi, G. Malavasi, L. Menabue, and M. Saladini, “Removal of cadmium ion by means of synthetic hydroxyapatite,” *Waste Management*, Vol. 22, pp. 853–857, 2002. [CrossRef]
- [33] F. Monteil-Rivera, and M. Fedoroff, “Sorption of inorganic species on apatites from aqueous solutions,” *Encyclopedia Surface Colloid Science*, Vol. 1, pp. 1–26, 2002.
- [34] M. J. Olszta, X. Cheng, S. S. Jee, R. Kumar, Y. Y. Kim, M. J. Kaufman, E. P. Douglas, and L. B. Gower, “Bone structure and formation: A new perspective,” *Materials Science and Engineering R: Reports*, Vol: 58, pp. 77–116, 2007. [CrossRef]
- [35] P. Fermo, F. Cariati, A. Pozzi, F. Demartin, M. Tetamanti, E. Collina, and U. Russo, “The analytical characterization of municipal solid waste incinerator fly ash: Methods and preliminary results,” *Fresenius' Journal of Analytical Chemistry*, Vol. 365, pp. 666–673, 1999. [CrossRef]
- [36] H. Kitamura, T. Sawada, T. Shimaoka, and F. Takahashi, “Geochemically structural characteristics of municipal solid waste incineration fly ash particles and mineralogical surface conversions by chelate treatment,” *Environmental Science and Pollution Research*, Vol. 23, pp. 734–743, 2016. [CrossRef]

APPENDIXS

Appendix 1. Definition of analytical quality control samples used in laboratory analysis

QC type	Definition	Frequency	Used to evaluate	Limits	Corrective action
Performance test standard (PT)	Certified reference standard	Per analytical method or manufacturer's specifications	Accuracy, precision	Per manufacture's specifications	Affected samples and associated quality control must be reanalyzed following successful instrument recalibration
Continuing Calibration (CC)	Standard solution at a concentration in the center of the calibration curve	Every 10 samples	Accuracy, comparability	80–120%	Analysis cannot proceed unless CCs pass. All samples/ QA after the last passing CC must be re-analyzed
Laboratory Control Sample (LCS)	Standard solution from a different vendor than that of the calibration standard spiked with compounds of interest into a clean water matrix	Every analytical batch or 20 samples, whichever is more frequent	Accuracy, comparability	80–120%	Perform instrument maintenance and prepare new standard solution if necessary. Samples and associated QA must be re-analyzed
Instrument or Analytical Blank (Lab Blank)	Clean water matrix, free of analyte. Analyzed in same manner as samples	Every analytical batch or 20 samples, whichever is more frequent	Accuracy	Measured value less than MDL ^a or RL ^b	In some cases, target compound values may be subtracted out, in other analyses target compounds present in blank must be flagged as contamination and may not be subtracted out
Laboratory Duplicate (Lab Dup)	Analytical duplicate	Every analytical batch or 20 samples, whichever is more frequent	Comparability, precision	RPD ^c <25% (n/a if native concentration of either sample <RL)	Rerun sample. If second result is not within limits, report with qualifier

a: MDL: Method detection limit; b: RL: Reporting limit; c: RPD: Relative percent difference.

Appendix 2. Summary of laboratory QA/QC for analyzed samples

QA/QC test	Fly ash, fishbone XRD	Fly ash XRF	Fly ash, fishbone SEM-EDX	Fly ash, treated fly ash samples FT-IR	JLT-46, treated samples ICP
Total number of samples analyzed*	10	2	6	4	26
Completeness of samples collected (%)	100	100	100	100	100
Samples completed on time (%)	100	100	100	100	100
CC's (%)	100	100	100	100	100
LCS passing (%)	100	100	100	100	100
Lab dup passing (%)	100	100	100	100	98.5
Lab blanks passing (%)	100	100	100	100	100
Overall (%)	100	100	100	100	99.8

*: Including duplicates.



Research Article

Characterisation study of solid wastes: A case of districts in Tekirdağ

Elçin GÜNEŞ¹, Kübra GÜMÜŞ BAYINDIR², Nesli AYDIN³, Deniz İzlen ÇİFÇİ¹

¹Department of Environmental Engineering, Tekirdağ Namık Kemal University, Çorlu Engineering Faculty, Tekirdağ, Türkiye

²Department of Environmental Protection and Control, Tekirdağ Metropolitan Municipality, Tekirdağ, Türkiye

³Department of Environmental Engineering, Karabük University, Faculty of Engineering, Karabük, Türkiye

ARTICLE INFO

Article history

Received: 07 December 2021

Revised: 14 February 2022

Accepted: 09 March 2022

Key words:

Co-mingled dry-recyclables;

Organic waste; Solid waste;

Waste characterisation

ABSTRACT

In this study, solid waste characterisation of high-income, middle-income, low-income regions and market areas in Tekirdağ Metropolitan Municipality was carried out in winter and summer, 2016. As a result, the amount of organic wastes (kitchen wastes, park and green wastes) and packaging waste (paper, cardboard, bulky cardboard, plastics, glass, metals and bulky metals) in Tekirdağ were determined as 41.02% and 32.4% respectively, by waste sampling. When waste characterisation was analysed based on the districts, it was seen that paper and plastic waste is mostly produced from the Çorlu district. The reason for this could be the high level of welfare of the citizens living in Çorlu and the high number of working people compared to other districts due to the high density of industrial facilities. It was also seen that the ash percentage of waste is high in the districts of Hayrabolu, Şarköy, Muratlı, Marmaraeğlisi, Malkara and Saray, which are the districts not covered by natural gas distribution grid. Waste samples were characterised in the Tubitak Energy Institute Laboratory to determine the moisture content, calorific value and glow loss. The results showed that there is a high moisture and organic matter in the wastes, which makes the incineration method not suitable for the treatment of solid wastes in Tekirdağ. The results of this study highlighted that there is a potential for introducing recycling schemes especially in high income regions in Tekirdağ. To initiate such programmes, collected municipal waste could be separated in two streams in place; organics and co-mingled dry-recyclables.

Cite this article as: Güneş E, Gümüş Bayındır K, Aydın N, Çifçi Dİ. Characterisation study of solid wastes: A case of districts in Tekirdağ. Environ Res Tec 2022;5:2:148–154.

INTRODUCTION

For the robust management of solid wastes, it is very important to properly characterise wastes and obtain accurate data about their composition. These data are used to determine the appropriate disposal methods, collection and separation systems for solid wastes [1].

As it is known, solid waste generation rises in parallel with increasing population, living standards and technological developments, especially in cities [2]. Similarly, an increase is observed in the amount and type of solid waste generated in Tekirdağ [3, 4]. The inadequacy of solid waste management in the province has led the local government to seek for new solutions [5].

*Corresponding author.

*E-mail address: nesli.ciplak.aydin@gmail.com



Characterisation studies guide the determination of alternative methods for the treatment and disposal of wastes. For instance, solid waste was characterised in Lagos, Nigeria for decision making and planning [6]. Similarly, it was determined that there is a high proportion of non-bio-degradable wastes in Covenant University, Nigeria and requirements of alternative waste management solutions for a more sustainable and environmentally friendly waste management system were determined [7]. Importantly, it was reported that there is a high percentage of putrescible matters and plastics in the composition of the waste stream in Reunion Island, France and a life-cycle analysis identified the most favourable waste management option in the region as a multiple waste-treatment process [8]. Another characterisation study was also conducted to determine various physico-chemical parameters of the waste, which was dumped at Gazipur landfill site in Delhi, India and results showed a high fraction of degradable organic components in the waste [9]. It was also determined that the main waste components in Lagos, Nigeria, are food, metal and plastic and a high power potential could be obtained by adopting incineration [10]. In Tekirdağ, there has been no published study so far investigating particularly the characteristics of the municipal solid wastes produced from the province, which were collected by the district municipalities and brought to the transfer stations to be disposed of to the Demirli Landfill Site.

This study aims to produce a data set based on the characterisation of the solid wastes generated in the summer and winter periods in the districts of Tekirdağ to develop a technically and economically feasible solid waste management system. In this context, the solid waste characterisation analyses of Süleymanpaşa, Hayrabolu and Muratlı districts were carried out in Demirli Landfill Facility, which is the only landfill site in the province and the analyses for other districts (Malkara, Şarköy, Marmaraeğlisi, Çorlu, Çerkezköy, Kapaklı, Saray and Ergene) were carried out in the districts. The waste samples taken for the characterisation study were also sent to the Tubitak Energy Institute Laboratory to determine moisture content, calorific value and glow loss. Within the scope of this study, waste samples were taken from all districts to determine the composition of solid wastes generated in Tekirdağ. Considering the income level of the people living in the districts, four regions were defined as low, medium, high-income regions and market areas.

MATERIALS AND METHODS

The equipment used for the characterisation study is given in Figure 1. A scale was used to weigh the waste. The fixed volume container (1 m x 1 m x 0.5 m) was used to ensure that the waste streams to be characterised were equal. A plastic cover (5 m x 10 m) was also laid on the floor to pre-



Figure 1. Equipment used for waste characterisation.

vent any loss from the waste samples. Component containers were used as discriminating containers on which the names of the waste groups (plastic, metal, glass, etc.) were noted. Shovels, rakes and brooms were also used for laying and filling waste. The sieve was used to shift waste piles.

The steps for the characterisation process are summarised below;

- 1 Each waste bag was emptied and levelled with a shovel and rake.
- 2 The fixed volume container was filled with the waste samples taken from different points of the waste pile,
- 3 After the fixed volume container was filled and then emptied on the plastic cover, the waste was separated and filled into component containers,
- 4 The waste containers were tared and absolute weight of the waste was recorded.
- 5 In the sieving step of the waste characterisation in winter, it was observed that the amount of ash contaminated and adhered to other wastes was negligibly low. For this reason, after each category was determined, the waste pile remaining on the ground was sieved through a 1 cm sieve. The part remaining under the sieve was defined as ash. Although there is no specific definition for size distribution of ash in municipal waste stream, it is known that it refers to remaining incombustible residues. Ash is a biologically inert material that can be managed in a more environmentally sound way [11]. The use of bottom ash in municipal solid waste incinerators, for example, could be used as a part of cement raw material or road base [12, 13].
- 6 2 kg solid waste samples were taken from each district and sent to the Tubitak Marmara Research Centre-Energy Institute Laboratory to determine moisture content, calorific value and glow loss.

For moisture determination, the samples were dried in an oven at 105°C for 24 hours and their water content was measured. The dried samples were processed by coarse and fine grinders in series. The product from the grinders was

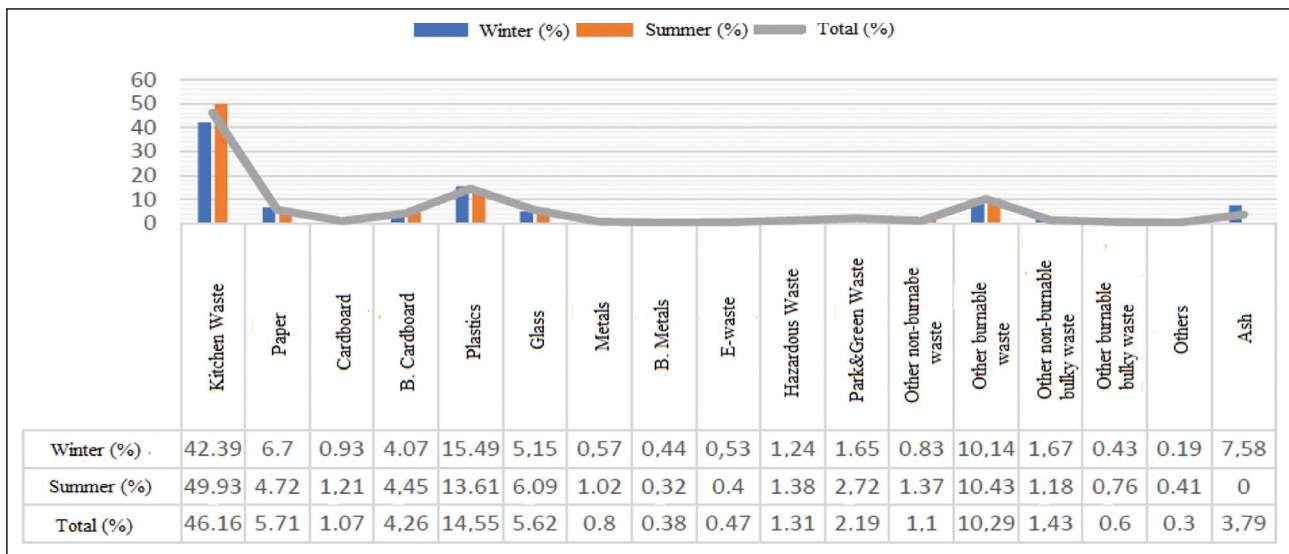


Figure 2. Seasonal characterisation of solid wastes in the districts of Tekirdağ.

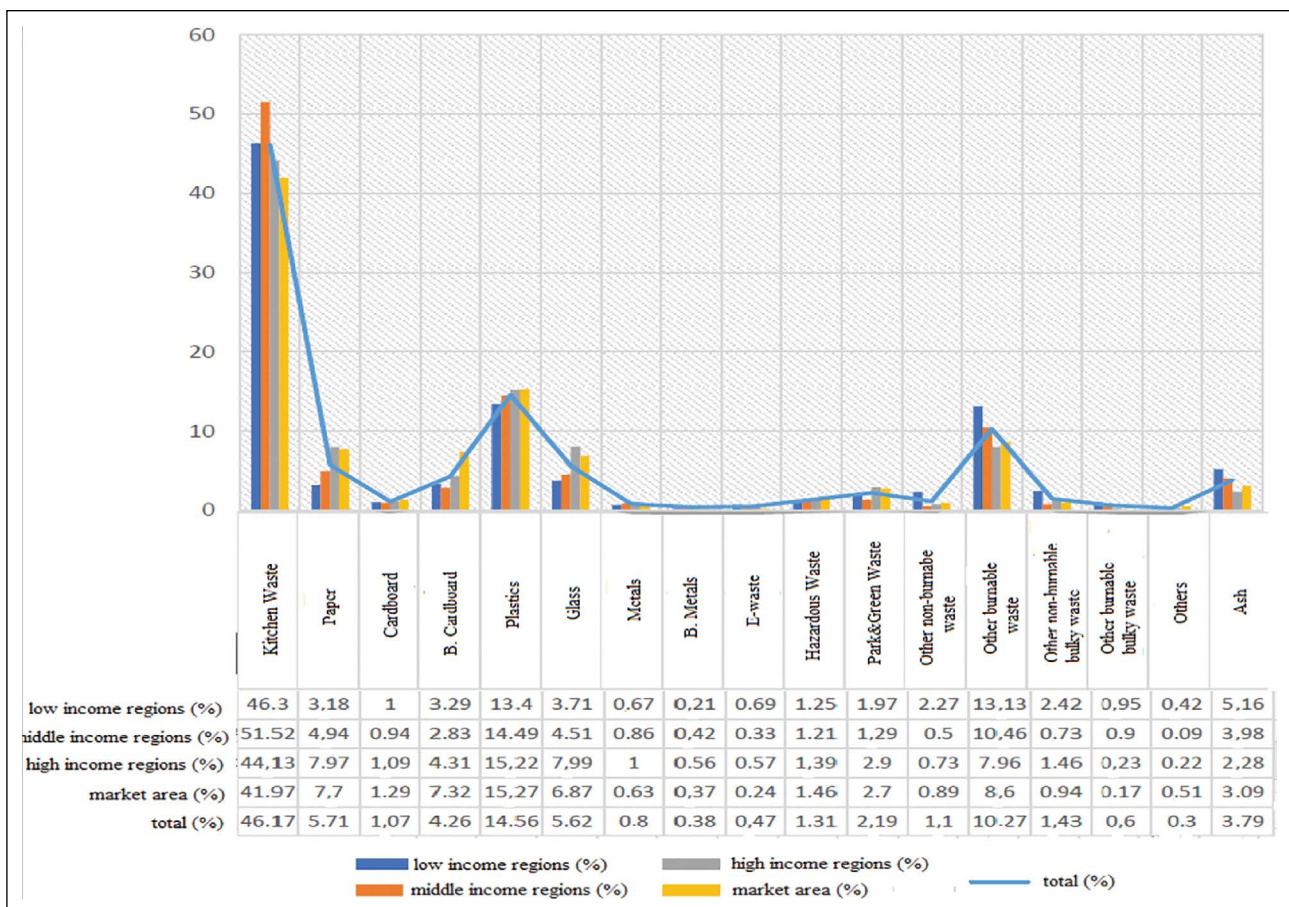


Figure 3. Solid waste characterisation by income level in districts of Tekirdağ.

sent for analyses. The calorific value of the wastes was determined based on the principle of calculating the mass of the substances released as gas by burning the dry waste sample at 550°C for at least 60 minutes [14].

RESULTS AND DISCUSSION

General Evaluation of Solid Waste Characterisation

The results of the characterisation study based on the

districts are given in Table 1. It is seen that the highest percentage of kitchen waste was produced in Çorlu, Çerkezköy and Süleymanpaşa districts. It is estimated that due to a large number of industrial facilities in Çorlu and Çerkezköy and the cooking activities taking place in the cafeterias located there, the kitchen waste component (53.59% in Çorlu and 48.67% in Çerkezköy) was comparatively high.

It is also seen that the highest (7.585%) and lowest percentage (3.365%) of the paper waste is produced in Çorlu, and Hayrabolu, respectively. The high income citizens living in Çorlu and number of working people compared to other districts, because of industrial activities in the district, may have resulted in Çorlu having the highest share of the paper waste.

When the generation rate of plastic wastes is investigated, it is seen that this rate is higher in Marmaraeğlisi, Şarköy and Çerkezköy with 19.175%, 17.85% and 17.19%, respectively. It is also seen that the highest percentage of ash waste comes from these districts, which are located out of natural gas distribution grid. Therefore, the use of coal continues and the ash component of the waste is significant.

Table 2 shows the moisture content, calorific value and glow loss of solid wastes generated in the districts of Tekirdağ. According to the results of the analysis conducted in Tubitak, the waste with the highest percentage of humidity is collected from in Malkara, Hayrabolu and Şarköy districts, respectively (Table 2). It is also seen that the district with the highest percentage of dry matter is Çerkezköy, while the district with the lowest percentage is Malkara.

In addition, the highest glow loss at 550°C was detected in waste produced from Marmaraeğlisi, Çorlu and Şarköy. It is estimated that this is due to contamination related to waste fractions. As it is known, flexographic inks, adhesives, wires, staples in papers and types of polymers in plastics could cause loss of heat depending on humid weather conditions and cross contamination of waste. The glow loss, which is an indicator of the percentage of volatile organic substances in the waste, was measured as 80.3% in Tekirdağ. It is advantageous if the waste has a high glow loss in terms of both thermal and biological methods.

It is seen that the district with the highest upper calorific value and the lowest calorific value is Marmaraeğlisi. The lower calorific value is an important indicator in terms of deciding whether thermal methods are efficient. For the treatment of wastes in incineration technology without using external additional fuel, a calorific value of waste must be at the level of a minimum of 1,500–1,600 kcal/kg waste [15, 16]. The low calorific value of combustible components and the high moisture value of the waste have a negative effect on combustion efficiency.

Seasonal Variation in Waste Characterisation in Tekirdağ

The seasonal variation of different waste categories is shown in Figure 2. It is seen that, kitchen waste has the largest percentage regardless of the season. It is also seen that kitchen and park-green waste increase relatively in summer. The main reason for this is the increase in consumption of thick-skinned fruits and vegetables such as melons and watermelons in summer.

There is a considerable increase in packaging waste such as glass and metals in summer (Fig. 2). It is expected that the reason for this is the high consumption of beverages in summer because of the hot and humid weather. It is also seen that the ash is produced relatively high in districts without natural gas (Hayrabolu, Şarköy, Muratlı, Marmaraeğlisi, Malkara and Saray). This is caused by the burning of charcoal for heating in the districts not covered by natural gas distribution grid, and as a result, the ash produced from the houses is mixed with municipal waste.

Waste Characterisation by Income Levels in the Districts

Solid waste characterisation by income levels in the districts is shown in Figure 3. It is seen that kitchen waste has by far the largest share in all of the income levels. Figure 3 also shows that kitchen waste production rate is the highest (51.52%) in middle-income regions. However, as stated in the section above, there are a large number of industrial facilities in Çorlu and Çerkezköy and cooking activities take place in the cafeterias located in Süleymanpaşa. The tendency to consume more packaged materials in these districts causes high proportion of kitchen and packaging waste to occur at the same time from high-income regions. This is reflected to Figure 3 which shows a higher proportion of packaging waste (38.14%), such as paper (7.97%), cardboard (1.09% and 4.31% for bulky cardboard), glass (7.99%), metals (1% and 0.56 for bulky metals) and plastics (15.22%), are produced in high-income regions compared to middle-income regions where packaging waste is only 28.99% [paper (4.94%), cardboard (0.94% and 2.83% for bulky cardboard), glass (4.51%), metals (0.86% and 0.42 for bulky metals) and plastics (14.49%)].

It is seen in Figure 3 that the category of paper-cardboard waste production is low in low-income regions in comparison to the other regions. In general, it is estimated that the consumption of packaged food, and so the production of packaging waste (such as paper and cardboard waste), is higher in high-income regions. However, there is no significant difference in the percentage of plastic wastes among high, medium, low income regions and market areas.

The other combustible materials category in Figure 3 includes diapers. The use of diapers seems to be widespread for every income group. This rate is higher in low-income regions than in other regions. This could be due to higher birth rates in low-income areas. The percentage of ash waste is also high in low-income regions where the use of natural gas is not widespread.

Table 1. Characterisation of solid wastes based on districts in Tekirdağ (%)

Waste categories	Districts waste composition (%)											
	Murathlı	Malkara	Hayrabolu	Şarköy	Mereğlisi	S.paşa	Çorlu	Ç.köy	Kapaklı	Saray	Ergene	Tekirdağ
Kitchen waste	35.3	43.1	39.845	35.59	32.815	46.37	53.59	48.67	45.28	39.35	38.7	46.16
Paper	6.1	5.1	3.365	4.36	5.765	6.81	7.585	4.335	4.86	4.43	3.83	5.71
Cardboard	1.5	2.4	1.505	2.665	2.11	0.675	0.89	0.99	0.935	1.35	0.675	1.07
Bulky cardboard	4.7	3.3	3.855	3.855	3.855	3.855	3.855	3.855	3.855	3.855	3.855	3.855
Plastics	16.3	15.6	14.46	17.85	19.175	15.92	11.97	17.19	14.015	10.22	14.665	14.55
Glass	4.7	6.5	4.12	5.775	5.65	6.945	5.995	4.46	3.845	4.975	5.87	5.62
Metal	1.9	1.9	0.87	2.27	2.57	0.79	0.56	0.43	0.46	0.665	0.545	0.795
Bulky metals	0.4	0.3	0.06	0.13	0	0.4	0.48	0.295	0.585	0.38	0.6	0.38
E-waste	0.8	0.6	0.47	0.86	0.855	0.81	0.325	0.195	0.205	0.54	0.415	0.465
Hazardous waste	2.0	1.2	1.41	2.115	1.975	1.445	1.145	1.11	1.08	1.67	1.345	1.31
Park and green waste	4.5	1.2	3.28	2.75	3.645	1.575	1.18	1.58	2.03	2.955	7.135	2.185
Other non-burnable waste	0.8	0.5	2.96	0.615	0.975	0.36	1.175	0.465	1.4	2.635	3.175	1.1
Other burnable waste	14.6	9.1	11.02	8.28	10.575	7.27	7.15	16.605	14.35	12.23	9.81	10.285
Other burnable bulky waste	0.6	0	1.37	0.38	0.115	2.99	1.45	0.735	1.705	0.71	1.765	1.425
Other non-burnable waste												
Bulky waste	0	0	0.77	0	0.255	0.18	0.195	0.17	0.355	3.66	3.26	0.595
Others	0	0	0	0	0.11	0.01	0.22	0.43	0.465	1.78	0.565	0.3
Ash	5.7	9.1	10.655	11.575	6.96	2.415	1.465	0.86	5.07	5.48	3.56	3.79
Total	100	100	100	100	100	100	100	100	100	100	100	100

Table 2. Moisture content, calorific value and glow loss of solid wastes in Tekirdağ

Waste properties	Districts waste composition (%)											
	Murathlı	Malkara	Hayrabolu	Şarköy	Mereğlisi	S.paşa	Çorlu	Ç.köy	Kapaklı	Saray	Ergene	Tekirdağ
Moisture content (%)	73.37	87.04	82.45	81.53	58.02	74.19	79.7	72.9	75.25	77.59	73.03	75.1
Dry matter (%)	26.63	12.96	17.55	18.47	21.98	25.81	20.3	28.36	24.75	22.41	26.97	24.9
Glow loss (%)	83.14	82.66	83.19	85.41	88.67	82.7	87.25	76.21	77.57	68.71	67.89	80.3
Upper calorific value (cal/g)	3643.75	3881.3	4118.25	3600.3	4193.13	3246.13	3935.1	3616.8	3757.7	3851.6	3076	3691
Lower calorific value (cal/g)	541.12	-6.17	240.42	188.02	1420.86	403.81	332.59	553.67	489.82	409.25	402.24	479.72

Waste characterisation provides useful information to city authorities in terms of planning to reduce waste, set up recycling programmes and hence, to protect resources. In this way, landfill diversion could also be maximised and recyclable waste could be captured and beneficially reused. The results of this study highlight that there is a potential for introducing recycling schemes especially in high income regions in Tekirdağ. To initiate such programmes, municipal waste could be separated in two streams, organics and co-mingled dry-recyclables at homes. Dry recyclables could further be segregated and reproduced as a secondary product by any proposed materials recycling facility in the province [17].

CONCLUSION

In this study, solid waste characterisation based on different income levels (low, middle, high-income regions and market area) in the districts of Tekirdağ was conducted in the summer and winter periods and moisture content, glow loss and lower-upper calorific value of the waste were determined.

As a result of this characterisation study, the rate of organic wastes (kitchen wastes, park and green wastes) and packaging waste (paper, cardboard, bulky cardboard, plastics, glass, metal and bulky metal) were determined as 42.02% and 32.4% in Tekirdağ, respectively. This shows similarity with the study conducted in Çorlu, which resulted that 170 tonnes of domestic waste are generated daily and 30% of this waste is recyclable materials [18]. In another study, it was found that almost 70% household waste in Eskisehir was food waste, while 20% of it was recycling waste including paper-cardboard, metals, glass and plastics [19]. It was also noted that the effects of socio-economical changes on waste composition plays a crucial role. High content of recyclables in waste stream was found significant in terms of pioneering on-site recycling schemes for residents. For instance, it was found that more than 65% of municipal wastes in the Campus Mexicali, Mexica are recyclable or potentially recyclable. This highlighted the feasibility of waste segregation and recycling in the campus and attracted recycling companies which could absorb all of these wastes [20].

It was also determined that the district with the highest production of kitchen and paper waste is Çorlu, because of the high level of welfare of the citizens living in the district and the high number of working people compared to other districts depending on the density of industrial facilities. It was also observed that the ash percentage is high in the districts of Hayrabolu, Şarköy, Muratlı, Marmaraeğlisi, Malkara and Saray, which are the districts not covered by natural gas distribution grid.

As a result of the analysis conducted in Tubitak, the humidity and dry matter was obtained as 75.1%, 24.9% in Tekirdağ, respectively. The glow loss at 550°C was measured as 80.3%. Upper and lower calorific values were determined as 3691 cal/g. and 479.72 cal/g. This shows similarity with

the outcomes of the study which presents that approximately 54% of domestic waste was organic in nature and average moisture content of samples was 62.41% in İstanbul [21]. These results indicate that incineration is not a suitable method for the solid wastes produced in Tekirdağ.

ACKNOWLEDGMENT

This study was produced from the master thesis of Kübra Gümüş Bayındır with the supervision of Prof. Dr. Elçin Güneş. The data used in this article were produced from Kübra Gümüş Bayındır's thesis, and Elçin Güneş, Nesli Aydın and Deniz İzlen Çifçi contributed to the production of this manuscript. The authors would like to thank the directors and employees of Tekirdağ Metropolitan Municipality for their contributions to providing the data used in the study.

DATA AVAILABILITY STATEMENT

The authors confirm that the data that supports the findings of this study are available within the article. Raw data that support the finding of this study are available from the corresponding author, upon reasonable request.

CONFLICT OF INTEREST

The authors declared no potential conflicts of interest with respect to the research, authorship, and/or publication of this article.

ETHICS

There are no ethical issues with the publication of this manuscript.

REFERENCES

- [1] S.S. Chung, and C.S. Poon, "Characterisation of municipal solid waste and its recyclable contents of Guangzhou," *Waste Management and Research*, Vol. 19(6), 2001. [\[CrossRef\]](#)
- [2] M.A. Sufian, and B.K. Bala, "Modeling of urban solid waste management system: The case of Dhaka city," *Waste Management*, Vol. 27(7), pp. 858–868, 2007. [\[CrossRef\]](#)
- [3] N. Aydın, "Electricity generation potential of municipal solid wastes produced in the province of Edirne," *Sustainable Engineering and Innovation*, Vol. 3(1), pp. 61-67, 2021. [\[CrossRef\]](#)
- [4] A. Hanedar, B. Gül, E. Güneş, G. Kaykıoğlu, and Y. Güneş, "Waste management and zero waste practices in educational institutions," *Environmental Research and Technology*, Vol.4(2), pp. 126–133, 2021. [\[CrossRef\]](#)
- [5] H. Sarı, "Assessment of Nutrient Status of Soil Around Municipal Soil Waste Disposal Site in Çorlu District of Tekirdağ Using GIS," *Turkish Journal of Agriculture - Food Science and Technology*, Vol. 7(2), pp. 377–383, 2019. [\[CrossRef\]](#)

- [6] L. Salami, and A.A. Susu, "Characterisation study of solid wastes: A case of Lagos State," *International Journal of Applied Science and Technology*, Vol. 1(3), pp. 47–52, 2011.
- [7] J.O. Okeniyi and E.U. Anwan, "Solid wastes generation in Covenant University, Ota, Nigeria: Characterisation and implication for sustainable waste management," *Journal of Materials and Environmental Science*, Vol. 3(2), pp. 419–424, 2012.
- [8] E. Lebon, N. Madushele, and L. Adelard, "Municipal solid wastes characterisation and waste management strategy evaluation in insular context: A case study in Reunion Island," *Waste and Biomass Valorization*, Vol. 11, pp. 6443–6453, 2020. [\[CrossRef\]](#)
- [9] S. Mor, K. Ravindra, A. D. Visscher, R.P. Dahiya and A. Chandra, "Municipal solid waste characterization and its assessment for potential methane generation: A case study," *Science of The Total Environment*, Vol. 371(1–3), pp. 1–10, 2006. [\[CrossRef\]](#)
- [10] A. Akinshilo, "Energy potential from municipal solid waste (MSW) for a developing metropolis," *Journal of Thermal Engineering*, Vol 5, pp. 196–204, 2019. [\[CrossRef\]](#)
- [11] H. Li, G. Liu, and Y. Cao, "Content and distribution of trace elements and polycyclic aromatic hydrocarbons in fly ash from a coal-fired chp plant," *Aerosol and Air Quality Research*, Vol. 14, pp. 1179–1188, 2014. [\[CrossRef\]](#)
- [12] R. Forteza, M. Far, C. Seguí, and V. Cerdá, "Characterization of bottom ash in municipal solid waste incinerators for its use in road base," *Waste Management*, Vol. 24(9) pp. 899–909, 2004. [\[CrossRef\]](#)
- [13] P. Krammart, and S. Tangtermsirikul, "A study on cement made by partially replacing cement raw materials with municipal solid waste ash and calcium carbide waste," *ScienceAsia*, Vol. 29, pp 77–84, 2003.
- [14] E. Aynur, "Comperative analysis of gasification and incineration systems for municipal solid waste of Is-tanbul," Master Thesis, Istanbul Technical Universi-ty, Turkey, 2011.
- [15] S. Kathirvale, M.N.M Yunus, K. Sopian, and A.H. Samsuddin, "Energy potential from municipal solid waste in Malaysia," *Renewable Energy*, Vol. 29, pp. 559–567, 2003. [\[CrossRef\]](#)
- [16] H. Liu, H. Xiao, B. Fu, and H. Liu, "Feasibility of sludge deep-dewatering with sawdust conditioning for incineration disposal without energy input," *Chemical Engineering Journal*, Vol. 313, pp. 655–662, 2017. [\[CrossRef\]](#)
- [17] N. Aydın, "Design and assessment of a material recycling facility in the middle-scale residential area," In: Jammi A, Güllü A, Yıman Z, Yalçınkaya S, editors. *Engineering and Technology Management*, İstanbul: Güven Plus Group Inc. Publications, 2021. [\[CrossRef\]](#)
- [18] E. Tinmaz and İ. Demir, "Research on solid waste management system: To improve existing situation in Çorlu Town of Turkey," *Waste Management*, Vol. 26(3), pp. 307–314, 2006. [\[CrossRef\]](#)
- [19] M. Banar, and A. Özkan, "Characterization of the municipal solid waste in Eskisehir city, Turkey," *Environmental Engineering Science*, Vol. 25(8), pp. 1213–1220, 2008. [\[CrossRef\]](#)
- [20] C.A.D. de Vega, S.O. Benitez, and M.E.R. Barreto, "Solid waste characterization and recycling potential for a university campus," *Waste Management*, Vol. 28(Suppl 1), pp. S21–S26, 2008. [\[CrossRef\]](#)
- [21] S. Yildiz, C. Yaman, G. Demir, H. K. Ozcan, A. Coban, H. E. Okten, K. Sezer, and S. Goren, "Characterization of municipal solid waste in Istanbul, Turkey," *Environmental Progress & Sustainable Energy*, Vol. 32(3), pp 734–739, 2013. [\[CrossRef\]](#)



Research Article

Assessing the efficiency of drinking water treatment plant and the impact of broken distribution systems on water quality of Wukari-Ibi plant

Ezekiel SAMAILA¹, Williams Abel GIN², Williams Kwari JOSHUA^{*3}

¹Department of Biological Sciences, Federal University Wukari, Faculty of Pure and Applied Sciences, Nigeria

²Department of Chemical sciences, Federal University Wukari, Pure and Applied Sciences, Nigeria

³Federal University Wukari, Faculty of Engineering and Technology, Nigeria

ARTICLE INFO

Article history

Received: 28 December 2021

Revised: 02 April 2022

Accepted: 10 April 2022

Key words:

Contaminants; Efficiency; Water quality; Water treatment; Water treatment plant

ABSTRACT

Water treatment is essential in the provision of potable drinking water to communities. However, studies have shown that many local conventional drinking water treatment plants in Nigeria are ineffective in removing contaminants. This study evaluated the efficiency of drinking water from Wukari-Ibi plant by assessing water samples before and after treatment and comparing results to national and international drinking water standards. Forty water samples were collected and selected physical and biological parameters were determined according to standard laboratory procedures. The results indicated that after treatment, turbidity (6.74 NTU) and coliform count (17 cfu/100 mL) were still significantly greater than standard guidelines, which suggest that the treatment plant is unable to reduce the concentration of these contaminants to a safe level for consumption. Furthermore, assessing water at consumer taps indicated that broken distribution system is likely serving as a potential pathway for contamination. The plant removal efficiency of colour, turbidity, Total Dissolved Solids, hardness, and coliform count was computed as 74.7%, 66.57%, 32.58%, 30.11%, and 59.88% respectively. Overall, the removal efficiency was 52.77% which is considered unacceptable for the supply of potable drinking water. The study concludes that cost and poor skilled personnel are the major factors in the inefficient treatment and therefore we suggest a low-cost treatment using activated carbon from locally sourced plants to be incorporated for effective removal of contaminants. There is also a need for government to invest in infrastructure and equipment so as to upgrade the treatment plant.

Cite this article as: Samaila E, Gin WA, Joshua WK. Assessing the efficiency of drinking water treatment plant and the impact of broken distribution systems on water quality of Wukari-Ibi plant. Environ Res Tec 2022;5:2:155–164.

INTRODUCTION

Next to oxygen, water is considered one of the most precious commodities for human survival. Therefore, without water, it is safe to say that the existence of life is impossible [1]. Despite the fact that around 70% of the earth is covered by

water, it has not been available when and where it is needed, and when it does, it is always not of sufficient quantity and quality for consumption [2–4]. This is particularly due to the unprecedented increase in population, accompanied by the increase in agricultural and industrial activities, which gives rise to waste generation and indiscriminate disposal

*Corresponding author.

*E-mail address: joshuakwari@fuwukari.edu.ng



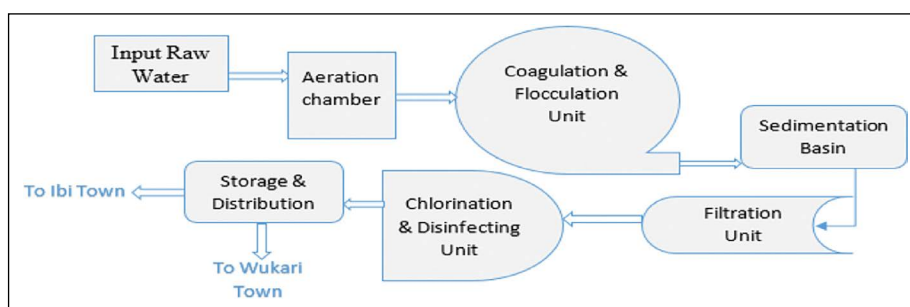


Figure 1. Schematic diagram of the treatment plant showing the various section.

into water bodies and the environment. Consequently, this has increased the rate and types of contaminants that are now identified in the environment [5–7]. These contaminants have been found in surface and groundwater and pose serious health concerns especially to rural people and areas where there are no water treatment facilities [8–11] or where the treatment facilities have either broken-down or are ineffective in removing contaminants.

Although pure water does not exist in its natural state due to the presence of gasses, dissolved and suspended solids, anthropogenic activities is now considered the biggest source of surface and groundwater pollution in many developing countries. Water quality has been identified as one of the key environmental indicators especially in areas susceptible to water contamination. Therefore, drinking water must be free from impurities and other hazardous chemicals and microorganisms that may adversely impact human health [7, 12–15]. This has led to the development of water treatment facilities across many communities for the provision of potable drinking water [12, 16]. However, even though the provision of safe, accessible, affordable, and sufficient drinking water is considered a fundamental human right [17], many communities still lack the facilities and infrastructure necessary for the treatment and distribution of adequate, safe, and sufficient water for all [3, 18, 19]. These communities are often in rural to semi-urban areas where there are engaged in large scale agricultural activities which contributes significantly to the high levels of nutrients, hormones, metals, and other chemicals found in drinking water [9, 20].

The Ibi-Wukari treatment plant uses the conventional coagulation and filtration process to treat and distribute water to consumers. The conventional treatment process involves the collection of raw water (from surface water sources), which is aerated, coagulated, filtered, and disinfected before distributed to consumers for consumption (Fig. 1). These processes however have been questioned due to poor maintenance and lack of monitoring of the water treatment and its infrastructure [3, 19]. There have been reports from residents who are often dissatisfied with the water from the treatment plant and hence result to water vendors as an alternative means of water supply [21]. This necessitates the

need to assess the efficiency of the treatment plant in removing the various contaminants, particularly those related to the aesthetics and biological properties of water.

MATERIALS AND METHODS

Water Quality Indicators

Physical and biological indicators were selected to assess how effective the treatment plant is in removing these parameters. The physical indicators assessed include pH, colour, turbidity, total dissolved solids (TDS), and total hardness while total coliform count was used to assess the removal of biological contaminants. These parameters were selected according to the Nigerian drinking water quality guidelines [22].

Sample Collection

Water samples were collected before treatment (raw water from the river source), after treatment (within the reservoir at the treatment plant), and at consumer taps within Wukari township. A total of 40 sampling sites (10, 15 & 15 sites before & after treatment and at consumer taps respectively) were randomly identified and water samples were subsequently collected. Water samples were collected in triplicates and the average was used to compute for both descriptive and inferential statistics. Water samples were collected in pre-treated 50cl bottle containers and pre-treatment was done by washing the bottle containers with 0.05M HCl and then rinsed with distilled water as specified by [23]. Furthermore, before collection, sample bottles were rinsed 3 times with the water samples before they were collected and subsequently transported to the laboratory in ice coolers under 4°C.

Sample Analysis

Temperature, pH and turbidity were measured using mercury thermometer, pre-calibrated digital electrode pH meter and turbid-meter respectively. Other physical and biological parameters comprising of colour, TDS, total hardness, and total coliform count were analysed in the laboratory according to standard laboratory procedures stipulated by [23, 24]. Colour was determined using the Hazen meth-

Table 1. Descriptive statistics of water samples before treatment

Parameters	NIS/WHO standards	Mean	St. Dev	SE mean	Range		P-values
					Min	Max	
Temperature (°C)	Ambient	20.276	0.335	0.0749	19.80	21.1	WR
pH	6.5–8.5	6.365	0.236	0.053	6.00	6.80	0.010***
Colour (TCU)	15	54.135	2.455	0.549	50.10	58.80	0.000***
Turbidity (NTU)	5	20.165	3.376	0.755	13.20	25.70	0.000***
TDS (mg/L)	500	633.38	25.27	5.65	588.70	684.20	0.000***
Hardness (mg/L)	150	212.81	16.30	3.65	182.50	241.00	0.000***
Total coliform (cfu/100 mL)	10	42.35	7.88	1.76	30	56.00	0.000***

Min: Minimum; Max: Maximum; St. Dev: Standard deviation; SE mean: Standard error mean; ***: Significantly exceeds WHO drinking water standard; *: Within WHO drinking water standard; WR-within stipulated range.

Table 2. Descriptive statistics of water samples after treatment

Parameters	NIS/WHO standards	Mean	St. Dev	SE mean	Range		P-values
					Min	Max	
Temperature (°C)	Ambient	21.93	0.50	0.113	21.00	22.8	WR
pH	6.5–8.5	7.5	0.18	0.041	7.10	7.8	*
Colour (TCU)	15	13.7	1.41	0.315	10.30	16.1	1.000*
Turbidity (NTU)	5	6.74	1.02	0.227	5.30	8.60	0.000***
TDS (mg/L)	500	427.02	13.95	3.12	400.10	448.8	1.000*
Hardness (mg/L)	150	148.73	5.38	1.20	140.00	158.2	0.847*
Total coliform (cfu/100 mL)	10	17	4.10	0.918	11.00	26.00	0.000***

Min: Minimum; Max: Maximum; St. Dev: Standard deviation; SE Mean: Standard error mean; ***: Significantly exceeds WHO drinking water standard; *: Within WHO drinking water standard; WR: Within stipulated range.

od, while TDS and total hardness were measured using the gravimetric methods and Winkler’s titration method as described by [23, 24]. The total coliform count was determined using membrane filtration techniques with the aid of Eosin Methylene Blue Agar (oxid), by incubating at 37°C since coliform bacteria is known to thrive well at 37°C [23].

Statistical Analysis

Descriptive and inferential statistics were used to draw conclusions and inform the discussion of this paper. Minitab statistical software version 20.0 was used to analyse the data and the mean, standard deviation, minimum and maximum values were tabulated and presented. A 1-sample student T-test was used to compare the result to the WHO/NIS guidelines to identify samples that failed to conform to the stipulated standards while Analysis of Variance (ANOVA) was used to indicate differences between water samples before treatment, after treatment, and at consumer taps during distribution. In addition, a 2-Sample T-test was also used to assess the difference in water quality after treatment and at consumer taps. This was done in order to assess the impact of broken distribution systems (pipes) on water quality.

RESULTS AND DISCUSSION

Comparing Results to WHO & NIS Stipulated Standards

The descriptive statistics of the results is shown in Table 1, 2 and 3 respectively. The results shows that the samples had a mean temperature of 20.3°C, 21.9°C and 21.5°C before, and after treatment and at consumer taps respectively. The sample pH before treatment was slightly acidic (6.4) but appears to be adjusted after treatment (7.5) and at the consumer taps (7.4). Comparing pH of samples at the various stages indicates that the water samples before treatment appears to be below the stipulated guideline of 6.5–8.5. This suggests acidity and acidity in water can aid dissolution of minerals which can likely influence the total dissolved solids (TDS) and colour of water [25]. Water samples before treatment generally showed high levels of contaminants above the stipulated drinking water guidelines with colour (54.13TCU), turbidity 20.16 NTU), TDS (633.38 mg/L), total hardness (212.81 mg/L) and total coliform count (42.35 cfu/100mL) significantly exceeding the drinking water guidelines. This was consistent with findings from similar studies [3, 10, 26] and was expected because surface water particularly in close

Table 3. Descriptive statistics of distributed water samples

Parameters	NIS/WHO standards	Mean	St. Dev	SE mean	Range		P-values
					Min	Max	
Temperature (°C)	Ambient	21.49	0.49	0.111	20.60	22.20	WR
pH	6.5–8.5	7.4	0.23	0.052	7.0	7.8	WR
Colour (TCU)	15	14.93	1.35	0.302	12.10	17.30	0.590*
Turbidity (NTU)	5	7.80	1.51	0.338	5.30	10.80	0.000***
TDS (mg/L)	500	496.58	23.89	5.34	450.10	535.70	0.735*
Hardness (mg/L)	150	150.88	10.00	2.24	130.10	168.5	0.350*
Total coliform (cfu/100 mL)	10	23.55	7.43	1.66	9.00	37.00	0.000***

Min: Minimum; Max: Maximum; St. Dev: Standard deviation; SE Mean: Standard error mean; ***: Significantly exceeds WHO drinking water standard; *: Within WHO drinking water standard; WR: Within stipulated range.

**Figure 2.** Broken pipes indicating potential contamination pathways within the city.

proximity to agricultural and residential areas is highly susceptible to contamination. In addition, studies by [2, 9] showed similar findings along the upstream of the case study area which indicates that high concentrations of contaminants have been recorded along the river which feeds the treatment plant.

However, the result after treatment showed a significant reduction and removal of some of the contaminants (Table 2) when compared with the samples before treatment. Findings indicates that the pH was improved from 6.4 to around 7.5 after treatment. In addition, colour (13.9 TCU), TDS (427.02 mg/L), and total hardness (148.73 mg/L) have been reduced significantly and are now within the stipulated drinking water guidelines. Although, turbidity (6.74 NTU) and total coliform count (17 cfu/100 mL) were still above the stipulated standards even after treatment, they were significantly reduced during the treatment process. The removal indicates that the treatment plant is effective in reducing some of the contaminants but not to the desired level stipulated by the WHO and NIS drinking water guidelines.

Water samples at the consumer's taps shows that although some of the parameters were significantly removed, there appears to be an increase in some parameters. For instance, colour which was 13.7 TCU after treatment increased to 14.93 TCU at the consumers tap within Wukari township. The same was noticed with turbidity (from 6.74 to 7.8 NTU), TDS (from 427.01 to 496.58 mg/L), total hardness (from 148.73 to 150.88 mg/L) and coliform count (from 17 to 23.55 cfu/100mL). This suggests that there was a source of contamination either within the distribution system or at the consumers tap. However, a site visit revealed broken pipes (Fig. 2) which not only accounts for loss of water but serves as a medium for contamination flowing back into the pipes. This could likely be the cause of disparity between the water samples after treatment and at the consumers tap.

Analysing Difference Before and After Treatment and at Consumer Taps

Analysing the differences in water quality before treatment, after treatment and at the distribution point showed that there were significant differences in the means of parameters which suggests that the treatment plant is removing

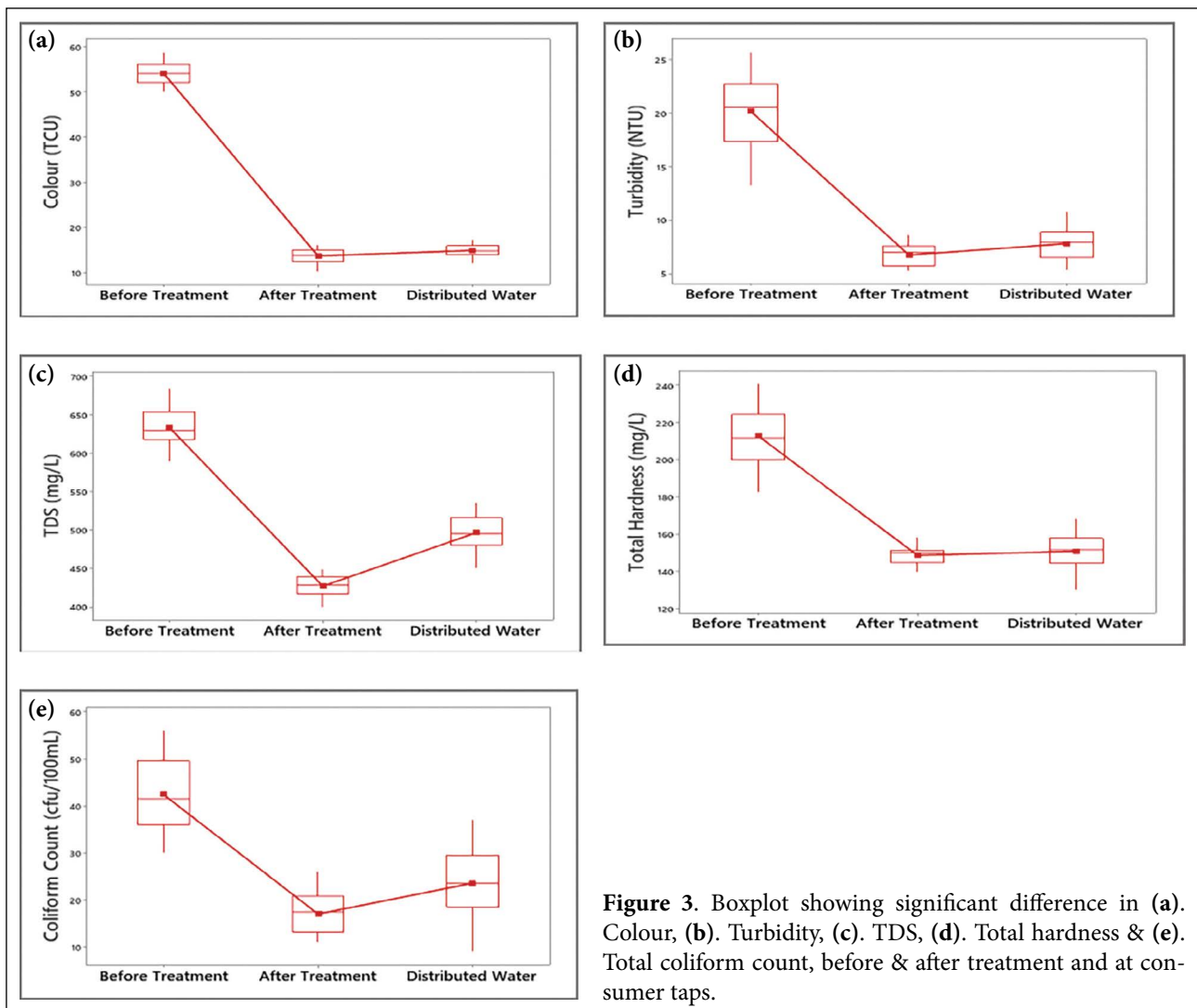


Figure 3. Boxplot showing significant difference in (a). Colour, (b). Turbidity, (c). TDS, (d). Total hardness & (e). Total coliform count, before & after treatment and at consumer taps.

the contaminants. However, the removal may not be to the desired level especially since there are still parameters that were not removed to conform to the stipulated drinking water standards. Analysis of variance (ANOVA) showed that the means of all parameters were significantly different (Table 4), particularly the means of samples before treatment and after treatment (Fig. 3). However, the means of samples after treatment and at consumer taps appears to be insignificant, a 2-sample test needs to be carried out to assess the difference in samples after treatment and during distribution at the consumer taps.

Analysing Difference Between Water After Treatment and Water at Consumer Taps

The results from a 2-Sample T-test indicates that there were significant differences between colour after treatment and at consumer taps with a p-value of 0.008. Similarly, the results for turbidity (p=0.014), TDS (p=0.000), and coliform count (p=0.002) were also found to be significant (Fig.

Table 4. ANOVA for difference in water before and after treatment and at consumer taps

Parameters	P-value	F-value	R-Sq (%)
Colour (TCU)	0.000	322.19	99.12
Turbidity (NTU)	0.000	227.03	88.85
TDS (mg/L)	0.000	471.09	94.30
Total Hardness (mg/L)	0.000	201.27	87.60
Total Coliform (cfu/100 mL)	0.000	77.43	73.09

4a–c, e). However, total hardness showed no significant difference (p=0.406) between water after treatment and at consumer taps (Fig. 4d). This analysis suggests that the rate of contamination of water during distribution is significant and can likely pose a serious health concern. Although the parameters that exceeded the standard after treatment, remained the same parameters that exceeded standard at the customer taps, the increase in concentration may like-

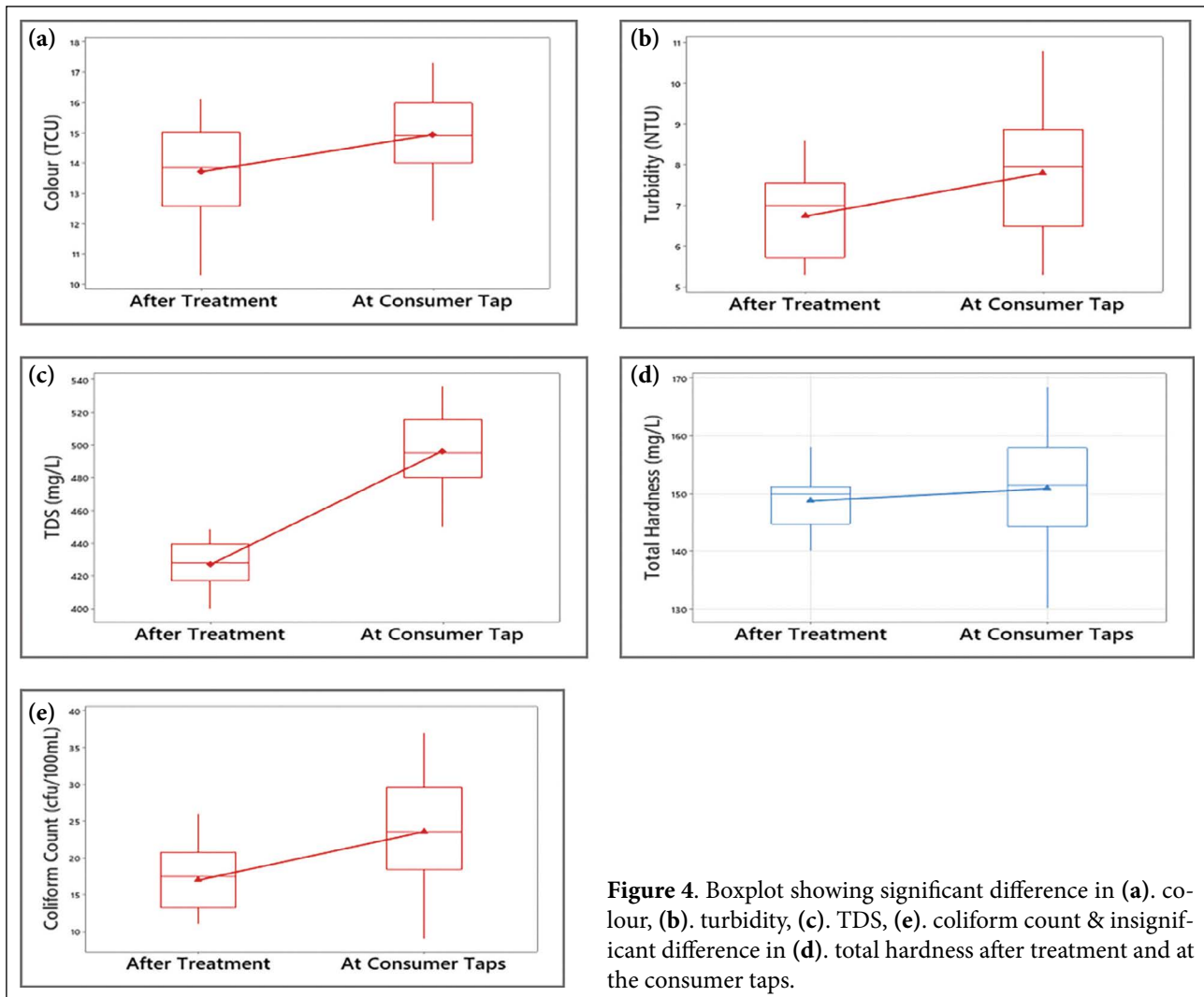


Figure 4. Boxplot showing significant difference in (a). colour, (b). turbidity, (c). TDS, (e). coliform count & insignificant difference in (d). total hardness after treatment and at the consumer taps.

ly impact vulnerable children, elderly people and visitors who have not been exposed to such level of contaminants. The difference may likely be due to broken pipes (Fig. 2) at various point in the distribution system. The findings of the study corroborate with findings from [19] which indicates that leakages from pipes can severely impact water quality.

Implication of Broken Pipes on Water Quality

Historically, the provision of piped water within homes have been associated with improve sanitation and hygiene and a significant decrease in water related diseases [19, 20]. However, with continuous stress, poor maintenance and ageing of water infrastructure, water distribution systems are likely to become vulnerable to contamination. The loss of water along the distribution system accounts for a substantial volume of water and energy annually, and although the water pipe system in the study area is not metered, and therefore water loss cannot be accounted for (Fig. 5), but however, the risk to water contami-

nation through these leaking pipes has been identified. Materials used in water distribution systems (including pipes) have different life span and therefore require monitoring to ensure that they do not deteriorate to the point that they pose severe risk to the quality of water that is being distributed [19].

Efficiency of the Treatment Plant

The efficiency of the treatment plant was computed based on the removal efficiency (RE) of each of the parameters assessed. The efficiency is computed and expressed as a percentage using the formula:

$$\text{Removal efficiency} = \frac{\text{influent} - \text{effluent}}{\text{influent}} \times 100 \quad (1)$$

The RE was computed and tabulated in Table 5. The computation indicates that colour had a removal efficiency of 74.69%, turbidity (66.57%), TDS (32.58%), total hardness (30.11%), and coliform form count (59.88%). The study result is in conformity to findings from [10, 11, 13]. This suggests that the treatment plant is indeed removing the



Figure 5. Water loss during pumping due to broken pipes within the city.

Table 5. Removal efficiency of the treatment plant

Parameters	Influent	Effluent	R.E (%)
Colour (TCU)	54.14	13.7	74.69
Turbidity (NTU)	20.17	6.74	66.57
TDS (mg/L)	633.38	427.02	32.58
Total Hardness (mg/L)	212.81	148.73	30.11
Coliform count (cfu/100 mL)	42.35	17	59.88

R.E: Removal efficiency expressed as percentage.

contaminants but however not to the desired level. For instance, in a study by [27], the removal of colour should be at least around 86% to ensure water is aesthetically acceptable by most consumers. This however indicates that all though colour in our study was removed to conform to drinking water standards, the RE was not adequate.

This can be seen in our study results indicating colour with mean value of 13.7 TCU at a RE of 74.7%. A further increase in RE to the minimum 80% suggested by [27] will likely decrease colour to under 12TCU. Similarly, the removal of turbidity at 66.6% was not sufficient to reduce turbidity to conform to drinking water standard. More so, findings from [28] suggests a RE of over 90% to adequately reduce turbidity which will increase the removal of bacterial contaminants. Total hardness and TDS having a low RE indicating failure of the plant in effectively removing contaminants. Ineffective removal efficiency of dissolved solids can suggest poor removal of metals and other chemical contaminants in water. Consequently, there was a low RE of biological contaminants which also suggest risk to public health particularly because coliform count was significantly greater than the stipulated drinking water standards. The treatment plant showed an overall efficiency of 52.77% (Fig. 6) which is not sufficient especially to service two local government areas with large scale agricultural activities. The study outcome therefore suggests the need to assess each stage of the treatment plant process to understand how each stage performs.

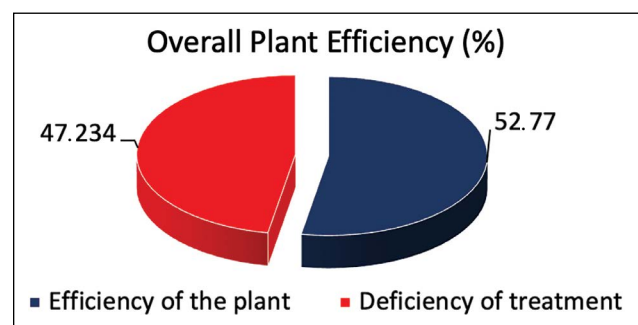


Figure 6. Overall treatment plant efficiency and deficiency (%).

A study by [19] showed that there could be improper dosage of coagulant and disinfectants during the treatment process. This can explain the inefficient removal of turbidity and bacteriological contaminants in water. A site visit indicates that the water treatment plant lacks a functional laboratory for testing and analysing water before and during every treatment stage. The addition of coagulating agents plays a key role in the removal of solids, colour and turbidity while disinfecting agents eliminates bacteriological parameters. Dosing these agents in the treatment plant requires adequate computation to ensure the right dosage is used at any given point. The findings suggests that these treatment agents are underutilised, probably because of poor funding or due to unqualified personals. There is therefore the need for adequate monitoring of water at every treatment stage to ensure that water leaving one stage for another is effectively treated before it gets to the final stage of disinfection and subsequent distribution.

Proposed Approach to Improve Water Treatment Using Low-cost Activated Carbon

Some of challenges confronting Ibi drinking water treatment plant is high treatment costs. Thus, there is dire need to explore alternatives ways to reduce costs without negatively affecting the quality of water delivery [21]. In this section, sustainable methods of improving drinking water properties using novel bio sorbent material developed from biomass waste as suggested by [29] is proposed. This will open a

new way of water treatment in Ibi by using low-cost activated carbon made from locally available organic waste and at the same time expand waste management options for these readily available biomass materials. Ibi climatic condition are conducive for cultivation of a large variety of biomasses. Due to the richness of the minerals in the parent rock; these soils are generally well suited for rice, maize, guinea corn likewise arable farming and tree crops production. According to [30], utilizing local residual biomass as a raw material for removal of organic micropollutants in water treatment plants may be advantageous in terms of sustainability.

It has been observed that state government resources and interventions towards sustaining water supply in Ibi town and environs have been insufficient [21]. The result has been constant water crisis and shortages over the years. This study recommends a paradigm shift from the use of conventional and costly coal-derived activated carbon to activated developed from green sources. In the literature, green activated carbon materials have been used extensively in drinking water treatment in various roles, including removal of colour, turbidity and micro-pollutants [31]. New materials have also been discovered in the world of natural coagulants and adsorbents [32, 33] to improve drinking water properties. Granular activated carbon (GAC) media [34, 35] of various origins coal, coconut shell [36] and bovine bone) and providing a range of physical characteristics with reference to pore size, have been appraised with reference to their capacity for natural organic matter [37].

CONCLUSION

The water quality before and after treatment was assessed and compared with the stipulated drinking water standard. The study showed that the treatment was not effective in removing some parameters and hence require further assessment. The overall efficiency was below expectation which could potentially impact public health. Additionally, dilapidated water distribution infrastructure is now a potential source of contamination which needs to be addressed in order to supply potable drinking water to the inhabitants of Ibi and Wukari town. Furthermore, low-cost activated carbon was proposed to compliment the conventional treatment process for effective removal of contaminants. In addition, the government needs to invest in infrastructure, skilled personal and operational inputs such as diesel and water treatment chemicals.

ACKNOWLEDGMENT

We wish to acknowledge Engr. Emmanuel Bassah, Dr. Wandia Yaduma and Mrs Mada Abass for their time, and positive feedback during the production of the first and final draft. We also like to appreciate the member of staff of Biological Sciences, Federal University Wukari and the staff of Ibi treatment plant without who this research project won't have been feasible. Your contribution and support during the collection and laboratory assessment of water sample is highly appreciated.

DATA AVAILABILITY STATEMENT

The authors confirm that the data that supports the findings of this study are available within the article. Raw data that support the finding of this study are available from the corresponding author, upon reasonable request.

CONFLICT OF INTEREST

The authors declared no potential conflicts of interest with respect to the research, authorship, and/or publication of this article.

ETHICS

There are no ethical issues with the publication of this manuscript.

REFERENCES

- [1] R. Kumar, V. Sharma, and R.C. Sharma, "Physico-chemical and Microbiological water quality of Asian wetland of Garhwal Himalaya, India," *International Journal of Ecological Science and Environmental Engineering*, Vol. 5(3), pp. 64–70, 2018.
- [2] W.K Joshua, Groundwater quality assessment: a case study of groundwater from hand-dug wells in Hawul Local Government Area of Borno State," *International Journal of Advance Research*, Vol. 3(2), pp. 537–546, 2015.
- [3] A.Q. Ibrahim, P.C. Onyenekwe, and I.M. Nwaedozie, "An efficiency assessment of lower usuma water treatment plant in abuja metropolis, Nigeria," *Journal of Environmental Science*, Vol. 8(12), pp. 46–53, 2014. [\[CrossRef\]](#)
- [4] A.G. Olufemi, O. Oghenechuko Utieyin, and O.M. Adebayo, "Assessment of groundwater quality and saline intrusions in coastal aquifers of lagos metropolis, Nigeria," *Journal of Water Resource and Protection*, Vol. 2(10), pp. 849–853, 2010. [\[CrossRef\]](#)
- [5] World Health Organization, "Guidelines for Drinking Water Quality", 3rd ed., Geneva: Switzerland: World Health Organization, 2006.
- [6] L.P. Chegbeleh, D.K. Aklika, and B.A. Akurugu, "Hydrochemical characterization and suitability assessment of groundwater quality in the saboba and chereponi districts, Ghana," *Hydrology*, Vol. 7(3), pp. 53–60, 2020. [\[CrossRef\]](#)
- [7] A. Shea, J. Poon, and S. Williamson, "Microbial risk assessment of drinking water to set health-based performance targets to improve water quality and treatment plant operations," *Water Practice and Technology*, Vol. 11(2), pp. 495–502, 2016. [\[CrossRef\]](#)
- [8] A.S. Al Chalabi, "Assessment of drinking water quality and the efficiency of the Al-buradieiah water treatment plant in Basra city," *Nature Environment and Pollution Technology*, Vol. 19(3), pp. 1057–1065, 2020. [\[CrossRef\]](#)

- [9] W.K. Joshua, "Assessing Rural Water Quality: comparing improved and unimproved drinking water sources in Hawul LGA," *SNRU Journal of Science and Technology*, Vol. 13(2), pp. 55–62, 2021.
- [10] M. Mustapha, M. Sridhar, and A.O. Coker, "Assess-ment of water supply system from catchment to consumers as framed in East Nigeria," *Sustainable Environment*, Vol. 7(1), pp. 1–14, 2021. [CrossRef]
- [11] M. Mustapha, M. Sridhar, A.O. Coker, A. Ajayi, and A. Suleiman, "Risk Assessment from catchment to consumers as framed in water safety plans: A study from Maiduguri water treatment plant, Northeast Nigeria," *Journal of Environmental Protection*, Vol. 10(10), pp. 1373–1390, 2019. [CrossRef]
- [12] A. Alver, "Evaluation of conventional drinking water treatment plant efficiency according to water quality index and health risk assessment," *Environmental Science and Pollution Research*, Vol. 26(26), pp. 27225–27238, 2019. [CrossRef]
- [13] B.O. Akinnuli, P.P. Ikubanni, E.A. Fadiji, and O.O. Agboola, "Drinking water quality assessment of a hand dug well using treatment plant installed in Akure, Nigeria," *Journal of Engineering and Applied Sciences*, Vol. 14(15), pp. 5236–5240, 2019. [CrossRef]
- [14] T. Sisay, A. Bevene, and E. Alemayehu, "Spatiotemporal variability of drinking water quality and the associated health risk in Southwestern towns of Ethiopia," *Environmental Monitoring and Assessment*, Vol. 189(11), pp. 208–212, 2017. [CrossRef]
- [15] B. Desye, B. Belete, Z. Asfaw Gebrezgi, and T. Terefe Reda, "Efficiency of treatment plant and drinking water quality assessment from source to Household, Gondar City, Northwest Ethiopia," *Journal of Environmental and Public Health*, Vol. 201, pp. 1–8, 2021. [CrossRef]
- [16] M.T. Martins, G. Castillo, and B. J. Dutka, "Evaluation of drinking water treatment plant efficiency in microorganism removal by the coliphage, total coliform and H2S paper strip tests," *Water Science and Technology*, Vol. 35(11), pp. 403–407, 1997. [CrossRef]
- [17] United Nations, "Ensuring Available Sustainable Management of Water and Sanitation for all," <https://sdgs.un.org/goals/goal6> Accessed November 6, 2021.
- [18] E.A. Badr, and A.A. Al-Naeem, "Assessment of drinking water purification plant efficiency in Al-Hassa, Eastern Region of Saudi Arabia," *Sustainability*, Vol. 13(11), pp. 6122–6129, 2021. [CrossRef]
- [19] A.S. Hassan, J. Musa Hayatu, and I.U. Mohammed, "An overview of water supply infrastructural chal- lenges in Nigeria: A case study of Taraba state," *Jour- nal of Mechanical and Civil Engineering*, Vol. 13(1), pp. 46–51, 2016.
- [20] E.A. Adams, Y.I. Adams, and C. Koki, "Water, sanitation and hygiene (WASH) insecurity will exacerbate the toll of COVID-19 on women and girls in low-income countries," *Sustainability, Science, Practice and Policy*, Vol. 17(1), pp. 86–90, 2021. [CrossRef]
- [21] H.T. Ishaku, M.A. Hussain, F.M. Dama, A.A. Zemba, and A.A. Peter, "Planning for water in Wukari," *Journal of Water Resources and Protection*, Vol. 2(1), pp. 916–922, 2010. [CrossRef]
- [22] Nigerian Industrial Standard, "Nigerian Standards for Drinking Water Quality," Abuja, Nigeria: Standard Organization of Nigeria, 2007.
- [23] American Public Health Association, "Standard Methods for Examination of Water and Wastewater". Washington D.C.: American Public Health Association, 1998.
- [24] M. Radojevic, and V.N. Bashkin, "Practical Environmental Analysis," 2nd ed., Cambridge, UK: Royal Society of Chemistry, 2006.
- [25] R. Amfo-Out, J.B. Agyenim, and G.B. Nimba-Bumah, "Correlation analysis of groundwater colouration from mountainous areas, Ghana," *Environmental Research, Engineering and Management*, Vol. 67(1), pp. 16–24, 2014. [CrossRef]
- [26] M.H. Geriesh, B.M.H. Mansour, and H. Farouk, "Assessment of drinking water quality along Port Said Canal treatment plants, Suez Canal corridor, Egypt," *Arabian Journal of Geosciences*, Vol. 12(23), pp. 1–13, 2019. [CrossRef]
- [27] M. Malakootian, and A. Fatehizadeh, "Colour removal from water by coagulation/caustic soda and lime". *Iranian Journal of Environmental Health Science and Engineering*, Vol. 7(3), pp. 267–275, 2010.
- [28] B. Ramavandi. "Treatment of water turbidity and bacteria by using a coagulant extracted from *Plantago ovata*," *Water Resources and Industry*, Vol. 6, pp. 36–50, 2014. [CrossRef]
- [29] S.K. Shukla, N. Al Mushaigri, S. Rashid, H.M. Al Subhi, K. Yoo, and H. Al Sadeq, "Low-cost activated carbon production from organic waste and its utilization for wastewater treatment," *Applied Water Science*, Vol. 10(2), pp. 1–9, 2020. [CrossRef]
- [30] B. Joseph, K. Kaetzl, F. Hensgen, B. Schäfer, and M. Wachendorf, "Sustainability assessment of activated carbon from residual biomass used for micropollutant removal at a full-scale wastewater treatment plant," *Environmental Research Letters*, Vol. 15(6), Article 064023, 2020. [CrossRef]
- [31] W.A. Abel, A. Jimoh, A.S. Abdulkareem, and A. Giwa, "Production of activated carbon from watermelon peel," *International Journal of Scientific and Engineering Research*, Vol. 5(2), pp. 66–71, 2014. [CrossRef]

- [32] K.J. Choi, S-G. Kim, and S-H. Kim, “Removal of antibiotics by coagulation and granular activated carbon filtration,” *Journal of Hazardous Materials*, Vol. 151(1), pp. 38–43, 2008. [\[CrossRef\]](#)
- [33] K. Konieczny, and G. Klomfas, “Using activated carbon to improve natural water treatment by porous membranes”. *Desalination*, Vol. 147(1), pp. 109–116, 2002. [\[CrossRef\]](#)
- [34] A.T. Alves, D.J. Lasmar, I.P. de Andrade Miranda, J. da Silva, and J. dos Santos Reis, “The potential of activated carbon in the treatment of water for human consumption, a study of the state of the art and its techniques used for its development,” *Advances in Biosciences and Biotechnology*, Vol. 12, pp. 143–153, 2021. [\[CrossRef\]](#)
- [35] J. Jjagwe, P.W. Olupot, E. Menya, and H.M. Kallibbala, “Synthesis and application of granular activated carbon from biomass waste materials for water treatment: A review,” *Journal of Biore-sources and Bioproducts*, Vol. 6(4), pp. 292–322, 2021. [\[CrossRef\]](#)
- [36] X. Xing, T. Li, Z. Bi, P. Qi, Z. Li, H. Wang, L. Lyu, Y. Gao, and C. H., “Efficiency removal of disinfection by-products precursors and inhibition of bacteria detachment by strong interaction of EPS with coconut shell activated carbon in ozone biofiltration,” *Journal of Hazardous Materials*, Vol. 392, Article 122077. [\[CrossRef\]](#)
- [37] D.M. Golea, P. Jarvis, B. Jefferson, G. Moore, S. Sutherland, S.A. Parsons, and S.J. Judd. “Influence of granular activated carbon media properties on natural organic matter and disinfection by-products precursor removal from drinking water,” *Water Research*, Vol. 174, Article 115613. [\[CrossRef\]](#)



Research Article

Principal component analysis in long term assessment of total viable plate count of municipal water distribution network system in healthcare facility

Mostafa ESSAM EISSA¹, Engy REFAAT RASHED², Dalia ESSAM EISSA³

¹Independent Researcher, Pharmaceutical and Healthcare Research Facility, Cairo, Egypt

²National Centre for Radiation Research and Technology, Cairo, Egypt

³Royal Oldham Hospital, Oldham, United Kingdom

ARTICLE INFO

Article history

Received: 25 January 2022

Revised: 19 April 2022

Accepted: 27 April 2022

Key words:

Eigen value; Loading plot;
Outlier diagram; PCA; Score
graph; Scree plot

ABSTRACT

The microbial quality of water is a critical safety aspect that should not be overlooked, especially when considering human consumption in the facilities for healthcare and the treatment of health compromised populations. The present work aimed to study a municipal network for city water within a healthcare facility microbiologically. The implementation of multivariate analysis was conducted over collected data to decipher trends of the microbiological count of samples from different points-of-use. The statistical study involved an Eigenvalue determination, score graph, loading plot study and outlier diagram. Data showed clustering tendency with aberrant values could be observed. The first component appeared to be associated with bioburden density in the water. While the other component showed a link to the relative locations of the distribution points in the facility and the length of the water lines from the source feeding city water to a great extent. The two components explained more than 55% of the variations in data. A property that highlighted a strong agreement between the order of points-of-use in the loading plot with that of ratio factor which was obtained from the Total Viable Count over the hypothetical distance of sampling port from the reference feeding entrance. Thus, there was evidence of variation in the microbial quality affected by the biological stability of the water distribution system that needed attention and an improvement plan for better control of microbial content in city water to prevent possible excursions in the future. The study showed a valuable perspective approach for the quantitative examination of the microbiological stability of the municipal water distribution network system.

Cite this article as: Essam Eissa M, Refaat Rashed E, Essam Eissa D. Principal component analysis in long term assessment of total viable plate count of municipal water distribution network system in healthcare facility. Environ Res Tec 2022;5:2:165–171.

INTRODUCTION

The microbiological quality of water is a crucial criterion that must be met for safe human use and consumption of city water as could be concluded from previous researchers' work [1]. This characteristic would become

even more demanding if it was to be considered in healthcare facilities such as hospitals where health-defected populations might be exposed to external sources of microbes and it is a subject of concern for international health organizations such as World Health Organization (WHO) [2].

*Corresponding author.

*E-mail address: mostafaessameissa@yahoo.com



Biological stability is one of the important properties of the municipal water distribution system as could be demonstrated by Gauthier et al. [3]. This stability ensures the predictable quality and consistency of the delivered water to the final consumers as could be demonstrated according to WHO (2017) [4]. Saha and Donofrio work showed a microbiological study of the metalworking which might lead to a concern that any uncontrolled excursions in the bioburden could lead to undesirable consequences, especially with significantly variable microbiological properties [5]. Several control techniques such as exposure to Ultraviolet (UV) irradiation and application of biocidal agents have been used [5, 6].

When considering a large amount of data gathered for microbiological trends of water distribution networks, the implementation of the multivariate analysis should be considered to analyze the biological quality of this type of complex system. Principal component analysis (PCA) is a multivariate data analysis tool commonly used to reduce the dimension (number of variables) of many interconnected variables while retaining as much information (variation) as possible. PCA calculates a set of uncorrelated variables (components or PCs). These components are ordered so that the first few hold the most variability that is present in all the original variables [7–10].

The present study aimed to investigate the microbiological stability of municipal water distribution network systems using a multivariate analysis approach. The study focused on the use of total bioburden count parameter in water examination as an indicator for the biological stability of city water. This work investigated the variability and the association in the microbiological quality between different sections of the water distribution system. Based on the outcome of the research herein, further investigation might be extended to cover other quality inspection criteria such as objectionable microorganisms' trend with dissemination profile, Total Organic Carbon (TOC) and conductivity.

MATERIALS AND METHODS

Long-term data collection – for 45 successive months - was performed for regular monitoring of the investigated subject for Multivariate Analysis (MVA) study following a discussion by Great Learning Team [11].

Subject Study

Healthcare facility with distribution water network system that gained its feed supply of city water from a municipal line was studied following the method described by Ainsworth [12]. The distribution of the piping network supplied different compartments in the plant and each section has its own sampling port from which routine samples of city water were collected for analysis.

Collection of Samples

Water samples were collected aseptically in sterile bottles from each functioning point-of-use after prior allowance for appropriate flushing as described by Essam Eissa and EMSL Analytical [13, 14]. Well-closed sample bottles were submitted for analysis immediately within two hours so that the aseptically collected samples would be analyzed freshly as soon as possible to avoid any variations from the original microbial count. The guidance provided with appropriate modifications were done following United States Environmental Protection Agency (USEPA) (2016) [15]. Storage of water bottles in refrigerator (2–8°C) was ensured for about eight hours, if samples would not be treated at once in the laboratory [15].

Microbiological Testing of Water Samples

Water samples were tested microbiologically using aseptic tools and techniques to avoid extraneous contamination. Sterile, single-use and 0.45 µm disposable membrane filters were used to collect microorganisms in a definite volume of water sample through a vacuum filtration system where filters were transferred aseptically over agar media for detection of coliforms and enumeration of the Total Viable Aerobic Count (TVAC) following method given by Eissa (2018a) [13]. The plates were incubated and counted for determination of the number of Colony Forming Unit (CFU) per unit volume of water and for detection of the characteristic appearance of the pathogen colonies. Francy et al. and Ngwa et al. [16, 17] had provided guidance for microbiological testing of water samples. Confirmatory biochemical tests were conducted for any suspicious colonies using appropriate identification kits such as API following Gram staining technique.

Data Collection and Processing

All observations of the results were recorded in the columns of the worksheets of commercial statistical software. Goldwater demonstrated the use of Excel program for data analysis [18]. Datasets were arranged in chronological order with all use points identification codes assigned for each column in GraphPad Prism program [19]. Each sampling port had a "C" letter followed by its serial number for location identification i.e. C1, C2, C3, etc. The processed database was subjected to statistical analysis and multivariate study using Principal Component Analysis (PCA) as could be described earlier by Eissa and colleagues [20].

RESULTS AND DISCUSSIONS

The present study covered the long-term trend monitoring of the total microbiological plate count of the city water in a limited location of the distribution network system in a selected healthcare facility over 45 months of regular sampling and analysis which was done as previously performed by similar work in other circumstances [13]. No objection-

Table 1. Eigen analysis of the Correlation Matrix for sampling ports from C1 to C13 of water distribution system

PCA of Correlation-Type Matrix [£]			
Component number [€]	Latent roots [£]	Proportion	Cumulative
1	6.0278	0.464	0.464
2	1.5004	0.115	0.579
3	1.1142	0.086	0.665
4	1.0200	0.078	0.743
5	0.8159	0.063	0.806
6	0.6216	0.048	0.854
7	0.5429	0.042	0.896
8	0.3502	0.027	0.923
9	0.2740	0.021	0.944
10	0.2477	0.019	0.963
11	0.2156	0.017	0.979
12	0.1651	0.013	0.992
13	0.1044	0.008	1.000

¥: Computation was done using Minitab® 17.1.0.0; £: Characteristic values: The variances of the principal components; € The components were studied as a linear combinations of the originally recorded variables.

able or pathogenic microorganisms were detected which followed the same working principle as done by Essam Eissa but with different outcome [21]. A low level of the microbial count was observed in most samples with all representative use points – for the different sections of water lines – were significantly ($p=0.05$) lower in bioburden content than the reference of the maximum threshold acceptance criterion of 100 CFU/mL which was similar in the outcome as in the previous work. A possible explanation for the observed low level of the microbial count could be attributed to the presence of the residual amounts of the sanitizing agent in the municipal water to deliver water with acceptable microbiological quality for human consumption.

Multivariate analysis using PCA in Table 1 showed Eigen values and the proportion of each component along with the cumulative contribution using the correlation-type of the matrix [22]. The first, second and third components contributed 46.4%, 11.5% and 8.6% of the variance that they could explain, respectively. Based on the selection for the Pareto principle of 60/40, the first three components would explain more than 66% of variations in the database [23]. Dimensionality reduction was ensured by including the highly influential and acceptable number of the principal components that could account for most of the variability [24]. With this respect, the fifth component was the first component number that yielded a characteristic value lower than unity with the cumulative contribution of the first five PCs above 80% from the total computed factors as

Table 2. Multivariate analysis of municipal water network of the first three principal components (PCs)

Dimensionality reduction [¥]			
Variables [€]	PC1	PC2	PC3
C1	0.305	0.307	-0.136
C2	0.279	0.347	-0.171
C3	0.303	0.347	-0.171
C4	0.172	0.332	0.693
C5	0.304	-0.297	0.214
C6	0.262	-0.254	0.470
C7	0.304	-0.171	-0.132
C8	0.333	-0.030	-0.331
C9	0.253	-0.116	0.178
C10	0.301	-0.263	-0.049
C11	0.307	-0.286	-0.131
C12	0.303	0.065	-0.141
C13	0.054	0.373	0.065

¥: Calculation was done using Minitab® 17.1.0.0; €: PCA was used to reduce the datasets into a smaller number of components.

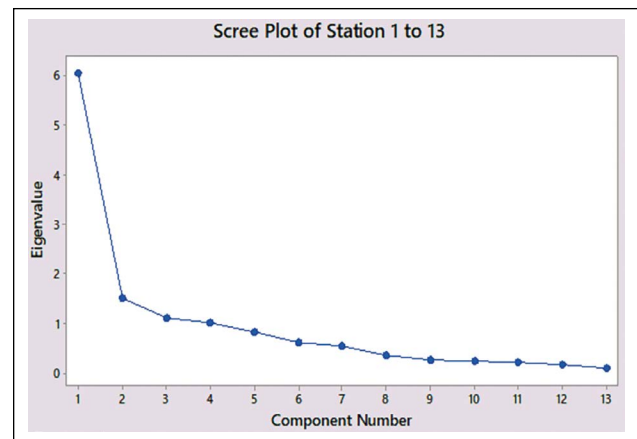


Figure 1. Scree diagram showing that the first five components could explain more than 80% of data variability.

could be seen in Figure 1. Based on the Kaiser criterion, PCs with latent values greater than one should be considered in the analysis [24]. Nevertheless, the scree graph started to form an almost straight line after the third component with a transition elbow curve between the second and the third components could be detected.

From the previous argument, the three first PCs would be considered in the present study for simplification and insight into data visualization. Table 2 showed the coefficient for each component calculated for each contributing variable i.e. use points representing different parts of the municipal water distribution system [24]. The greater the absolute fig-

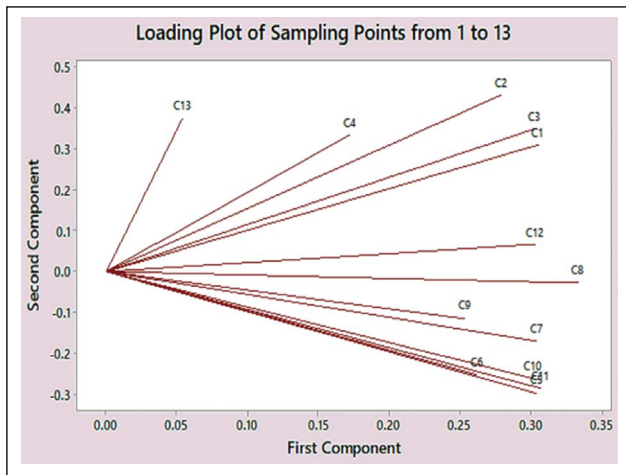


Figure 2. Loading diagram showing the influence of different points-of-use in the water distribution network on both the first and second components.

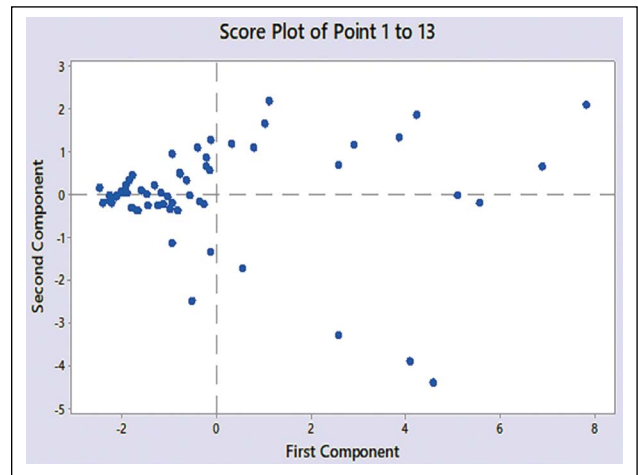


Figure 3. Score diagram showing data distribution, trend and pattern surrounding the reference zero point, in addition to the detection of outliers and clustering tendency.

Table 3. Aberrant values detection and removal statistically using ROUT method

Method*	ROUT [‡] (Q=1.000%)**													Overall network
	Distribution points in facility													
	C1	C2	C3	C4	C5	C6	C7	C8	C9	C10	C11	C12	C13	Average
Number of points Analyzed	59	59	59	59	59	59	59	59	59	59	59	59	59	59
Outliers [€]	12	6	12	8	9	11	8	10	6	11	13	8	10	7

*: Q is the maximum False Discovery Rate (FDR); **: Computation was done using GraphPad Prism for Windows version 6.01; ‡: Robust regression and Outlier removal combination technique; €: Aberrant values extracted from a non-linear regression.

ure of the coefficient, the more influential the corresponding water distribution section is in calculating that component. From Table 2, the descending order for the effect of points-of-use on the first component was as the following: C8, C11, C1, C5, C7, C3, C12, C10, C2, C6, C9, C4 and C13. Concerning the second component, the decrease in the coefficient was as the following: C13, C3, C2, C4, C1, C12, C8, C9, C7, C6, C10, C11 and C5. Finally, the last component showed the following descending order: C4, C6, C5, C9, C13, C10, C11, C7, C1, C12, C3, C2 and C8. A more in-depth focus on the first two components was desired since these two PCs only accounted for about 58% of the variability in the database of the total microbiological water plate count.

The loading plot in Figure 2 showed the contribution of each section of the municipal water distribution network on the first two principal components that demonstrated the main impact on the data variability of microbiological plate count [25]. The first component appeared to be affected by the microbiological density expressed as CFU/mL where all points were located at the positive side of the x-axis (PC1). Accordingly, monitoring ports C13 and C4 showed a lower trend in HPC. PC2 likely added another dimensionality of the relative locations for different lines with respect to the feeding source

[25]. Thus, the microbial burden in water over the length of the water line might determine a positive quality (+y-axis) versus negative municipal water quality (-y-axis), a marker that could be used as one of the indicators for microbiological stability through the facility network system. This marker would explain bioburden quality as total microbial count over distance from the reference entry point of the distribution water section. Moreover, the graph demonstrated correlated points at minor and gross levels [26]. Normally, the biological quality of the feeding source influences that of the distribution network. However, at a smaller scale the microbiological quality level would be affected by the flow pattern of water in different sections, in addition to the state of the distribution system at different affected sections ex. corruptions. Other factors such as hygiene level, microbial sources and human population density cannot be ruled out as possible influential factors in the observed microbial trend. At a gross level, three groups were identified C1→C4, C5→C12 and solitary C13 that stands alone. On the other hand, small-scale correlation showed a closer association between C5, C6, C10 and C11 following GraphPad Software LLC guiding manual [27]. In the same line, a binary closer correlation was found between C1 and C3, in addition to C7 and C9.

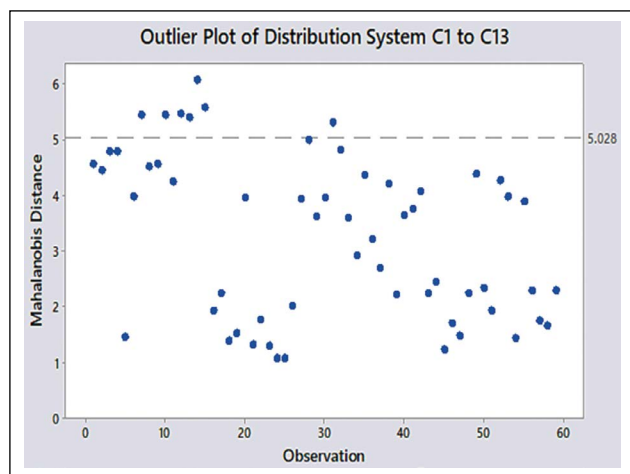


Figure 4. Outlier diagram showing outlier values due to unusual high values in microbiological count data.

The score plot was used as a scatterplot charting for the first component against the second one. There was a shred of strong evidence for clustering tendency that could be observed in the left side of the y-axis in the score plot in Figure 3. Moreover, outlier values could be expected also as some remote and isolated values were spotted toward the edges at the right position above and below the +x-axis [20, 26, 28]. Sporadic high values in the database records were detected, despite no Out-Of-Specification (OOS) results could be detected as all results were below the regulatory acceptance specification limit of 100 CFU/mL. In addition, Points were not randomly dispersed in the graph [25]. Accordingly, data did not show the expected behavior of the normal distribution spreading with possible skewness would be expected due to solitary excursions in the microbial count of water samples.

Since aberrant values could be spotted in the preceding section, the presence of excursion would be analyzed. Possible reasons for such abnormal results include the quality state of the piping system and the nature of water circulation and flushing, in addition to the design geometry. Also, the presence of dead ends and/or stagnant spots cannot be ruled out. A preliminary analysis for detection of the excursions was done using ROUT method – at recommended $Q=1.000\%$ - in GraphPad Prism version 6.01 [29]. The results obtained in Table 3 showed the following ascending order of the outlier rates (expressed as percent): (C2, 10.17%), (C9, 10.17%), (C4, 13.56%), (C7, 13.56%), (C12, 13.56%), (C5, 15.25%), (C8, 16.95%), (C13, 16.95%), (C6, 18.64%), (C10, 18.64%), (C1, 20.34%), (C3, 20.34%) and (C11, 22.03%). The rate of the emergence of the aberrant values for the mean of all distribution points for the overall facility assessment was 0.1186. The outlier plot displayed the Mahalanobis distance in Figure 4 for all observations, in addition to a reference line to identify outliers. The Mahalanobis distance is defined as the distance separating each data point from the centroid of multivariate space (in layman's term: the overall

mean) [25]. Examining Mahalanobis distances was viewed as a more powerful mean for discovering the outliers better than looking at a single variable at a time because it took into consideration the diverse scales between the variables and the correlations between them.

CONCLUSIONS

In conclusion, multivariate analysis was surfaced in this study when we aimed to measure the microbiological quality (in terms of TVC) of the city water within a specific facility. The first dimension was the degree of the stability of microbial count over a certain time for each water line in the plant. The outlier rate of the HPC results – even there was no OOS - over a specific period might indicate a state of abnormal variation in the quality of water which should be investigated and eliminated. The second one could be found through the PCA where the position of each segment of the water network showed considerable variation in the average total microbial count from the neighbor lines with clustering tendency was obvious indicating a significant association between the correlated points that formed grouping environment. The first PC demonstrated the imparted difference in the bioburden associated with each use point. Moreover, the tested sampling ports showed unique PC2 because of its expected link to the relative location of each point-of-use from the source feed to a great extent. No doubt that the original quality of the municipal water was basically affected by the feeding source from the supplementing city water station. However, it was out-of-scope in this study and would be evaluated in another future analysis. Nevertheless, the distribution network system within a specific facility had its influential contributing factor over water quality before reaching the consumers. Importantly, it was the methodology and the findings herein which could find their room in broader applications likewise such as different types of water including purified water and Water for Injection (WFI), in addition to the inspection of other quality characteristics of water such as Total Organic Carbon (TOC) and conductivity.

DATA AVAILABILITY STATEMENT

The authors confirm that the data that supports the findings of this study are available within the article. Raw data that support the finding of this study are available from the corresponding author, upon reasonable request.

CONFLICT OF INTEREST

The authors declared no potential conflicts of interest with respect to the research, authorship, and/or publication of this article.

ETHICS

There are no ethical issues with the publication of this manuscript.

REFERENCES

- [1] M. D. Sobsey, C. E. Stauber, L. M. Casanova, J. M. Brown, and M. A. Elliott, "Point of use household drinking water filtration: A practical, effective solution for providing sustained access to safe drinking water in the developing world," *Environmental Science & Technology*, Vol. 42(12), pp. 4261–4267, 2008. [CrossRef]
- [2] G. Duce, J. Fabry and L. Nicolle, "Prevention of hospital-acquired infections," 2nd ed., World Health Organization, Geneva, 2002.
- [3] V. Gauthier, B. Gérard, J. Portal, J. Block and D. Gatel, "Organic matter as loose deposits in a drinking water distribution system," *Water Research*, Vol. 33(4), pp. 1014–1026, 1999. [CrossRef]
- [4] World Health Organization (WHO), "Potable Re-use: Guidance for producing safe drinking-water," 2017. <https://apps.who.int/iris/bitstream/handle/10665/258715/9789241512770-eng.pdf> Accessed on Jan 5, 2022.
- [5] R. Saha and R. Donofrio, "The microbiology of metalworking fluids," *Applied Microbiology and Biotechnology*, Vol. 94(5), pp. 1119–1130, 2012. [CrossRef]
- [6] M. E. Eissa, "Assessment for Sporicidal activity of two types of peroxygen/silver-based disinfectants: A comparative study," *Journal of Pharmaceutical Technology, Research and Management*, Vol. 4(2), pp. 161–169, 2016. [CrossRef]
- [7] C. B. Cordella, PCA: The basic building block of chemometrics, In I. S. Krull, (Eds.). *Analytical Chemistry*, IntechOpen, London, United Kingdom, 2012.
- [8] I. Jolliffe and J. Cadima, "Principal component analysis: a review and recent developments," *Philosophical Transactions of the Royal Society A: Mathematical, Physical and Engineering Sciences*, Vol. 374(2065), Article 20150202, 2016. [CrossRef]
- [9] S. Salata and C. Grillenzoni, "A spatial evaluation of multifunctional Ecosystem Service networks using Principal Component Analysis: A case of study in Turin, Italy," *Ecological Indicators*, Vol. 127, Article 107758, 2021. [CrossRef]
- [10] M. E. Eissa, E. Rashed and D. E. Eissa, "Quality improvement in routine inspection and control of healthcare products using statistical intervention of long-term data trend," *Dicle University Journal of the Institute of Natural and Applied Science*, Vol. 10(2), pp. 163–184, 2021.
- [11] Great Learning Team, "Overview of multivariate analysis | what is multivariate analysis and model building process?," *GreatLearning Blog: Free Resources what Matters to shape your Career!*, 2020. <https://www.mygreatlearning.com/blog/introduction-to-multivariate-analysis/> Accessed on Jan 5, 2022.
- [12] R. Ainsworth, "Safe piped water: Managing microbial water quality in piped distribution systems," *Water Intelligence Online*, Vol. 12, 2013. [CrossRef]
- [13] M. Essam Eissa, "Investigation of microbiological quality of water from the feed source to the terminal application in the healthcare facility: A case study," *Health Research*, Vol. 2(1), pp. 16, 2018. [CrossRef]
- [14] EMSL Analytical, Inc, "Legionella, fecal coliform & total coliform sampling guide," *Emsl.com*, 2022. https://www.emsl.com/PDFDocuments/Sampling-Guide/legionella_coliform_guide.pdf. Accessed on Jan16, 2022.
- [15] United States Environmental Protection Agency, "Quick guide to drinking water sample collection," *Epa.gov*, 2022. https://www.epa.gov/sites/default/files/2015-11/documents/drinking_water_sample_collection.pdf. Accessed on Jan15, 2022.
- [16] D. Francy, E.A. Stelzer, A.M. Brady, C. Huitger, R.N. Bushon, H.S. Ip, M.W. Ware, E.N. Villegas, V. Gallardo and H.D. Lindquist, "Comparison of filters for concentrating microbial indicators and pathogens in lake water samples," *Applied and Environmental Microbiology*, Vol. 79(4), pp. 1342–1352, 2012. [CrossRef]
- [17] G. Ngwa, R. Schop, S. Weir, C. León-Velarde and J. Odumeru, "Detection and enumeration of *E. coli* O157:H7 in water samples by culture and molecular methods," *Journal of Microbiological Methods*, Vol. 92(2), pp. 164–172, 2013. [CrossRef]
- [18] E. Goldwater, "Using excel for data analysis," *People.umass.edu*, 2022. <https://people.umass.edu/evagold/excel.html>. Accessed on Jan 19, 2022.
- [19] H. Motulsky, "Home - GraphPad", *Graphpad.com*, 2022. <https://www.graphpad.com/> Accessed on Jan 18, 2022.
- [20] M. Essam Eissa, "Determination of the microbiological quality of feed city water to pharmaceutical facility: distribution study and statistical analysis," *Athens Journal of Sciences*, Vol. 4(2), pp. 143–160, 2017. [CrossRef]
- [21] M. Eissa, "Evaluation of microbiological purified water trend using two types of control chart," *European Pharmaceutical Review*, Vol. 23(5), pp. 36–38, 2018.
- [22] P. Praus, "Urban water quality evaluation using multivariate analysis," *Acta Montanistica Slovaca*, Vol. 12(2), pp. 150–158, 2007.
- [23] L. Almagro, X. Llabres and P. Cintas, "Industrial Statistics with Minitab," Hoboken, N.J., Wiley, 2013.
- [24] W. Ojok, J. Wasswa and E. Ntambi, "Assessment of seasonal variation in water quality in River Rwizi using multivariate statistical techniques, Mbarara Municipality, Uganda," *Journal of Water Resource and Protection*, Vol. 9(1), pp. 83–97, 2017. [CrossRef]

- [25] Minitab® 18 Support. 2019, "Interpret all statistics and graphs for Factor Analysis - Minitab", Support.minitab.com, 2022. <https://support.minitab.com/en-us/minitab/18/help-and-how-to/modeling-statistics/multivariate/how-to/factor-analysis/interpret-the-results/all-statistics-and-graphs/> Accessed on Jan 12, 2022.
- [26] D. Weragama, V. Weerasingha, L. Jayasumana, J. Adikari, J. Vidanarachchi and H. Priyashantha, "The physicochemical, microbiological, and organoleptic properties and antioxidant activities of cream cheeses fortified with dried curry leaves (*Murraya koenigii* L.) powder," *Food Science & Nutrition*, Vol. 9(10), pp. 5774–5784, 2021. [CrossRef]
- [27] GraphPad Software LLC, "GraphPad Prism 9 Statistics Guide - How to: Correlation," Graphpad.com, 2022. https://www.graphpad.com/guides/prism/latest/statistics/stat_how_to_correlation.htm. Accessed on Jan 13, 2022.
- [28] C. Charoux, L. Free, L.M. Hinds, R.K. Vijayaraghavan, S. Daniels, C.P. O'Donnell and B.K. Tiwari, "Effect of non-thermal plasma technology on microbial inactivation and total phenolic content of a model liquid food system and black pepper grains," *LWT*, Vol. 118, Article 108716, 2020.
- [29] M.E. Eissa, "Role of statistical process control of pharmaceutical product to monitor consistency of the manufacturing operation," *EC Pharmacology and Toxicology*, Vol. 6, pp. 439–444, 2018.



Research Article

Indoor air CO₂ concentrations and ventilation rates in two residences in İzmir, Turkey

Aybüke TAŞER^{1,2}, Sedef UÇARYILMAZ¹, Ilgın ÇATAROĞLU¹, Sait Cemil SOFUOĞLU³

¹Department of Architecture, İzmir Institute of Technology, İzmir, Türkiye

²Department of Architecture, İzmir University of Economics, İzmir, Türkiye

³Department of Environmental Engineering, İzmir Institute of Technology, İzmir, Türkiye

ARTICLE INFO

Article history

Received: 07 March 2022

Revised: 19 April 2022

Accepted: 30 April 2022

Key words:

Air exchange rate; Building monitoring, CO₂ concentration; Infiltration rate; Ventilation rate

ABSTRACT

Houses are the places where people spend most of their time. That is why indoor air quality at home is essential for public health. Sufficient ventilation is the factor to avoid accumulation of pollutants in indoor air, which include microorganisms, such as SARS-CoV-2. Therefore, adequate ventilation is needed to provide good indoor air quality for human health and reduce infection risk at home. There are no reports of residential ventilation rates in Turkey. In this study, CO₂ concentrations were measured in two residences in İzmir, Turkey. Three experiments were conducted to determine background concentrations and the rate of natural ventilation with infiltration and opening windows. Results show that air exchange provided by infiltration is low for both case rooms, while adequate ventilation could be achieved with natural ventilation under the studied conditions. Infiltration provided air exchange and ventilation rates of 0.18 h⁻¹ and 5.9 m³/h for Case 1 and 0.29 h⁻¹ and 8.23 m³/h for Case 2, respectively. Air exchange and ventilation rates were increased to 2.36 h⁻¹ and 76.9 m³/h for Case 1 and 1.2 h⁻¹ and 34 m³/h for Case 2, respectively, by opening the windows. Although ventilation can be provided by opening the windows, the other factors that determine its rate, e.g., meteorological variables, cannot be controlled by the occupants. Consequently, people cannot ensure the good indoor air quality in bedrooms and sufficient reduction in transmission of pathogenic microorganisms; therefore, risk of spreading diseases such as COVID-19 at home.

Cite this article as: Taşer A, Uçaryılmaz S, Çataroğlu I, Sofuoğlu SC. Indoor air CO₂ concentrations and ventilation rates in two residences in İzmir, Turkey. Environ Res Tec 2022;5:2:172–180.

INTRODUCTION

Ventilation is the key to good indoor air quality in any built environment. When a space lacks it, there starts an accumulation of – especially indoor-generated – pollutants [1].

The accumulation results in indoor air pollutant concentrations of 2 to 5, and sometimes 100 times, higher than those outdoors. Indoor sources of pollutants include people. In cases when there is a respiratory infection, people become a source of pathogenic microorganisms. When this occurs in

*Corresponding author.

*E-mail address: aybuketaser@iyte.edu.tr; aybuke.taser@ieu.edu.tr



a space that lacks sufficient ventilation, there starts accumulation and transmission of the microorganisms, including SARS-CoV-2, the virus that causes COVID-19 disease [2–5]. Therefore, the ventilation rate or fresh air exchange rate becomes a significant factor for public health for indoor air quality and associated human health risks [2, 6].

Houses are the built environments where the most time is spent in a day. Family members sharing the same house regularly interact with each other while doing everyday activities such as watching TV, eating, or using the same bathroom. It is challenging to act by social distance rules at home; therefore, if any family member gets infected, this increases the probability of transmission to the other family members. Like all built environments, houses need to be resilient due to many anticipated pandemics and climate change.

Ventilation at home is essential to ensure good indoor air quality and a reduced risk of pathogenic microorganism transmission [7]. Although natural ventilation plays an active role in improving indoor air quality, the rate of fresh air exchange it provides is not controlled by people. It generally cannot provide adequate outdoor airflow in residences [8]. The average air exchange rate (AER) was reported to be $0.64 \pm 0.30 \text{ h}^{-1}$ in apartments and $0.45 \pm 0.22 \text{ h}^{-1}$ in houses in Europe [9], in which $\text{AER} < 0.5 \text{ h}^{-1}$ occupants are more likely to experience non-specific symptoms.

Although there is no worldwide standardized definition of indoor air quality, various standards have been published in different countries. For example, EN 15251, one of the most widely used standards, is the first European standard to include criteria for four indoor environmental factors: thermal comfort, air quality, lighting, and acoustics. Turkey has no national ventilation standard, but the EU standard, EN 15251 is valid as TS [10]. ASHRAE 62.2 [11] specifies the minimum ventilation requirements for acceptable indoor air quality in residences in USA, applicable to both new and existing homes (Table 1).

The literature shows that indoor air quality and occupant health can be improved by retrofitting a mechanical ventilation system [12]; Kang et al. [13] studied 40 homes in Chicago and showed that putting an HVAC system into operation resulted in significant reductions in CO_2 , NO_2 , PM_1 , $\text{PM}_{2.5}$, and PM_{10} concentrations with an average between 33 and 42%. In Portugal, indoor air quality of 10 residences was investigated for suitability of the ventilation during the sleep period [14]. AER was measured using CO_2 as the tracer gas, which the occupants emit. It was determined that all bedrooms had average AERs greater than the minimum value of 0.7 h^{-1} [15]. Pollutant concentrations indoors and outdoors of 40 typical residences in the temperate climate zone in Australia were measured [16]. Energy-efficient designs of newer, more airtight homes generally result in high indoor air pollutant concentrations as they trap the pollutants indoors. Therefore, a negative correlation was observed between res-

Table 1. Ventilation rate recommended for residences by ASHRAE [11]

Building type	People outdoor air rate (Rp)		Area outdoor air rate (Ra)	
	Cfm/person	(L/s) x person	Cfm/ft ²	L/s x m ²
Residential	5	2.5	0.006	0.3

idential age and selected indoor air pollutants. In addition, pollutant concentrations found during the study were lower than those found in other Australian and overseas studies.

Although there are many studies abroad in the literature, three of which are exemplified above, there are no reports of ventilation rates in houses in Turkey. This study aimed to determine the ventilation rate by measuring CO_2 as the tracer gas in two residential dwellings in İzmir, Turkey. Real-time monitoring of CO_2 levels was conducted for three days indoors and outdoors with two ventilation scenarios.

MATERIALS AND METHODS

Residences

The Case 1 building is located in the Karşıyaka district of İzmir, at $38^\circ 27' 54.2''$ North and $27^\circ 06' 03.7''$ East. It is a ground + 4 apartment building with five apartments, occupying 140 m^2 areas on the ground floor. The building has a double facade, North and South. There are three bedrooms on the South facade. There is a kitchen and a living room on the North facade. A 9-meter-long balcony connects these. There is a distance of 10 m between the North facade (i.e., the main facade facing the road) and the neighboring building opposite it. Therefore, it can be said that it is highly hindered in terms of wind and daylight, especially since it is on the North side. There is a neighboring building on the east side of the building. There is a distance of two meters between the West facade and the neighboring building. Despite this, the absence of any windows on the West facade indicates that the land on which this building is located is an adjacent array according to the regulation. The examined apartment has a gross area of 120 m^2 . It is a 3+1 apartment with three rooms facing South and a kitchen and living room facing North. The room in which the experiment was conducted in the family room facing the South. The gross floor area of the room is 14.42 m^2 , and the net floor area is 11.41 m^2 . In addition to floor areas, the total volume of the family room is calculated as 41.10 m^3 , and the net volume is 32.52 m^3 . There are two windows and one door in the case room.

The Case 2 building is a dwelling located in the Örnekköy neighborhood, Karşıyaka, İzmir. The coordinates are $38^\circ 29' 2''$ N $27^\circ 6' 9''$ E, and the elevation above the sea level is 94.1 meters. The building is located in a housing complex with two buildings. The case building is constructed with two

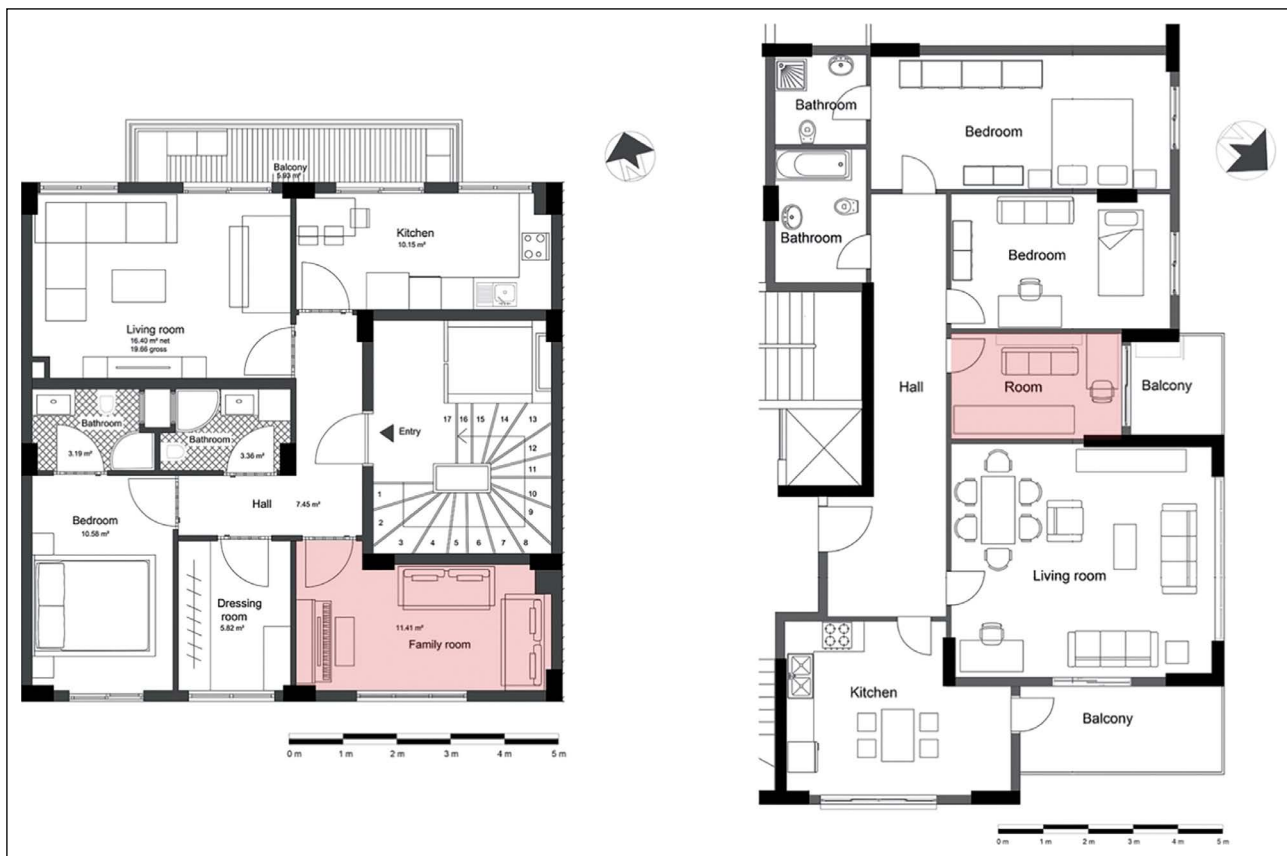


Figure 1. Left: Case 1 floor plans of case buildings and case rooms indicated with red color hatch. Right: Case 2 floor plans of case buildings and case rooms marked with red color hatch.

different entrances and two other cores, but the roof and walls are typical. There are nine flats, and each flat has two apartments. On the ground floor, there is one apartment, so the entire building has 10 stories. The surrounding of the building is quite empty. It is located next to a small hill. The case building is oriented to the North at 21° degrees. The gross dwelling area is 155 m², the net usable space is 122.20 m², and the total volume is 387 m³. The dwelling contains three bedrooms, one kitchen, one living room, two bathrooms, and two balconies. The case room is a bedroom that is not being used. The case room's gross and net floor areas are 13.5 m² and 11.3 m². The gross volume is 36.45 m³, and the net volume is calculated as 28.25 m³. There is a balcony door and a room door in the case room. The floor plans of the two cases are presented in Figure 1.

Monitoring

A monitoring device (Testo 400) was used to measure the indoor and outdoor CO₂ levels of case rooms (Fig. 2). The device was located in the center of the room and placed on a chair. It was set to a 10-minute recording interval for three days. On the first day, outdoor CO₂ concentration levels were measured, and indoor CO₂ level was monitored for 12 hours representing the general (background)

conditions. On the second day, 500 gr amount of dry ice was located in the room, and a monitoring process was conducted for 24 hours. Windows and the room door were kept closed to measure ventilation by infiltration. After 24 hours, CO₂ concentration levels were decreased to the general condition levels. Then, the door and windows were opened to reduce the concentration to the outdoor levels. On the last day, 250 gr of dry was located in the case room. After two hours of the monitoring process, the windows were opened to increase the natural ventilation. During monitoring with dry ice, a fan was used to obtain better mixing in the room. The range and accuracy values of the monitoring device are shown in Table 2.

Ventilation Rate Estimation

CO₂ is an important indoor air pollutant frequently used in such studies to investigate indoor air quality. CO₂ in the outdoor air varies between 330 and 500 ppm depending on the characteristics of the environment. The CO₂-based method is divided into three segments. The first is the occupancy phase or the concentration trend into build-up, the second is the steady-state, and the third is the decay (or "step-down") phase [17]. When an area is populated with people and then emptied (or when a controlled loading is

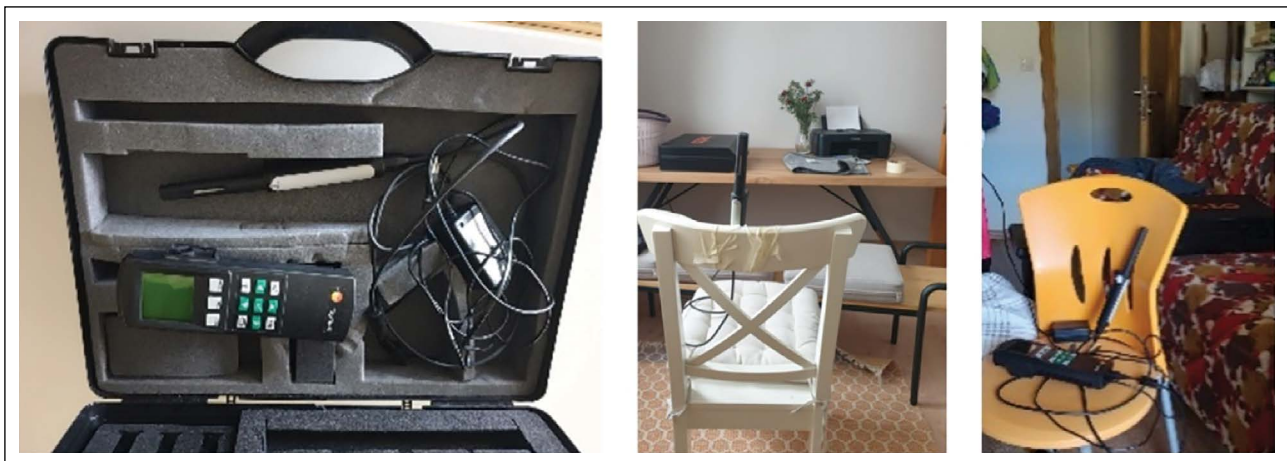


Figure 2. Testo data-logger placement.

Table 2. Indoor-outdoor monitoring equipment specifications

Sensor	Measuring range	Resolution	Accuracy
Testo 400 data-logger	0–10,000 ppm	1 ±	±(50 ppm+3% interval value) (0–5,000 ppm) (100 ppm+5% measurement value) (5,001–10,000 ppm)

done and left to monitor), or if there is a gradual decrease in occupancy, it makes sense to use decay or reduction to estimate the ventilation rate of the environment. The decay method is a technique that uses tracer gas dilution to determine the air exchange of a single zone with the outside environment induced by weather conditions. This test method is not limited to any single tracer gas [18]. The associated data analysis assumes that a single value can characterize the tracer gas concentration within the zone. Dry ice was used in this experiment to increase the CO₂ level in the indoor environment. In experiments, occupant density in the room could also be used for CO₂ production since people give CO₂ to the indoor environment due to breathing. A person engaged in a typical job produces 20 liters (0.02 m³) of CO₂ per hour [19]. For this experiment, 21 people were required for 1 hour in a room with a volume of 30 m³ for a CO₂ level of 10,000 ppm. Therefore, dry ice was preferred for ease of testing.

The monitoring results were imported to MS Excel for analysis. Equation-1 was used to calculate the air exchange rate in the room. In this equation, *AER* is the air exchange rate, and it is calculated by using duration and indoor and outdoor CO₂ concentration levels (Eq. 2). *t* is defined as the period during measurement. *C_o* and *C_i* are measured CO₂ concentrations over the decay period (ppm). *C_{ext}* is CO₂ concentrations level (ppm) outdoors [19]. Although there is no exact value as the limit for CO₂ concentration, 1,000 ppm is the most commonly used value [11, 20] since Pettenkofer first proposed it in the 1800s. Therefore, the acceptable limit value of carbon dioxide in the room for this experiment was set as 1,000 ppm.

$$AER=Q/V \tag{1}$$

$$AER=t^{-1} \times \ln((C_o - C_{ext}) / (C_i - C_{ext})) \tag{2}$$

where *AER* is Air Exchange Rate, *t* is the period between measurements (h), *C_o* and *C_i* are the measured CO₂ concentrations (ppm) over the decay period, and *C_{ext}* is outdoor CO₂ concentration (ppm) [17].

$$Q \text{ (m}^3\text{/h)}=AER \times \text{room volume (m}^3\text{)} \tag{3}$$

where *Q* is ventilation rate.

RESULTS AND DISCUSSION

Experiments were conducted in two residential cases, i.e., Cases 1 and 2. Three experiments were conducted in each house. Firstly, indoor CO₂ levels were monitored for 12 hours without any dry ice or potential CO₂ source to assess the background concentration levels. In the second experiment, dry ice was placed in the room to increase CO₂ levels. Doors and windows were kept closed to measure ventilation by infiltration. In the last experiment, windows were opened after CO₂ levels exceeded a specified level, to measure an increased natural ventilation rate.

Background Concentrations

Indoor air CO₂ concentration levels were monitored for 12 hours. This experiment aimed to estimate general (background) CO₂ levels of the indoor environment without any potential CO₂ source. For the first case, the concentration levels varied between 437–562 ppm with an average value of 479 ppm (Fig. 3). For the second case, concentration lev-

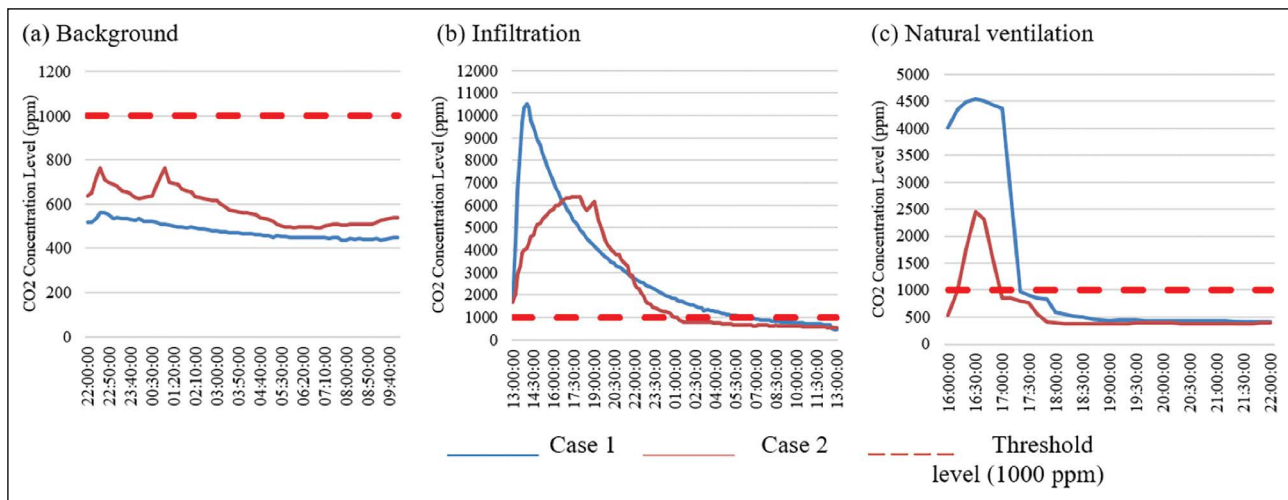


Figure 3. CO₂ concentrations measured during the experiments: (a) background, (b) infiltration, (c) natural ventilation.

els varied between 491–764 ppm with an average value of 584 ppm. It can be seen that CO₂ concentration decreases during nighttime. Variation in concentration was probably caused by occupant activity in the remainder of the house and the decrease during nighttime may be related to reduced activity. For both of the cases, indoor CO₂ levels have never exceeded the threshold level of 1,000 ppm.

Concentrations During Experiments

In the infiltration experiment, 500 grams of dry ice was included in the rooms. A fan was used during the experiment to distribute the emitted CO₂ by the dry ice homogeneously throughout the room. Windows and doors were kept closed throughout the experiment. In this process, the change in the mass of solid dry ice was observed and the increase in the CO₂ level was monitored. Throughout this time, the CO₂ level reached its maximum level, and then it started to decrease gradually. For the first case, the maximum level for CO₂ concentration was recorded as 10,510 ppm, and it took 1 hour to reach this level. After 23 hours of reaching the maximum level, the concentration level was decreased to 457 ppm. During this 24-hour experiment, the average concentration was recorded as 2,925 ppm.

In this experiment, 72% of the measured levels were above the 1,000-ppm threshold. However, after 17 hours and 20 minutes, CO₂ concentration was decreased back to below 1,000 ppm. For the second case, the highest level of CO₂ concentration was recorded as 6,392 ppm, and it took 5 hours to reach this level. After 18 hours and 50 minutes of reaching the highest level, the concentration level was decreased to 531 ppm. The average value was 2,363 ppm. Fifty percent of the measured values were >1,000 ppm threshold level. After 12 hours and 10 minutes, CO₂ concentrations were decreased back to background levels.

In the natural ventilation experiment, 250 grams of dry ice was included in the rooms. Similarly, a fan was used during

the experiment to homogenize CO₂ levels throughout the room. The different aspect from the first experiment was that windows were opened when the CO₂ concentration reached its maximum level. This experiment aimed to estimate the effect of opening the windows on the natural ventilation rate. For the first case, the peak level for CO₂ concentration was recorded as 4,537 ppm. After 4 hours and 50 minutes of reaching the highest level, it decreased back to 417 ppm. During this 6-hour experiment, the average concentration was 1,302 ppm, in which 22% of the recorded concentrations were above the threshold level. However, CO₂ concentration levels were decreased back to below 1,000 ppm in just 1 hour and 20 minutes. The highest CO₂ concentration was recorded as 2,453 ppm for the second case. After 4 hours and 40 minutes of reaching the highest level, it was decreased to 372 ppm. The average value was 631 ppm. Nine percent of the measured concentrations were above the threshold level. However, after only 30 minutes, CO₂ concentration levels were decreased back to below 1,000 ppm-level.

Air Exchange Rates

Figure 4 shows the calculated air exchange rates for the two case houses during the infiltration and natural ventilation experiments. The infiltration rate was relatively stable in Experiment-2 in Case-1 at about 0.15 h⁻¹, while it fluctuated in the 2nd house roughly around 0.3 h⁻¹. In Experiment-3, it is seen in the graph that the air exchange rate started to increase when the windows were opened. However, due to concentrations reducing back to background levels relatively quickly, the time was insufficient to observe a stabilized AER, especially for Case-2. In contrast, for Case-1, an AER of 2 h⁻¹ could be assumed based on values at 100, 110, and 120th minutes. Both cases show that opening windows had a critical effect on the air exchange rate during the meteorological conditions of the time of the experiments.

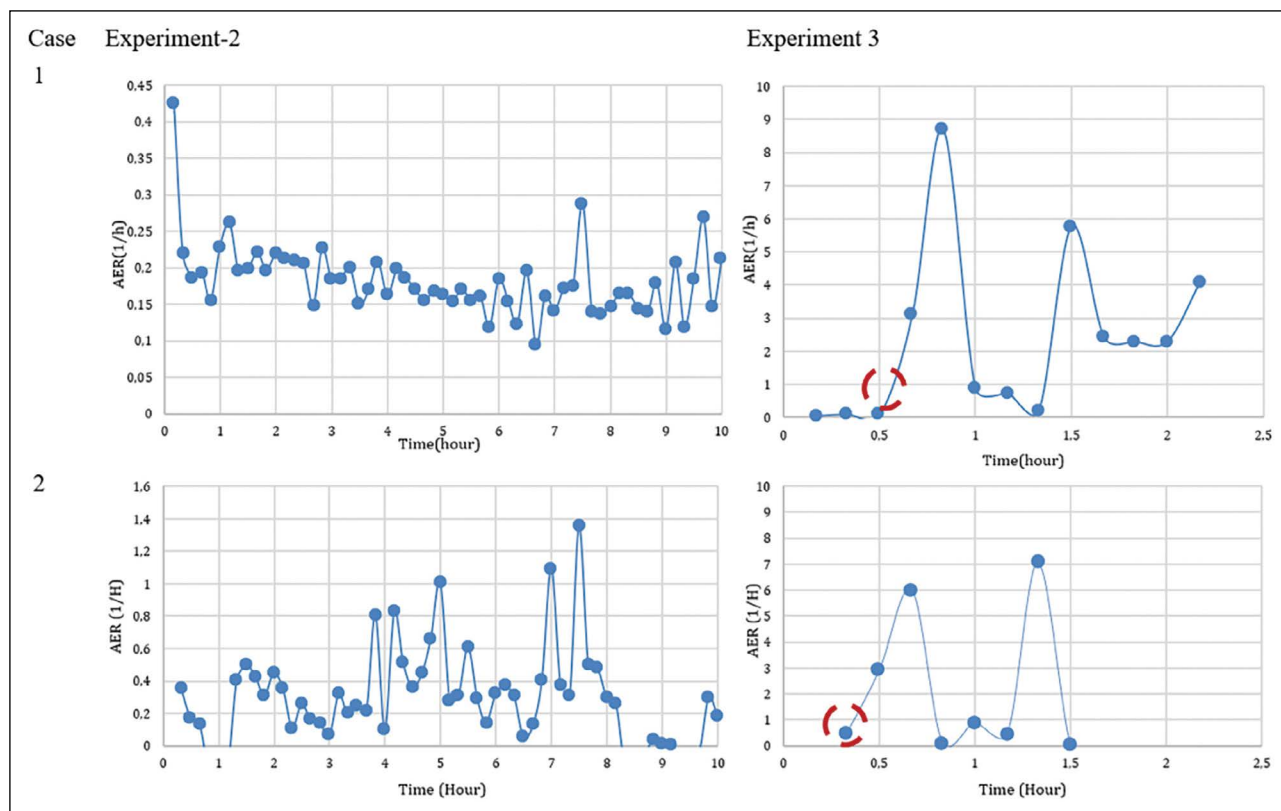


Figure 4. Plot of calculated air exchange rate (AER) values during the experiments.

When the two case houses are compared, it is seen that the maximum CO₂ values in the rooms did not reach the same concentration level, although the same amount of dry ice (500 gr) was used. In the second case, the infiltration rate was higher. This may depend on the height of the house, the number of windows, and the number of leakage areas other than the meteorological conditions outside, e.g., wind speed and direction. The results of the third experiment gave increased natural ventilation by opening the windows. As soon as the windows were opened, we observed sharp changes in the air exchange rate due to increased natural ventilation. While the high CO₂ level in Case 1 fell below 1,000 ppm in 1 hour and 30 minutes, it happened in an hour in Case 2. This shows the effect of increased natural ventilation for both cases compared to low AERs provided by infiltration.

Figure 5 shows the difference between the two case houses' infiltration and windows-open ventilation rates as boxplots. In both cases, estimated ventilation rates were increased considerably by window opening compared to the ventilation provided by infiltration. Many studies monitored CO₂ concentrations in the literature, as shown in Table 3. The literature shows that CO₂ concentration levels can be a useful indicator of the building's overall performance, affecting occupant health [14].

It was reported that CO₂ levels considerably relate to indoor air quality [21]. There is a correlation between indoor CO₂ level, building airtightness, and energy efficiency [16]. In

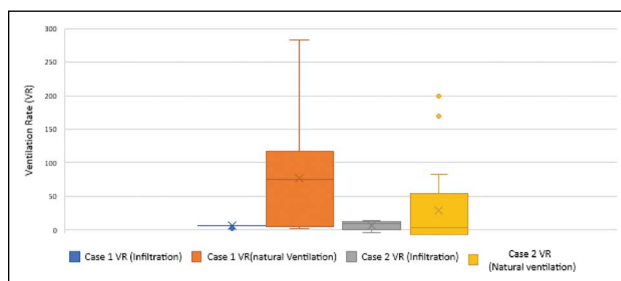


Figure 5. Variation in the estimated ventilation rates.

this study, the indoor CO₂ level was measured to be below the acceptable level of 1,000 ppm (Table 4). In the first and second cases, average indoor CO₂ levels were 479 and 584 ppm. However, these levels were consciously increased to assess the buildings' air exchange and ventilation rates. In the second experiment average air exchange rate was calculated as 0.18 and 0.29 h⁻¹ for Case 1 and 2, respectively. The average ventilation rate was 5.9 m³/h and 8.23 m³/h for cases 1 and 2. Both of the cases are newly constructed buildings located in the same district of İzmir. However, the second case is located on a higher sea elevation and exposed to an intense wind load, resulting in a higher infiltration potential. According to the results of the second experiment, in the second case, average air exchange rate and ventilation rate due to infiltration was calculated to be higher than the first case. The

Table 3. Comparative literature review

Year	Authors	Location	Building type	Ventilation type	Tools	Findings
2012	Bulut [20]	Undefined	Residential, office, and education building	Natural Natural Natural	Real-time monitoring, numerical methods	The relationship between CO ₂ concentrations and other parameters (i.e., temperature, humidity, etc.) is discussed. There found a correlation between CO ₂ levels and humidity with particulate matter concentration.
2012	Molloy et al. [15]	Australia	Residential		Real-time monitoring	Energy-efficient designs of newer, more airtight residences can result in high concentrations of pollutants indoors, as they trap pollutants indoors. Therefore, a negative correlation was observed between residential ages and selected indoor air pollutants.
2020	Canha et al. [13]	Portugal	Residential		Real-time monitoring, tracer gas method	Air exchange rates are insufficient to provide good indoor air quality during sleep by reducing the dilution rate of emitted pollutants, even though they are always above the set guideline (0.7 h ⁻¹).

Table 4. Comparison of experimental results

Experiment	Data	Case 1	Case 2
Experiment 1	Average background CO ₂ (ppm)	479	584
Experiment 2	Average air exchange rate (h ⁻¹)	0.18	0.29
Experiment 3	Average air exchange rate (h ⁻¹)	2.36	1.2

third experiment aimed to estimate natural ventilation AER achieved by opening the windows. The average AER was determined as 2.36 h⁻¹ and 1.2 h⁻¹ while the average ventilation rate was calculated as 76.9 h⁻¹ and 34 h⁻¹ for cases 1 and 2, respectively. The lower rate estimated for Case-2 than that of Case-1 may have occurred due to not reaching a similar peak concentration before gradual decrease, meteorological conditions, and the window opening area. While the ratio of opening area to volume in 1st case is calculated as 0.085 m²/m³, it is calculated as 0.067 m²/m³ in the second case. In the second experiment, different levels of CO₂ were obtained despite adding the same amount of dry ice. This was due to the different infiltration levels of the rooms. Since higher CO₂ concentration occurred in the first case, the air exchange rate was lower. This experiment shows the importance of windows on ventilation and indoor air quality. The results of this study are found to be consistent with those reported in the literature. Buildings' air leakage potential, thus infiltration and thermal performance, closely relates to indoor air quality [16]. The literature also clearly concluded that indoor air quality is strongly related to the spread of various diseases through ventilation rate [14]. This study shows that AERs due to infiltration were very low and can be considerably

increased when natural ventilation was acquired by opening the windows. Therefore, natural ventilation can play an essential role in maintaining a better indoor air quality and decreasing the risk of virus and disease spread indoors.

CONCLUSIONS

The effect of natural ventilation on reducing the indoor CO₂ concentration is apparent when the two experiments are compared. Factors such as housing type, sea-level elevation, location, window size, airtightness, the number of outdoor facing facades, and window size may determine its rates through infiltration and opening windows. Both case rooms are between the minimum and maximum ventilation rates specified in ASHRAE [11] and contribute to indoor air quality. However, the rates estimated in this study are relatively low and natural ventilation is a result of factors that cannot be controlled by the occupants, which is uncertain to supply a sufficient decrease in the risk of infection spread, e.g., COVID-19.

ACKNOWLEDGMENT

Authors thank Assoc. Prof. Dr. Zeynep Durmuş Arsan and Building Physics Laboratory at İzmir Institute of Technology for the monitoring devices.

DATA AVAILABILITY STATEMENT

The authors confirm that the data that supports the findings of this study are available within the article. Raw data that support the finding of this study are available from the corresponding author, upon reasonable request.

CONFLICT OF INTEREST

The authors declared no potential conflicts of interest with respect to the research, authorship, and/or publication of this article.

ETHICS

There are no ethical issues with the publication of this manuscript.

REFERENCES

- [1] L. Morawska, G.A. Ayoko, G.N. Bae, G. Buonanno, C.H.Y. Chao, S. Clifford, S.C. Fu, O. Hännineng, C. He, C. Isaxonh, M. Mazaheri, T. Salthammer, M. S. Waring, and A. Wierzbickah “Airborne particles in indoor environment of homes, schools, offices and aged care facilities: the main routes of exposure,” *Environment International*, Vol. 108, pp. 75–83, 2017. [\[CrossRef\]](#)
- [2] L. Morawska and J. Cao, “Airborne transmission of Sars-Cov-2: the World should face the reality,” *Environment International*, Vol. 139, Article 105730, 2020. [\[CrossRef\]](#)
- [3] L. Morawska, J.W. Tang, W. Bahnfleth, P.M. Bluyssen, A. Boerstra, G. Buonanno, J. Cao, S. Dancer, A. Floto, F. Franchimon, C. Haworth, J. Hogeling, C. Isaxon, J. L. Jimenez, J. Kurnitski, Y. Li, M. Loomans, G. Marks, L. C. Marr, L. Mazzearella, A. Krikor Melikov, S. Miller, D. K. Milton, W. Nazaroff, P. V. Nielsen, C. Noakes, J. Peccia, X. Querol, C. Sekhar, O. Seppänen, S. Tanabe, R. Tellier, K. Wai Tham, P. Wargocki, A. Wierzbicka, and M. Yaoai, “How can airborne transmission of Covid-19 indoors be minimised?” *Environment International*, Vol. 142, Article 105832, 2020. [\[CrossRef\]](#)
- [4] V.T. Chu, A.R. Yousof, K. Chang, N.G. Schwartz, C.J. McDaniel, S.H.Lee, C.M. Szablewski, M. Brown, C. L. Drenzek, E. Dirlikov, D. A. Rose, J. Villanueva, A. M. Fry, A. J. Hall, and H. L. Kirking, “Household transmission of Sars-Cov-2 from children and adolescents,” *Journal of Medicine*, Vol. 385, pp. 954–956, 2021. [\[CrossRef\]](#)
- [5] Y. Li, G.M. Leung, J.W. Tang, X. Yang, C.Y.H. Chao, J.Z. Lin, J.W. Lu, P.V. Nielsen, J. Niu, H. Qian, A.C. Sleigh, H.J.J. Su, J. Sundell, T.W. Wong, and P.L. Yuen, “Role of ventilation in airborne transmission of infectious agents in the built environment - a multidisciplinary systematic review,” *Indoor Air*, Vol. 17, pp. 2–18, 2007. [\[CrossRef\]](#)
- [6] S.C. Sofuoglu and M. Töksoy, “COVID-19 ve okularda mekanik havalandırmanın aciliyeti,” *TTMD Dergisi*, Vol. 129, pp. 40–42, 2021.
- [7] A. Frattolillo, L. Stabile, and M. Dell’Isola, “Natural ventilation measurements in a multi-room dwelling: critical aspects and comparability of pressurization and tracer gas decay tests,” *Journal of Building Engineering*, Vol. 42, Article 102478, 2021. [\[CrossRef\]](#)
- [8] L. Zhao, J. Liu, and J. Ren, “Impact of various ventilation modes on IAQ and energy consumption in Chinese dwellings: “First long-term monitoring study in Tianjin, China,” *Building and Environment*, Vol. 143, pp. 99–106, 2018. [\[CrossRef\]](#)
- [9] C. Dimitroulopoulou, “Ventilation in European dwellings: A review,” *Building and Environment*, Vol. 37, pp. 109–125, 2012. [\[CrossRef\]](#)
- [10] EN 15251, “Indoor Environmental Input Parameters for Design and Assessment of Energy Performance of Buildings Addressing Indoor Air Quality, Thermal Environment, Lighting and Acoustics,” 2007.
- [11] ASHRAE, “ANSI/ASHRAE Standard 62.2-2017, ventilation for acceptable indoor air quality,” American Society of Heating, Refrigerating and Air-Conditioning Engineers, Inc.: Atlanta, GA, USA, 2017.
- [12] K. Insung, A. McCreery, P. Azimi, A. Gramigna, G. Baca, K. Abromitis, M. Wang, Y. Zeng, R. Scheu, T. Crowder, A. Evens, and B. Stephens, “Indoor air quality impacts of residential mechanical ventilation system retrofits in existing homes in Chicago, IL,” *Science of The Total Environment*, Vol. 804, Article 150129, 2022.
- [13] I. Kang, A. McCreery, P. Azimi, A. Gramigna, G. Baca, K. Abromitis, M. Wang, Y. Zeng, R. Scheu, T. Crowder, A. Evens, and B. Stephens. “Indoor air quality impacts of residential mechanical ventilation system retrofits in existing homes in Chicago, IL,” *Science of The Total Environment*, Article 150129, 2022. [\[CrossRef\]](#)
- [14] N. Canha, A. C. Alves, C. S. Marta, J. Belo, J. Lage, T. Faria, S. Cabo Verde, C. Viegas, C. Alves, and S. M. Almeida, “Compliance of indoor air quality during sleep with legislation and guidelines – A case study of Lisbon dwellings,” *Environmental Pollution*, Vol. 264, Article 114619, 2020. [\[CrossRef\]](#)
- [15] EN 16798-1 “Energy Performance of Buildings – Ventilation for Buildings Part 1: Indoor Environmental Input Parameters for Design and Assessment of Energy Performance of Buildings Addressing Indoor Air Quality, Thermal Environment, Lighting and Acoustics,” European Committee for Standardization (CEN), 2019.
- [16] S.B. Molloy, M. Cheng, I. E. Galbally, M. D. Keywood, S. J. Lawson, J. C. Powell, R. Gillett, E. Dunne, and P. W. Selleck, “Indoor air quality in typical temperate zone Australian dwellings,” *Atmospheric Environment* Vol. 54, pp. 400–417, 2012. [\[CrossRef\]](#)
- [17] S. Batterman, “Review and extension of CO₂-based methods to determine ventilation rates with application to school classrooms,” *International Journal of*

- Environmental Research and Public Health, Vol. 14, pp. 145, 2017. [[CrossRef](#)]
- [18] V.R. Phillips, D.S. Lee, R. Scholtens, J.A. Garland, and R.W. Sneath, “A review of methods for measuring emission rates of ammonia from livestock buildings and slurry on manure stores, part 2: monitoring flux rates, concentrations and airflow rates,” *Journal of Agricultural Engineering*, Vol. 78, pp. 1–14, 2001.
- [19] A. Persily, “Evaluating building IAQ and ventilation with indoor carbon dioxide,” *American Society of Heating Refrigerating and Air Conditioning Engineers*, Vol. 103, pp. 193–204, 1997.
- [20] E. Schramek, “Recknagel-Sprenger Schramek Isıtma ve Klima Tekniđi El Kitabı,” 11 Nolu Teknik Yayın, TTMD, Ankara, 2003. [Turkish]
- [21] H. Bulut, “Havalandırma ve iç hava kalitesi açısından CO2 miktarının analizi,” *Plumbing Engineering*, pp. 61–70, 2012. [Turkish]



Research Article

Degradation and mineralization of tetracycline by Fenton process

Engin GÜRTEKİN¹, Murat ÇELİK¹, Ekrem AYDIN¹, Aytekin ÇELİK¹

Department of Environmental Engineering, Fırat University, Elazığ, Türkiye

ARTICLE INFO

Article history

Received: 16 March 2022

Revised: 10 May 2022

Accepted: 02 June 2022

Key words:

Antibiotics; Degradation;
Fenton process; Mineralization;
Tetracycline

ABSTRACT

In this study, we aimed to systematically optimize the operating parameters in the degradation and mineralization of tetracycline by Fenton process. For this purpose; optimum values were found for Fe^{2+} concentration, H_2O_2 concentration and pH, reaction time, sedimentation times which are effective operating parameters in Fenton process. In this study where initial tetracycline concentration was used as 100 mg/L; optimum values were found as 4 for pH, 30 mg/L for Fe^{2+} concentration, 100 mg/L for H_2O_2 concentration and 10 min for reaction time and 90 min for sedimentation time. Under these conditions, the TC degradation was 100%, while the COD removal efficiency was approximately 94%. As a result of kinetic studies, BMG is the most suitable kinetic model in terms of tetracycline degradation, while it is seen that the most suitable kinetic model for tetracycline mineralization in terms of COD is the first-order kinetic model. The cost of removing 1 kg of tetracycline from the unit costs of chemicals and energy used in the Fenton process was found to be 1.527\$.

Cite this article as: Gürtekin E, Çelik M, Aydın E, Çelik A. Degradation and mineralization of tetracycline by Fenton process. Environ Res Tec 2022;5:2:181–187.

INTRODUCTION

Tetracycline (TC) antibiotics are a group of broad-spectrum synthetic antibiotics against a wide range of Gram positive and Gram-negative bacteria, so they are widely used in human and veterinary medicine for controlling diseases and promoting growth [1]. Tetracyclines are the second largest group of antibiotics in terms of production and use [2]. A very small amount of tetracycline taken into human and animal bodies is metabolized or degraded, the remaining tetracycline being excreted into the environment in active form through humans and animals feces or urine [3]. The release of antibiotics to the environment promotes the proliferation of antibiotic-resistant bacteria and genes,

and consequently affects human health and ecosystem [4, 5]. Although conventional biological wastewater treatment has advantages such as low cost, high stability and easy operation; tetracyclines cannot be effectively removed because of its chemical stability and biological resistance [6, 7]. Therefore, effective and environmentally friendly alternative technologies are required to effectively degrade and remove these compounds [2]. Advanced oxidation processes are efficient alternative methods for treating organic wastewater pollutants with low biodegradable and high toxicity. Advanced oxidation methods such as Fenton, photo-Fenton, ozonation, electrochemical oxidation and photo catalysis are commonly used in the removal of recalcitrant and non-biodegradable organic contaminants in wastewa-

*Corresponding author.

*E-mail address: egurtekin@firat.edu.tr



ter [8]. Fenton process, which is one of the advanced oxidation processes, is one of the most widely used processes for removing of a wide variety of non-degradable organic contaminants because it has advantages such as high performance, technology simplicity, low cost and low toxicity of the chemicals used [8, 9]. The Fenton process involves the formation of hydroxyl radical formed by the catalytic reaction between hydrogen peroxide and iron ions (Eq. 1). The hydroxyl radical has an oxidation potential of 2.80 V and can degrade and mineralize a wide range of organic matter [10]. The Fenton process is influenced by H_2O_2 and Fe^{2+} and pollutant concentrations. In addition, other factors such as reaction time, pH, temperature are important operating parameters in the Fenton process.



There are many studies using the Fenton process for the removal of different drugs [11–16]. Also, different processes such as UV, UV/ H_2O_2 , UV/persulfate, photo-Fenton, solar photo-Fenton, sono-Fenton, ozonation have been tried in tetracycline removal [17–22]. In this study, it was aimed to systematically optimize the operating parameters such as pH, Fe^{2+} concentration, H_2O_2 concentration, reaction time and precipitation time in the degradation and mineralization of tetracycline by Fenton process. The kinetics of tetracycline degradation and mineralization by Fenton process were determined. The cost of tetracycline removal by Fenton process was calculated.

MATERIALS AND METHODS

Experimental System

All experiments were performed in amber colored glass bottles with a total volume of 250 mL to minimize light effect (Fig. 1). Stirring was done with a magnetic stirrer. The pH was initially adjusted with the aid of the Thermo Scientec brand pH meter and no further pH adjustment was made during the reaction. The desired concentrations of Fe^{2+} and H_2O_2 were added to the tetracycline solution prepared at a specific concentration for each experiment. H_2SO_4 and NaOH were used for pH adjustment. At the end of the reaction, the pH was adjusted to 9–10 and the reactions were stopped and settled for 90 min. At the end of sedimentation time, clear liquid was removed from the top of the reactor and tetracycline and COD were analyzed.

Reagents

Tetracycline (TC) hydrochloride salt (CAS No. 64-755) was purchased from Sigma-Aldrich and 35% purity Hydrogen peroxide (H_2O_2) was purchased from Merck. Iron sulfate heptahydrate was obtained from Biochem. The pH of the solution was initially adjusted with dilute 98% sulfuric acid (0.2 and 0.02 N H_2SO_4) and sodium hydroxide (0.2 N NaOH).

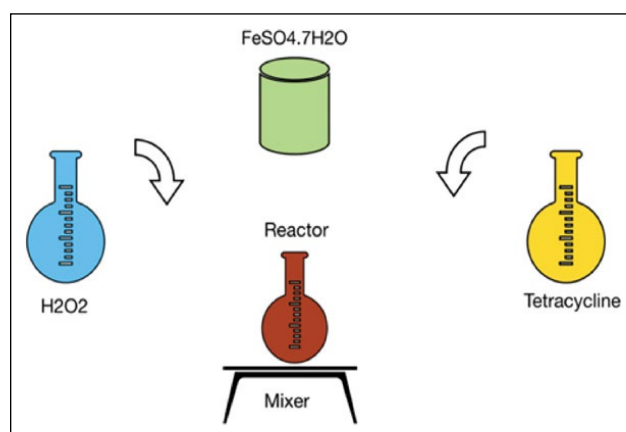


Figure 1. Experimental setup.

Analytical Methods

To determine the performance of Fenton process, tetracycline and COD analyzes were performed on the samples taken at the end of the sedimentation period. Determination of tetracycline was performed by Shimadzu brand High Performance Liquid Chromatography (HPLC). As the mobile phase, a mixture of 20 mM $(NH_4)_2 H_2PO_4$ and HPLC grade acetonitrile with pH adjusted to 2.45–2.55 was used and the flow rate was adjusted to 1.2 mL/min and the injection volume to 100 μ L. The determination of COD was made with Merck code 114895.

RESULTS AND DISCUSSIONS

Effect of pH

Tetracycline is an amphoteric compound containing two acidic (tricarboxyl amide and phenolic diketone) and one basic functional groups (dimethyl amine) in its structure. Therefore, different forms of TC will occur in the environment depending on the pH. At $pH < 3.30$ (pK_{a1}), TC molecules are available as TC^+ form; at $3.30 < pH < 7.68$ (pK_{a2}) TC molecules available as TC^0 ; at $7.68 < pH < 9.70$ (pK_{a3}) TC molecules are present as TCH^- , and at $pH > 9.70$, TC molecules are present as TC^{2-} [23]. In the Fenton process, the pH value has an important effect on the formation of hydroxyl radical and therefore on the oxidation efficiency [24]. Hence, pH is important in terms of both tetracycline and Fenton process. Experimental studies were carried out at pH 2, 3 and 4 to determine the effect of pH in Fenton process. Initial TC concentration, Fe^{2+} concentration and H_2O_2 concentration were selected as 100, 30 and 300 mg/L, respectively. At all pH values, the effluent TC concentration were found to be 0 mg/L and the corresponding TC removal efficiencies were 100% (Fig. 2). The COD removal efficiencies were 81%, 74% and 94% mg/L at pH 2, 3 and 4, respectively. Compared to pH 4, the efficiency of COD removal is lower at pH 2 and 3. Because it is stated that TC molecules have hydroxyl groups in ring 1 in undissolved

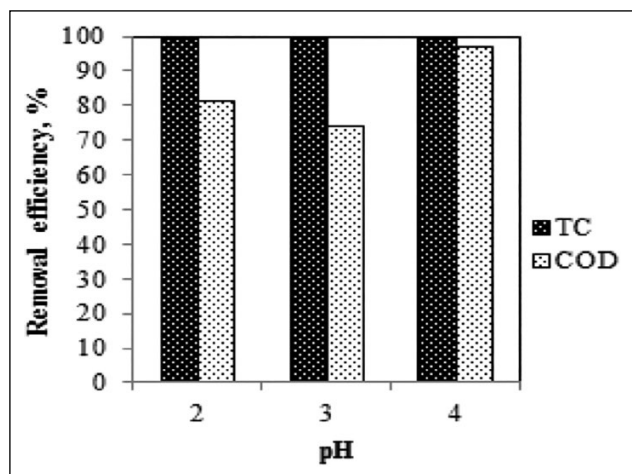


Figure 2. TC and COD removal efficiency at different pH values (TC: 100 mg/L, Fe²⁺: 30 mg/L, H₂O₂: 300 mg/L).

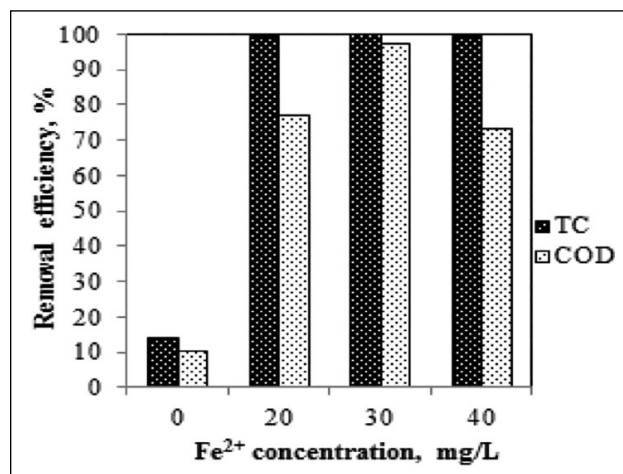


Figure 3. TC and COD removal efficiency at different Fe²⁺ values (TC: 100 mg/L, pH: 4, H₂O₂: 300 mg/L).

form at pH <3.3, while hydroxyl groups in ring 1 in the structure of TC molecules dissolve at pH > 3.3. These experimental results were evaluated and the optimum pH value was selected as 4 in terms of TC and COD removal and pH 4 value was used in the rest of the study. The results of this study were similar with the results of the study in which the degradation of tetracycline with ozonation was investigated [17]. In addition, in the literature, it is stated that the low removal rate in the Fenton process at pH 1 and 2 is due to hydroxyl radical reacting with H⁺ ions. Furthermore, H₂O₂ can be dissolved at a high H⁺ ion concentration to form an oxonium ion. An oxonium ion makes it electrophilic to increase the stability of hydrogen peroxide and reduces its reactivity with iron ion. On the other hand, it is stated that the oxidation efficiency decreases due to the precipitation of dissolved iron at pH > 4 and the decrease in the disintegration of H₂O₂ to hydroxyl radical [7]. The optimum pH value found in this study was consistent with the pH range in the literature [7, 25].

Effect of Fe²⁺ Concentration

Increased iron concentration leads to the formation of more hydroxyl radical and accelerates the redox reaction. Experimental studies were carried out at 0, 20, 30 and 40 mg/L concentrations in order to determine the effect of Fe²⁺ concentration on TC and COD removal efficiency. Figure 3 shows the TC and COD removal efficiency at different Fe²⁺ concentration. The highest TC and COD removal was achieved at a Fe²⁺ concentration of 30 mg/L, where the removal efficiencies were 100% and 97%, respectively. However, there was a decrease in COD removal in Fe²⁺ concentration of 40 mg/L. The use of a much higher Fe²⁺ concentration causes scavenging of •OH, resulting in a decrease in the rate of degradation and mineralization. Furthermore, the use of a lower iron concentration in the Fenton process will result in reduced sludge volume and

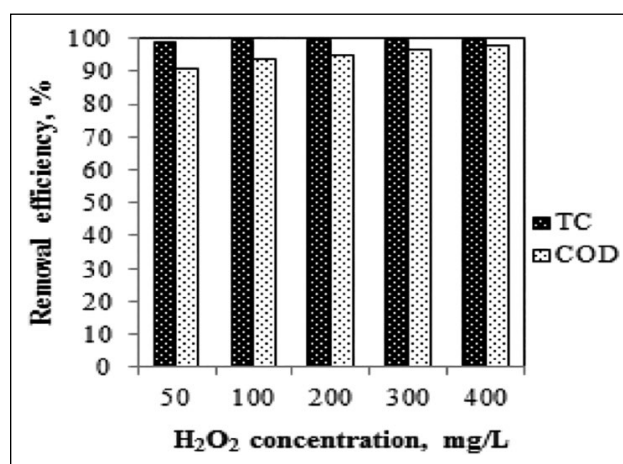


Figure 4. TC and COD removal efficiency at different H₂O₂ values (TC: 100 mg/L, pH: 4, Fe²⁺: 30 mg/L).

treatment costs [26]. Therefore, it was seen that Fe²⁺ concentration of 30 mg/L was the most appropriate value. Similarly, it was obtained complete degradation of amoxicillin (AMX) at a concentration of 30 mg/L Fe²⁺ for an initial concentration of AMX of 10 mg/L [16].

Effect of H₂O₂ Concentration

Figure 4 shows the TC and COD removal efficiency at different H₂O₂ concentrations. Based on TC and COD removal efficiencies, 100 mg/L H₂O₂ concentration could be considered as the optimum value. The TC and COD removal efficiencies at this H₂O₂ concentration were 100% and 94%, respectively. When the optimum H₂O₂ concentration was evaluated in terms of TC and COD removal efficiencies; higher H₂O₂ concentration was not necessary. In the literature, it is stated that the rate of degradation increases as H₂O₂ concentration increases until critical H₂O₂ concentration is obtained. The reduction in the rate of degradation at

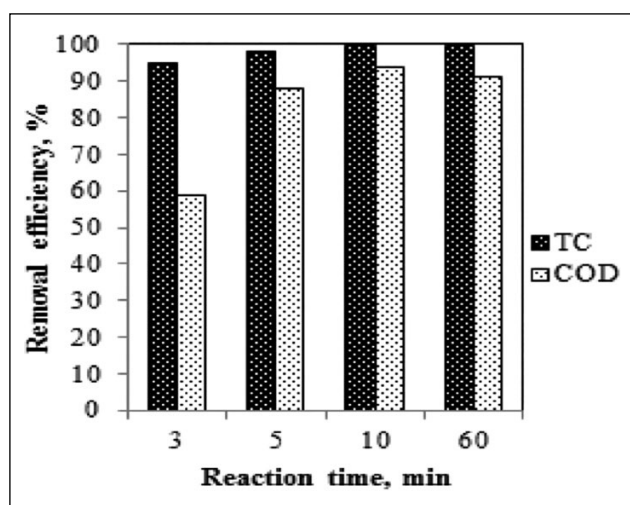


Figure 5. TC and COD removal efficiency at different reaction time (TC: 100 mg/L, pH: 4, Fe²⁺: 30 mg/L, H₂O₂: 100 mg/L).

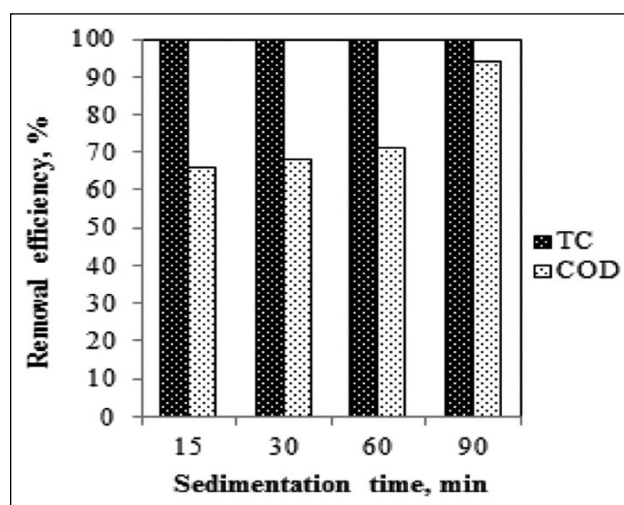


Figure 6. TC and COD removal efficiency at different sedimentation time (TC: 100 mg/L, pH: 4, Fe²⁺: 30 mg/L, H₂O₂: 100 mg/L, Reaction time: 10 min).

Table 1. The parameters of kinetic models and correlation coefficients (R²) for the degradation of tetracycline

	First-order kinetic model		Second-order kinetic model		BMG kinetic model		
	k ₁ (1/min)	R ²	k ₂ (L/mg.min)	R ²	1/m	1/b	R ²
R TC	0.6989	0.57	3.0014	0.88	Undefined	1.0	1.00
COD	0.422	0.99	0.0342	0.83	1.1	1.0395	0.95

higher concentrations results from both the recombination of hydroxyl radical and the scavenging effect of the $\cdot\text{OH}$ of H₂O₂ [27]. However, such a critical H₂O₂ concentration value was not found in this study. In another study, the optimum H₂O₂ concentration was found to be 375 mg/L in the degradation of amoxicillin (initial concentration: 10 mg/L) with Fenton process [16].

Effect of Reaction Time

As could be seen in Figure 5, the degradation of tetracycline was completed in 10 min. The tetracycline removal efficiency was increased until the reaction time of 10 min. In the Fenton process, it can be said that the effect of the reaction time on the process efficiency is important since the degradation efficiency increases with increasing reaction time [8]. However, the further increase in reaction time (>10 min) did not show a positive effect on the efficiency of the Fenton process. Besides, the increase in reaction time would increase the operating cost. So, the reaction time of 10 min was considered optimum. In a similar study, complete degradation of amoxicillin by the Fenton process took place at a reaction time of 12 min [16].

Effect of Sedimentation Time

The TC and COD removal efficiency depending on the sedimentation time is given in Figure 6. The TC removal effi-

ciencies were found to be 100% after 15, 30, 60 and 90 min of sedimentation time. The highest COD removal efficiency was obtained at the end of the 90 min of sedimentation time which has a value of 94%. Therefore, the sedimentation time of 90 min was found to be the optimum value when the COD removal efficiencies were considered. The reason why the COD removal efficiency is lower than the TC removal efficiency is due to the formation of intermediates and the incomplete mineralization of TC and intermediates to CO₂ and H₂O.

Kinetic Study

The kinetics of the degradation of tetracycline with Fenton process was evaluated using first-order, second-order and Behnajady-Modirshahla-Ghanbery (BMG) [28]. For this purpose, the change in tetracycline concentration and the value of tetracycline in terms of COD depending on the reaction time was investigated. Kinetic calculations were made according to the reaction time of 10 minutes. R² value is taken into account in determining the suitability of the kinetic model. For the tetracycline concentration, the R² value for the first-order was 0.57, the R² value for the second-order was 0.88, and the R² value for BMG was 1 (Fig. 7 and Table 1). In the degradation of tetracycline in terms of COD, R² value is 0.99 for first-order, R² value is 0.83 for second-order and 0.95 for BMG. When R² values

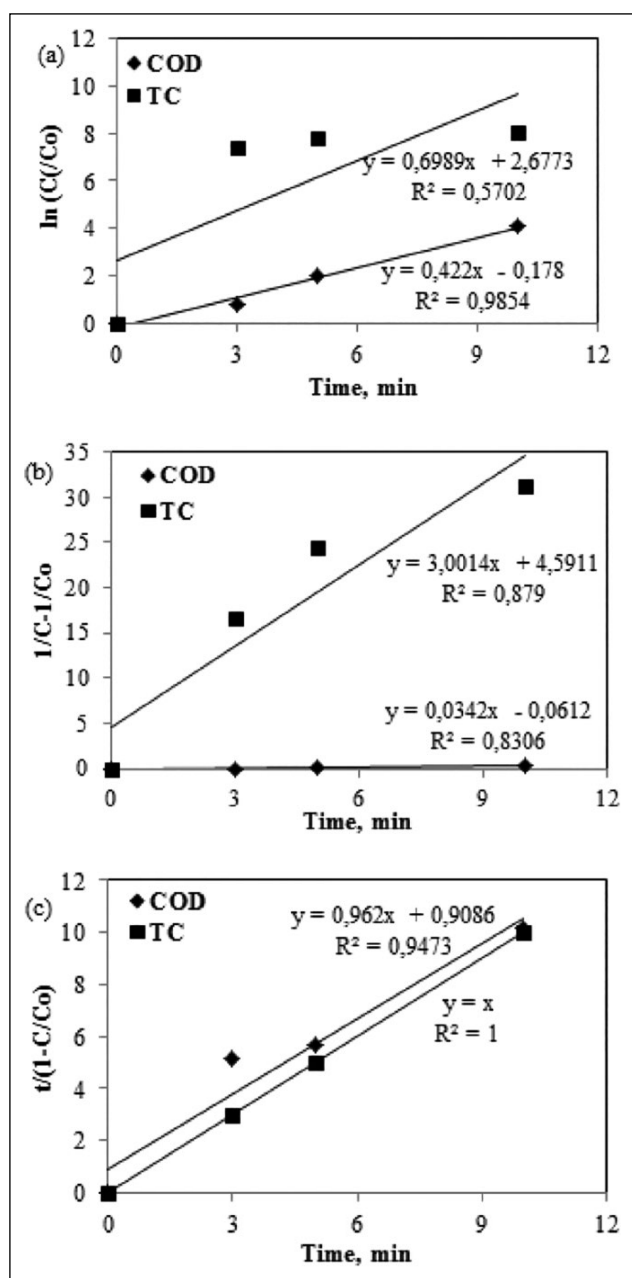


Figure 7. (a) First-order, (b) second-order, (c) BMG kinetics of the degradation of tetracycline with Fenton process.

are taken into consideration, when mineralization is evaluated in terms of COD concentration, it is seen that it fits the first-order kinetics. In terms of tetracycline concentration, it is seen that the BMG kinetic model is suitable. This is due to the fact that the tetracycline concentration decreases very quickly at the beginning and then slows down. The fact that the decrease in tetracycline in terms of COD concentration corresponds to first-order kinetics is due to the intermediate products originally formed during oxidation. It has been reported that the degradation of tetracycline in the schorl/H₂O₂ system fits first-order kinetics [1].

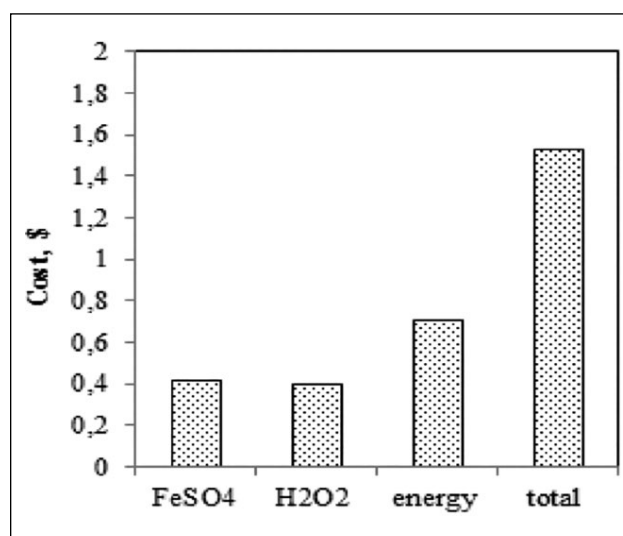


Figure 8. The operating cost in Fenton process (in \$ per kg tetracycline removal).

Operating Cost Analysis

The factors affecting the operating cost in Fenton process are chemicals and the energy cost spent for the mixer. The calculation was made by taking FeSO₄·7H₂O cost as 0.28\$/kg, H₂O₂ cost as 0.4\$/kg and mixer power as 3 W and unit energy cost as 0.071\$. For 1 kg tetracycline removal, FeSO₄ cost was calculated as 0.417\$, H₂O₂ cost was 0.4\$ and energy cost was 0.71\$. The total cost is 1.527\$ (Fig. 8). In the study in which phenol removal was done with the Fenton and electro-Fenton method, the calculation using the same numbers found that the removal cost of 1 kg phenol was 1.337\$ with the Fenton process [29]. It was stated that the operating cost for 1 kg of tetracycline removal was 330.06\$ for the ozone method, 405.59\$ for the ozone+ultrasound method, 193.63\$ for the ozone+Fenton method, and 229.71\$ for the ozone+ultrasound+Fenton method [30]. It was seen that the Fenton process had lower operating costs compared to other methods.

CONCLUSIONS

Experimental study results showed the optimum values for pH, Fe²⁺, H₂O₂, reaction time and sedimentation time in Fenton process were found to be 3, 30 mg/L, 100 mg/L, 10 min and 90 min, respectively. Under these conditions, TC degradation is 100%. The COD removal efficiency was about 94%. As a result of kinetic studies, it was the most appropriate kinetic model BMG in tetracycline degradation and first-order in tetracycline mineralization. The cost of tetracycline removal by Fenton process was calculated as 1.527\$ per 1 kg. The operating cost of the Fenton process for tetracycline removal was lower compared to other methods.

DATA AVAILABILITY STATEMENT

The authors confirm that the data that supports the findings of this study are available within the article. Raw data that support the finding of this study are available from the corresponding author, upon reasonable request.

CONFLICT OF INTEREST

The authors declared no potential conflicts of interest with respect to the research, authorship, and/or publication of this article.

ETHICS

There are no ethical issues with the publication of this manuscript.

REFERENCES

- [1] Y. Zhang, J. Shi, Z. Xu, Y. Chen, and D. Song, "Degradation of tetracycline in a schorl/H₂O₂ system: Proposed mechanism and intermediates," *Chemosphere*, Vol. 202, pp. 661–668, 2018. [\[CrossRef\]](#)
- [2] J. Jeong, W. Song, W. J. Cooper, J. Jung, and J. Greaves, "Degradation of tetracycline antibiotics: mechanisms and kinetic studies for advanced oxidation/reduction processes," *Chemosphere*, Vol. 78(5), pp. 533–540, 2010. [\[CrossRef\]](#)
- [3] M. K. Liu, Y. Y. Liu, D. D. Bao, G. Zhu, G. H. Yang, J. F. Geng, and H. T. Li, "Effective removal of tetracycline antibiotics from water using hybrid carbon membranes," *Scientific Reports*, Vol. 7(1), pp. 1–8, 2017. [\[CrossRef\]](#)
- [4] Y. Zhang, J. Geng, H. Ma, H. Ren, K. Xu, and L. Ding, "Characterization of microbial community and antibiotic resistance genes in activated sludge under tetracycline and sulfamethoxazole selection pressure," *Science of the Total Environment*, Vol. 571, pp. 479–486, 2016. [\[CrossRef\]](#)
- [5] E. Aydın, M. Şahin, E. Taşkan, H. Hasar, and M. Erdem, "Chlortetracycline removal by using hydrogen based membrane biofilm reactor," *Journal of Hazardous Materials*, Vol. 320, pp. 88–95, 2016. [\[CrossRef\]](#)
- [6] M. G. Alalm, A. Tawfik, and S. Ookawara, "Degradation of four pharmaceuticals by solar photo-Fenton process: kinetics and costs estimation," *Journal of Environmental Chemical Engineering*, Vol. 3(1), pp. 46–51, 2015. [\[CrossRef\]](#)
- [7] M. Zouanti, M. Bezzina, and R. Dhib, "Experimental study of degradation and biodegradability of oxytetracycline antibiotic in aqueous solution using Fenton process," *Environmental Engineering Research*, Vol. 25(3), pp. 316–323, 2020. [\[CrossRef\]](#)
- [8] S. A. Mousavi, F. Farrokhi, N. Kianirad, and F. Falahi, "Degradation of aniline from aqueous solution by Fenton process: modeling and optimization," *Desalination and Water Treatment*, Vol. 125, pp. 68–74, 2018. [\[CrossRef\]](#)
- [9] E. Gürtekin, and N. Şekerdağ, "An advanced oxidation process: Fenton process," *Pamukkale University Journal of Engineering Sciences*, Vol. 14(3), pp. 229–236, 2008.
- [10] V. Kavitha, and K. Palanivelu, "Destruction of cresols by Fenton oxidation process," *Water Research*, Vol. 39(13), pp. 3062–3072, 2005. [\[CrossRef\]](#)
- [11] E. Elmolla, and M. Chaudhuri, "Optimization of Fenton process for treatment of amoxicillin, ampicillin and cloxacillin antibiotics in aqueous solution," *Journal of Hazardous Materials*, Vol. 170(2-3), pp. 666–672, 2009. [\[CrossRef\]](#)
- [12] S. P. Sun, H. Q. Guo, Q. Ke, J.H. Sun, S. H. Shi, M. L. Zhang, and Q. Zhou, "Degradation of antibiotic ciprofloxacin hydrochloride by photo-Fenton oxidation process," *Environmental Engineering Science*, Vol. 26(4), pp. 753–759, 2009. [\[CrossRef\]](#)
- [13] O. Rozas, D. Contreras, M. A. Mondaca, M. Pérez-Moya, and H. D. Mansilla, "Experimental design of Fenton and photo-Fenton reactions for the treatment of ampicillin solutions," *Journal of Hazardous Materials*, Vol. 177(1–3), pp. 1025–1030, 2010. [\[CrossRef\]](#)
- [14] A. S. Giri, and A. K. Golder, "Ciprofloxacin degradation from aqueous solution by Fenton oxidation: reaction kinetics and degradation mechanisms," *RSC Advances*, Vol. 4(13), pp. 6738–6745, 2014. [\[CrossRef\]](#)
- [15] G. Dalgic, I. F. Turkdogan, K. Yetilmezsoy, and E. Kocak, "Treatment of real paracetamol wastewater by Fenton process," *Chemical Industry and Chemical Engineering Quarterly*, Vol. 23(2), pp. 177–186, 2017. [\[CrossRef\]](#)
- [16] M. Verma, and A. K. Haritash, "Degradation of amoxicillin by Fenton and Fenton-integrated hybrid oxidation processes," *Journal of Environmental Chemical Engineering*, Vol. 7(1), Article 102886, 2019. [\[CrossRef\]](#)
- [17] M. H. Khan, H. Bae, and J. Y. Jung, "Tetracycline degradation by ozonation in the aqueous phase: proposed degradation intermediates and pathway," *Journal of Hazardous Materials*, Vol. 181(1–3), 659–665, 2010. [\[CrossRef\]](#)
- [18] J. J. López-Peñalver, M. Sánchez-Polo, C. V. Gómez-Pacheco, and J. Rivera-Utrilla, "Photodegradation of tetracyclines in aqueous solution by using UV and UV/H₂O₂ oxidation processes," *Journal of Chemical Technology and Biotechnology*, Vol. 85(10), pp. 1325–1333, 2010. [\[CrossRef\]](#)
- [19] A. M. Cahino, M. M. A. de Andrade, E. S. de Araújo, E. L. Silva, C.D.O. Cunha, and E.M.R. Rocha, "Degradation of tetracycline by solar photo-Fenton:

- Optimization and application in pilot photoreactor,” *Environmental Quality Management*, Vol. 28(1), pp. 101–106, 2018. [\[CrossRef\]](#)
- [20] C. H. Han, H. D. Park, S. B. Kim, V. Yargeau, J.W. Choi, S.H. Lee, J.A. Park, “Oxidation of tetracycline and oxytetracycline for the photo-Fenton process: Their transformation products and toxicity assessment,” *Water Research*, Vol. 172, Article 115514, 2020. [\[CrossRef\]](#)
- [21] M. Xu, J. Deng, A. Cai, X. Ma, J. Li, Q. Li, and X. Li, “Comparison of UVC and UVC/persulfate processes for tetracycline removal in water,” *Chemical Engineering Journal*, Vol. 384, Article 123320, 2020. [\[CrossRef\]](#)
- [22] Y. Aşcı, The effect of pH on the removal of tetracycline antibiotic from aqueous solutions by ultrasound/H₂O₂ and sono-fenton methods, In Y. Aşcı, (Ed.). “Engineering sciences innovative approaches,” pp. 136–145, 2021.
- [23] Y. Y. Chen, Y. L. Ma, J. Yang, L. Q. Wang, J. M. Lv, and C. J. Ren, “Aqueous tetracycline degradation by H₂O₂ alone: removal and transformation pathway,” *Chemical Engineering Journal*, Vol. 307, pp. 15–23, 2017. [\[CrossRef\]](#)
- [24] G. K. Turkay, and H. Kumbur, “Investigation of amoxicillin removal from aqueous solution by Fenton and photocatalytic oxidation processes,” *Kuwait Journal of Science*, Vol. 46(2), pp. 85–93, 2019.
- [25] N. Modirshahla, M. A. Behnajady, and F. Ghanbary, “Decolorization and mineralization of CI Acid Yellow 23 by Fenton and photo-Fenton processes,” *Dyes and Pigments*, Vol. 73(3), pp. 305–310, 2007. [\[CrossRef\]](#)
- [26] L. V. de Souza Santos, A. M. Meireles, and L. C. Lange, “Degradation of antibiotics norfloxacin by Fenton, UV and UV/H₂O₂,” *Journal of Environmental Management*, Vol. 154, pp. 8–12, 2015. [\[CrossRef\]](#)
- [27] M. Y. Ghaly, G. Härtel, R. Mayer, and R. Haseneder, “Photochemical oxidation of p-chlorophenol by UV/H₂O₂ and photo-Fenton process. A comparative study,” *Waste Management*, Vol. 21(1), pp. 41–47, 2001. [\[CrossRef\]](#)
- [28] M. A. Behnajady, N. Modirshahla, and F. Ghanbary, “A kinetic model for the decolorization of CI Acid Yellow 23 by Fenton process,” *Journal of Hazardous Materials*, Vol. 148(1–2), pp. 98–102, 2007. [\[CrossRef\]](#)
- [29] D. Gümüş, and F. Akbal, “Comparison of Fenton and electro-Fenton processes for oxidation of phenol,” *Process Safety and Environmental Protection*, Vol. 103, pp. 252–258, 2016. [\[CrossRef\]](#)
- [30] C. K. Wang, and B.M. Huang, “Degradation, of tetracycline by advanced oxidation processes: Sono-Fenton and ozonation processes,” *Desalination and Water Treatment*, Vol. 96, pp. 161–168, 2017. [\[CrossRef\]](#)



Research Article

Calculation of rainwater harvest in greenhouses for semi-arid and continental climate zones

Abdullah Nafi BAYTORUN¹, Zeynep Binnaz ZAIMOĞLU², Fatma Elçin ERKURT²,
Behzat BALCI², Hasan Kıvanç YEŞİLTAŞ²

¹Department of Agricultural Structures and Irrigation, Çukurova University, Adana, Türkiye

²Department of Environmental Engineering, Çukurova University, Adana, Türkiye

ARTICLE INFO

Article history

Received: 25 April 2022

Revised: 20 Mayıs 2022

Accepted: 13 June 2022

Key words:

Irrigation in greenhouses; Water consumption; Water harvesting; Plant water consumption

ABSTRACT

In this study, it is aimed to determine the irrigation water required due to solar radiation in high technology greenhouses where soilless cultivation is carried out according to TS825 standards, and to determine the annual water consumption and storage capacity with the harvested rainwater. As a result of the calculations made for Turkey Mediterranean region, it has been determined that if 90% of the rainfall in the western Mediterranean region is harvested, 72% of the annual water consumption can be met, and 45% in the eastern Mediterranean region. In the inner regions where the terrestrial climate is dominant, 22%–32% of the annual water consumption can be met with 90% of the rain harvested depending on the amount of rainfall. The required storage volume in the western Mediterranean is 0.420 m³.m⁻², while it is 0.096 m³.m⁻² in the eastern Mediterranean and 0.044 m³.m⁻² in Kırşehir, where the continental climate prevails.

Cite this article as: Baytorun AN, Zaimoğlu ZB, Erkurt FE, Balcı B, Yeşiltaş HK. Calculation of rainwater harvest in greenhouses for semi-arid and continental climate zones. Environ Res Tec 2022;5:2:188–196.

INTRODUCTION

The increasing need for food in parallel with the population growth in the world increases the demand for agricultural products as well. It is estimated that by the year 2026, the world population will have reached 8.3 billion, with an increase of 35% compared to 2000 [1]. In order to ensure the food security of the growing population in our country, it is necessary to increase agricultural production and productivity in agricultural production. It is not possible to say that our country has sufficient land and water resources, which are the two main elements of agricultural production. One

of the most effective ways to increase production and efficiency is to increase the yield per unit area of land. This is possible by using new technologies in agriculture and increasing irrigated areas.

According to the State Hydraulic Works (DSI), average annual precipitation in Turkey is 574 mm. The average above ground and underground water potential of Turkey is 112 billion m³ per year [2]. Turkey's current water consumption is 44 km³.year⁻¹. 74% of this water is used in agriculture while 15% is consumed as domestic water and 11% is used in the industrial sector [3]. When water use

*Corresponding author.

*E-mail address: zeynepzaimoglu6@gmail.com



in our country is analysed by sectors, it is seen that the agricultural sector has the highest share. The pressure on resources in order to meet the increasing requirements of Turkey shows an upward trend [4].

Irrigation is the agricultural activity that has the highest effect on the yield increase in crop production. Water use efficiency (WUE), which is the ratio of yield to irrigation water usage, is generally used as a measure of water use in irrigation systems. Due to diminishing water resources, increasing water use efficiency is of great importance. WUE values in tomato production using greenhouses vary between 20.47 kg.m^{-3} and 47.7 kg.m^{-3} [5–7]. A significant amount of water is consumed in vegetative production in greenhouses. The ratio of tomato production in Turkey's under cover vegetative production is 48%. Studies have shown that 193 liters of water are consumed for 1 kg of tomato production [8]. This reveals that water saving should be especially taken into consideration in the coming years in order to benefit more from the water resources that have diminished due to global warming.

Studies are being carried out to establish an optimum irrigation program for vegetables grown in greenhouses with medium technology on the Mediterranean coastline. In these studies, generally open water surface evaporation is used to determine the water requirement [9]. In their study on watering tomatoes in a glass greenhouse on the Mediterranean coastline, Tari and Sapmaz (2017) took advantage of the Class A-Pan evaporation vessel and determined the water consumption to be 1.8 mm.day^{-1} in January-April, 3.33 mm.day^{-1} in May and 5 mm.day^{-1} in June [10]. Using the FAO-Penman Monteith equality, Zabeltitz (2011) has determined the values as $0.86\text{--}3.5 \text{ mm.day}^{-1}$ for January-April, 4.75 mm.day^{-1} for May and 5.9 mm.day^{-1} for June in his calculations of water consumption in Antalya, based on average daily temperatures [11].

Irrigation scheduling determines the amount of water applied to the plant (irrigation dose) and the application timing (irrigation frequency). Irrigation scheduling is made one in two different ways, depending water budget based on climatic data or soil and plant sensors [12].

In Turkey, irrigation for soilless agriculture production in high technology greenhouses established in recent years is scheduled according to the intensity of solar radiation. In soilless culture, normal planning for irrigation according to solar radiation intensity is one irrigation application per 80 J.cm^{-2} . In this method, plants can be directed towards the desired growth characteristics by decreasing or increasing irrigation intervals. Increasing the irrigation interval can increase salinity in the growing medium, which increases fruit sugar and generative growth as it increases plant stress [13].

Rainwater harvesting is the collection and accumulation of the portion of the rainwater that passes to the surface

flow and the provision of water necessary for plant and animal production as well as domestic consumption [14]. The biggest problem that global climate change will create in terms of sustainable agriculture in the future will be water scarcity. In the future, in areas where water resources are not sufficient, it will be of great importance to collect rainwater and use it for greenhouse irrigation. However, under these conditions, the gutters collecting rainwater and their storage volumes water should be calculated based on the amount of rainfall and daily water consumption [11].

In storing rainwater, the factors to be taken into consideration when determining the storage capacity are the area of the greenhouse area and the size of the storage area, the distribution of rainfall, the total amount of rainfall, the water requirement of the plant grown, and whether the storage tanks to be planned will be used only for storing rainwater or for a mixture made with waste or salt water [11]. In large greenhouse enterprises with high technology, storage structures are constructed by taking into account the daily maximum water consumption during the production period.

This study aims to determine storage capacity for different harvest rates and determine the rates of meeting water consumption requirements with harvested rainwater by taking into account the monthly rainfall and daily water consumption for tomato production in high technology greenhouses in three different climate zones in Turkey, established in compliance with TS 825 standards.

MATERIALS AND METHODS

In this study, the calculations are based on high technology greenhouses in Turkey in different provinces set in compliance with TS 825, where greenhouse cultivation is common and the daily solar radiation in these provinces: Antalya, Mersin and Adana in Region I, Denizli, Yalova and Şanlıurfa in Region II, Kırşehir and Kütahya in Region III where there are geothermal resources.

Determining Plant Water Consumption

Daily water consumption in greenhouses where soilless agriculture is carried out has been determined according to the intensity of solar radiation. In Table 1, monthly average solar radiation values for the 2004–2018 ($\text{kWh.m}^{-2}\text{day}^{-1}$) provided by the General Directorate of Meteorology for provinces located in different climatic regions are given. In the calculation of daily water consumption depending on the months, based on the values given in Table 1, 3 mL.m^{-2} irrigation water was calculated for 1 J.cm^{-2} radiation energy.

Determining Storage Pool Capacity

In determining the accurate rainwater storage capacity, daily repetitions of rainfall are used. However, since these values are not known for many areas, in this study monthly

Table 1. Average daily radiation values of different provinces based on months (kWh.m².day⁻¹)

Region	Province	January	February	March	April	May	June	July	August	September	October	November	December
Region I	Adana	1.98	2.42	4.12	4.98	6.07	6.68	6.46	5.91	4.90	3.78	2.33	1.81
	Antalya	2.12	2.57	4.37	5.47	6.36	6.93	6.65	6.14	5.16	3.93	2.51	1.92
	Mersin	2.11	2.65	4.27	5.24	6.28	6.86	6.66	6.08	5.04	3.84	2.47	1.91
Region II	Denizli	2.01	2.45	4.11	5.26	6.22	6.73	6.62	6.00	4.99	3.75	2.39	1.79
	Şanlıurfa	1.94	2.48	4.09	5.08	6.18	6.83	6.58	5.94	5.02	3.79	2.42	1.80
Region III	Yalova	1.40	2.23	3.24	4.44	5.63	6.05	5.82	5.30	4.20	2.90	1.70	1.22
	Kırşehir	1.78	2.38	3.89	4.83	6.09	6.47	6.42	5.85	4.84	3.43	2.08	1.58
	Kütahya	1.77	2.36	3.75	4.93	6.08	6.48	6.38	5.72	4.69	3.28	2.04	1.51

Table 2. Daily water consumption based on solar radiation in greenhouses in different climatic regions established according to TS 825 standards (L.m².day⁻¹)

Region	Province	January	February	March	April	May	June	July	August	September	October	November	December
Region I	Adana	2.1	2.6	4.4	5.4	6.6	7.2	7.0	6.4	5.3	4.1	2.5	2.0
	Antalya	2.3	2.8	4.7	5.9	6.9	7.5	7.2	6.6	5.6	4.2	2.7	2.1
	Mersin	2.3	2.9	4.6	5.7	6.8	7.4	7.2	6.6	5.4	4.1	2.7	2.1
Region II	Denizli	2.2	2.6	4.4	5.7	6.7	7.3	7.1	6.5	5.4	4.1	2.6	1.9
	Şanlıurfa	2.1	2.7	4.4	5.5	6.7	7.4	7.1	6.4	5.4	4.1	2.6	1.9
	Yalova	1.5	2.4	3.5	4.8	6.1	6.5	6.3	5.7	4.5	3.1	1.8	1.3
Region III	Kırşehir	1.9	2.6	4.2	5.2	6.6	7.0	6.9	6.3	5.2	3.7	2.2	1.7
	Kütahya	1.9	2.5	4.1	5.3	6.6	7.0	6.9	6.2	5.1	3.5	2.2	1.6

Table 3. Daily and monthly water consumption based on solar radiation in greenhouses under climatic conditions of Antalya

Consumption	January	February	March	April	May	June	July	August	September	October	November	December
L.m ² .day ⁻¹	2.3	2.8	4.7	5.9	6.9	7.5	7.2	6.6	5.6	4.2	2.7	2.1
L.m ² .mon ⁻¹	71.3	78.4	145.7	177.0	213.9	225.0			168.0	130.2	81.0	65.1

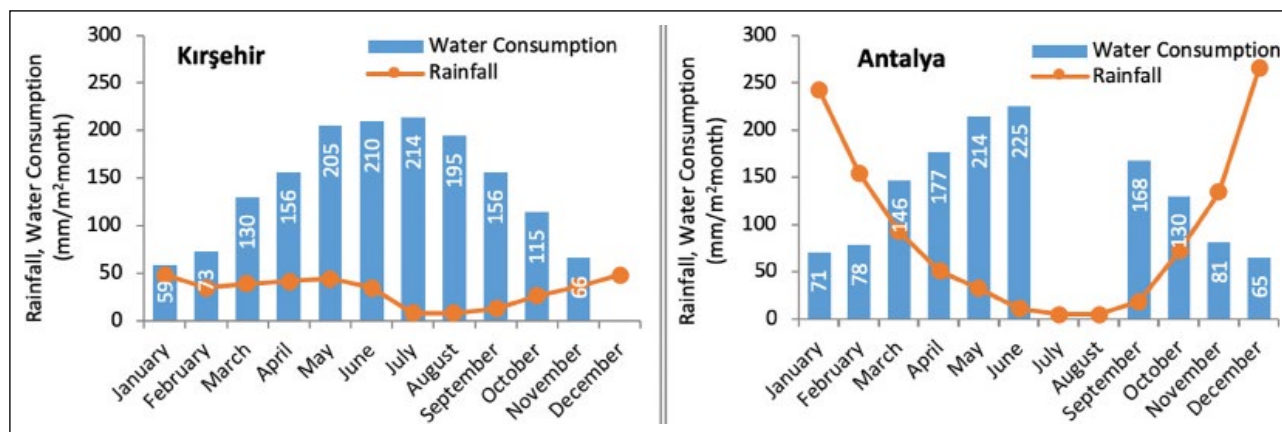


Figure 1. Amounts of water consumption based on monthly rainfall and intensity of solar radiation in Antalya, where greenhouse cultivation is intensively carried out, and in Kırşehir, where geothermal greenhouse cultivation has become a practice.

rainfall amounts were used in order to determine the storage capacity. The monthly amount of rainwater that can be stored was calculated with Equation 1 [11].

$$CV_m = Pre \cdot R_c \quad (L \cdot m^{-2} \cdot month^{-1}) \quad \text{(Equation 1.)}$$

In the equation;

CV_m : Amount of water harvested ($L \cdot m^{-2} \cdot month^{-1}$), R_c : Water harvest rate (%), Pre : Monthly precipitation ($mm \cdot month^{-1}$). In the calculations made, the R_c value was taken as 40–90%.

Storable monthly rainfall was calculated with the help of Equation 2:

$$STP_m = CV_m - CWR_m - EV_{pond} \quad (L \cdot m^{-2} \cdot month^{-1}) \quad \text{(Equation 2.)}$$

In the equation:

STP_m : Monthly stored rainfall ($L \cdot m^{-2} \cdot month^{-1}$), CWR_m : Monthly plant water consumption ($L \cdot m^{-2} \cdot month^{-1}$), EV_{pond} : Evaporation losses in the storage pool ($L \cdot m^{-2} \cdot month^{-1}$)

In the calculations made, evaporation losses from the storage pool were taken as 0, assuming that the pool surface is covered with PE plastic. As a result of the calculations, when the monthly storable precipitation amount (STP_m) is positive, the pool is filled, and when STP_m is negative, the water in the pool decreases.

Storable annual precipitation depending on the stored rainfall per month was determined with Equation 3:

$$STP_y = \sum(+)STP_m \quad (L \cdot m^{-2} \cdot month^{-1}) \quad \text{(Equation 3.)}$$

The annual deficit due to plant water consumption was calculated with Equation 4:

$$Def_y = \sum(-)STP_m \quad (L \cdot m^{-2} \cdot month^{-1}) \quad \text{(Equation 4.)}$$

The stored annual precipitation amount was calculated with Equation 5:

$$STB_y = STP_y - Def_y \quad (L \cdot m^{-2} \cdot month^{-1}) \quad \text{(Equation 5.)}$$

While determining the storage capacity, the following conditions were taken into account [15].

1- When $STB_y > 0$ or $STP_y > Def_y$ the amount of stored water will meet the water needs of the plants during the production period. In this case, the storage capacity should be taken as $VST = Def_y \quad (L \cdot m^{-2})$.

When the precipitation changes over the months are large, the storage volume should be increased. In this case, the storage volume should be taken as $VST = Def_y \cdot (1 + V_c) \quad (L \cdot m^{-2})$.

2- If $STB_y < 0$ or $STP_y < Def_y$ then stored rainfall is not sufficient for irrigation. In this case, two conditions must be considered:

(a) If the amount of stored rainfall is greater than the monthly maximum rainfall collected ($STP_y > CV_{mmax}$) then the storage volume should be $VST = STP_y$, and when the precipitation variation due to months is large, it should be determined as $VST = STP_y \cdot (1 + V_c)$.

(b) If the amount of stored rainfall is less than the monthly maximum rainfall collected ($STP_y < CV_{mmax}$) then the storage volume should be $VST = CV_{mmax}$, and when the precipitation variation due to months is large, it should be determined as $VST = CV_{mmax} \cdot (1 + V_c)$.

FINDINGS

The plant water requirements calculated based on solar radiation in soilless agriculture practices in high technology greenhouses established in provinces located in different climatic regions according to TS 825 are given in Table 2. As can be seen from the Table 2, the highest daily water requirement in all three climatic regions is in July.

The plant production period in greenhouses varies depending on the climate of the region. The production in high technology greenhouses in the provinces within Region I starts in the last week of August and continues until the end of June. The water consumption amounts during the production period depending on the daily total radiation intensities of the Antalya province located in Region I are given in Table 3.

Table 4. The monthly rates of meeting water requirement and the required storage capacities in Antalya climate conditions when 90% of rainwater is harvested

Month	Pre mm/m ² mon.	CV _m mm/m ² mon.	d _m	CWR _d L/m ² day	CWR _m L/m ² mon	STP _m L/m ² mon.	STP _m L/m ² mon.	IW _m L/m ²
January	242.1	217.9	31	2.3	71.3	146.6	359.5	0.0
February	154.4	139.0	28	2.8	78.4	60.6	420.0	0.0
March	97.2	87.5	31	4.7	145.7	-58.2	361.8	0.0
April	50.4	45.4	30	5.9	177.0	-131.6	230.2	0.0
May	32.1	28.9	31	6.9	213.9	-185.0	45.2	0.0
June	10.9	9.8	30	7.5	225.0	-215.2	-170.0	170.0
July	4.5	4.1	0	7.2	0.0	4.1	4.1	0.0
August	4.6	4.1	0	6.6	0.0	4.1	8.2	0.0
September	18.1	16.3	30	5.6	168.0	-151.7	-143.5	143.5
October	72.1	64.9	31	4.2	130.2	-65.3	-208.8	65.3
November	133.6	120.2	30	2.7	81.0	39.2	39.2	0.0
December	265.3	238.8	31	2.1	65.1	173.7	212.9	0.0
Total	1085.3	976.8			1355.6			378.8
Rate of meeting irrigation water		0.72						

If it is assumed that there is no vegetative production in the greenhouse due to the high temperature during July and August in Antalya climatic conditions, the amount of water consumed during the production period is 1.356 m³.m⁻²a⁻¹. According to different resources, the average water requirement in greenhouses for summer months can be taken as 5 L.m⁻² plant area per day or 0.15 m³.m⁻²month⁻¹. The annual requirement is 0.8–2.0 m³.m⁻². Annual water requirement in irrigation with fogging method can be 3 m³/m² or more [15].

The fact that Turkey has different climate zones leads to different temperatures and different quantities of rainfall. In Figure 1, monthly water consumption amounts in the greenhouse based on monthly rainfall and intensity of solar radiation have been given. The values are given for Antalya, where greenhouse cultivation is a common practice and for Kırşehir, where geothermal greenhouse cultivation has become widespread in recent years.

In Antalya, where greenhouse cultivation is a common practice, the amounts of rainfall in November–February period exceed the water required for the plant production in the greenhouse (Fig. 1). In the case of harvesting and storing rainfall during this period, a significant part of the plant water required in the following months will be met.

Inner parts of Anatolia are insufficient in terms of rainfall. When the rainfall and water consumption are examined in Kırşehir, which is located in Central Anatolia and where geothermal greenhouse cultivation has gained momentum in recent years, it is seen that in the case of storing monthly rainfall, a very small part of the monthly water consump-

tion can be met, yet this amount is not for storage (Fig. 1). In Kırşehir, while rainfall cannot fully meet the water consumption of the greenhouse in any month, it does not provide any possibility for storage.

The required storage capacities and the rate of meeting irrigation water with rainfall according to the water consumption quantities calculated depending on the monthly amount of precipitation and intensity of solar radiation in Antalya are given in Table 4. The highest precipitation in Antalya climate conditions falls is observed in December and the total annual precipitation is 1085.3 mm.m⁻². Considering that 90% of the rainfall on the greenhouse cover surface is harvested, the amount of rainfall that can be stored is 976.8 mm.m⁻²year⁻¹.

Under the climatic conditions of Antalya, when it is considered that greenhouse cultivation starts in the last week of August and ends at the end of June, 8.2 L.m⁻² water can be stored by collecting the rainfall in the months of July and August. Assuming that 90% of the rainfall in September is collected (16.3 L.m⁻²month⁻¹) and that 8.2 L.m⁻² water kept in the tanks is used, only 14.6% of the 168 L.m⁻²month⁻¹ water requirement in September will be met by precipitation. The remaining amount of the irrigation water required in September (143.5 L.m⁻²month⁻¹) must be met from different sources. While the amount of required irrigation based on solar radiation decreases in October, with the increasing amount of rainfall, the amount of irrigation water needed from external sources is 65.3 L.m⁻²month⁻¹.

In Antalya climate conditions, the collection of rainwater starts in November. As can be seen from Table 4, the

Table 5. The monthly rates of meeting water requirement and the required storage capacities in Kırşehir climate conditions when 90% of rainwater is harvested

Month	Pre mm/m ² mon.	CV _m mm/m ² mon.	d _m	CWR _d L/m ² day	CWR _m L/m ² mon	STP _m L/m ² mon.	STP _m L/m ² mon.	IW _m L/m ²
January	48.4	43.6	31	1.9	58.9	-15.3	28.4	0
February	35.2	31.7	28	2.6	72.8	-41.1	-12.8	12.8
March	39.3	35.4	31	4.2	130.2	-94.8	-107.6	94.8
April	41.5	37.4	30	5.2	156	-118.7	-226.2	118.7
May	44.8	40.3	31	6.6	204.6	-164.3	-390.5	164.3
June	34.6	31.1	30	7	210	-178.9	-569.4	178.9
July	8.3	7.5	31	6.9	213.9	-206.4	-775.8	206.4
August	7.9	7.1	31	6.3	195.3	-188.2	-964.0	188.2
September	12.9	11.6	30	5.2	156	-144.4	-1108.4	144.4
October	26.7	24.0	31	3.7	114.7	-90.7	-1199.1	90.7
November	36.4	32.8	30	2.2	66	-33.2	-1232.3	33.2
December	48.5	43.7	0	1.7	0	43.7	43.7	0
Total	384.5	346.05			1578.4			1232.4
Rate of meeting irrigation water		0.22						

amount of irrigation water required due to the decreasing solar radiation in November is 81 L.m⁻²month⁻¹ and the amount of rainwater collected is 120.2 L.m⁻²month⁻¹. Under these conditions, the remaining 39.2 L.m⁻²month⁻¹ of the collected rainfall can be stored. In the case of collecting 90% of the rainfall after November in Antalya, it is possible to meet the irrigation water in the greenhouse without the need for water supply from external sources until the end of May.

The water requirement and storage capacity calculated based on monthly amounts of rainfall and water consumption in Kırşehir, a province in Central Anatolia, are given in Table 5. As can be seen from the Table 5, in the case of greenhouse cultivation all year under Kırşehir climate conditions, planting in the greenhouse starts in the last week of December and continues until the first week of December of the following year. Under these conditions, the storage of the rainfall in December takes place, and the storage capacity of 43.7 L/m² is sufficient as the rainfall in the following months meets only a small part of the monthly water requirement. When 90% of the precipitation is harvested in Kırşehir climate conditions, only 22% of the annual water consumption can be met.

The rates of meeting irrigation water requirement with rainwater depending on different rainwater harvest rates in provinces located in different climatic zones according to TS 825 standards are given in Table 6. By harvesting 90% of rainwater in Antalya climate conditions, 72% of the annual water requirement can be met. In the event that harvest rate drops to 70%, this rate drops to 56%.

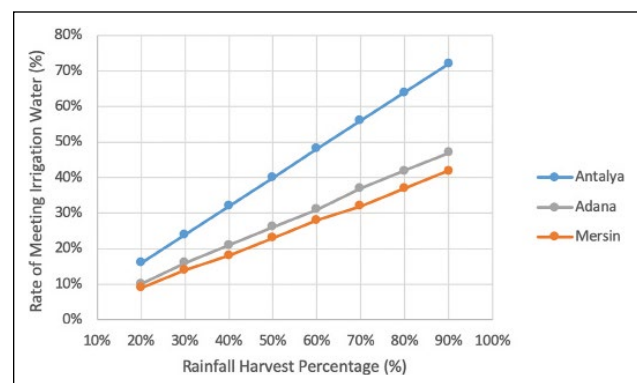


Figure 2. Rates of meeting irrigation water requirement in different provinces according to TS 825 based on rainfall harvest rates.

As can be seen from Table 6, the rates of meeting irrigation water with harvested rainwater show significant differences in the provinces located in Region I. If the rainwater harvest rate is 90% in Antalya, the irrigation water is met 72%, while this rate is 47% in Adana and 42% in Mersin. This shows that the rate of meeting irrigation water requirement is influenced by the amount of precipitation rather than the temperatures in different regions.

In Figure 2, the rates of meeting the irrigation water with rainwater for different rainfall harvest rates are given for the provinces of Antalya, Adana and Mersin, which are located in Region I according to TS 825 standards and where greenhouse cultivation is intensely carried out. As can be seen from the figure, depending on the increase

Table 6. Rates of meeting irrigation water requirement with rainfall in different climatic regions according to ts 825 based on rainfall collection rates

TS825 region	Region I			Region II			Region III	
	Antalya	Adana	Mersin	Yalova	Denizli	Şanlıurfa	Kütahya	Kırşehir
Rainfall (mm/m ²)	1085	671	616	757	572	464	562	385
Harvest rate (%)								
90	72	47	42	54	40	32	32	0.22
80	64	42	37	48	35	29	29	19
70	56	37	32	42	31	25	25	17
60	48	31	28	36	26	21	22	15
50	40	26	23	30	22	18	18	12
40	32	21	18	24	18	14	14	10

Table 7. Storage volumes based on rainwater harvest rates in different climatic regions according to TS 825 (L.m²)

TS825 region	Region I			Region II			Region III	
	Antalya	Adana	Mersin	Yalova	Denizli	Şanlıurfa	Kütahya	Kırşehir
Rainfall (mm/m ²)	1085	671	616	757	572	464	562	385
Harvest rate (%)								
90	420.0	95.9	95.9	117.7	36.9	28.3	76.4	43.7
80	340.5	64.0	70.1	89.1	20.8	11.5	62.5	38.8
70	261.0	40.1	44.3	60.3	18.2	3.8	54.7	34.0
60	182.3	16.3	18.7	37.2	15.6	3.2	46.9	29.1
50	117.4	10.0	9.3	17.1	13.0	2.7	39.1	24.3
40	66.5	8.0	7.4	12.7	10.4	2.2	31.2	19.4
30	15.8	6.0	5.6	9.5		1.6	23.4	

in rainwater harvest rate, irrigation water coverage rate increases linearly. Among the provinces located in Region I, the highest rainfall occurs in Antalya, while the amount of rain decreases from the western Mediterranean to the eastern Mediterranean. When 90% of the rainfall is collected in Adana climate conditions, 47% of the irrigation water need can be met, while this value is 42% in Mersin.

The rate of meeting irrigation water requirement from rainwater is the lowest in Kırşehir, which is located in Region III. Table 6 shows the percentages of meeting irrigation water requirements at different rainfall collection rates in provinces located in different climatic zones.

It is necessary to know the volumes calculated according to the monthly rainfall and water consumption in order to resize the tanks to be established for storing rainwater. In Table 4, the storage volumes calculated depending on the monthly rainfall and plant water requirement in Antalya climatic conditions are given. As can be seen from the calculations made, if 90% of the rainwater is harvested, the highest storage volume is in February with 420 L.m⁻²month⁻¹.

When the rainfall harvested in the regions with low amount of rainfall covers some of the water consumption, storage cannot be made. As can be seen from the calculations in Table 5 made for Kırşehir, where rainfall amounts are low, rainfall is not stored as the monthly rainfall amounts meet only a small part of the water consumption. Since irrigation water is not needed only in December, when planting is carried out, it is possible to store rainfall in this month.

Storage volume varies depending on harvested rainfall and water requirement. In Table 7, the maximum storage volumes calculated based on different rainwater harvest rates in provinces in different climatic zones according to TS 825 standards are given. As can be seen from the Table, depending on the amount of rainfall, the highest storage volume occurs in Antalya, while the lowest storage volume is calculated for Kırşehir, where geothermal greenhouse cultivation is practiced.

CONCLUSION AND EVALUATION

74% of Turkey's current water consumption is in agriculture while domestic use and industrial use are 15% and 11%

respectively. Turkey's growing need for water has increased the pressure on resources. Global climate change and the gradual reduction of water resources may put the sustainability of agricultural production, which has important contributions to human nutrition, at risk in the coming years.

Reducing water consumption in agriculture will be possible by increasing water use efficiency (WUE). In Turkey, which follows Spain in Europe in terms of greenhouse area, increasing water use efficiency will be possible by collecting the rainwater that reaches greenhouse surface and using it for irrigation rather than implementing water constraints.

For harvesting and storing the rain water reaching the greenhouse cover surface, it is necessary to resize the water gutters in the greenhouse structures and to accurately determine the storage volumes to be installed. When determining an accurate storage volume, daily rainfall and daily water consumption quantities should be known. However, it is not possible to obtain the daily amount of rainfall for every location. For the stated reason, monthly total precipitation is taken as a basis in determining the storage volume.

Along the Mediterranean coastline, where greenhouse cultivation is a common practice, rainfall shows significant differences. While the annual precipitation amount in Antalya is 1085 mm.year⁻¹, it is 671 mm.year⁻¹ in Adana and 616 mm.year⁻¹ in Mersin. In the case of harvesting 90% of rainwater in the production under cover in Antalya, 72% of the annual water consumption can be met, while in Adana and Mersin the rates are 47% and 42%. In the case of harvesting 90% of rainwater, the required storage volume in Antalya is 420 L.m⁻², while it is 96 L.m⁻² in Adana and Mersin.

In areas where terrestrial climate is dominant and geothermal greenhouse cultivation is carried out, the amount of rainfall is considerably low. Total annual precipitation in Kütahya is 562 mm.year⁻¹, and in Kırşehir it is 385 mm.year⁻¹. In the study conducted, it has been shown that in the case of harvesting 90% of the rainwater in Kütahya climatic conditions, 32% of the annual water consumption can be met, while only 22% of it can be met in Kırşehir.

In order for the irrigation water in the greenhouses to rest and not to risk the product in the greenhouse, the water tanks installed should be of a sufficient size to meet the irrigation water need for at least two days. Considering that the effective size of greenhouses established as large enterprises is 20160 m², the maximum water requirement in June in the Mediterranean region and in July where the continental climate prevails is 150 m³.day⁻¹. In this case, the capacity of the water tank to be installed should be at least 300 m³. Whenever possible, the tanks to be established for storing rainwater should be built in a closed area within a greenhouse tunnel. Under these conditions, evaporation of water is prevented during hot periods, and frostbite can be prevented during cold periods. The diameter of the pipes that will carry the water to the collection tanks varies depending

on the greenhouse floor area. The diameter of the collecting pipe should be 125 mm if the area where the rainwater will be harvested is 400–700 m² and 150 mm when the collection area is 700–1200 m² [11].

ACKNOWLEDGMENT

The authors would like to thank the Turkish State Meteorological Service and Çukurova University for their support.

DATA AVAILABILITY STATEMENT

The authors confirm that the data that supports the findings of this study are available within the article. Raw data that support the finding of this study are available from the corresponding author, upon reasonable request.

CONFLICT OF INTEREST

The authors declared no potential conflicts of interest with respect to the research, authorship, and/or publication of this article.

ETHICS

There are no ethical issues with the publication of this manuscript.

REFERENCES

- [1] OECD/FAO. "OECD-FAO Agricultural Outlook 2021-2030," OECD Publishing, Paris, 2021.
- [2] E. Askan, Y. Topcu, and A. N Sahin, "Determining consumption preferences of consumers considering quality attributes of drinking water: A case of Igdir," Italian Journal of Food Science, Vol. 33(2), pp. 156–165, 2021. [CrossRef]
- [3] Presidency of the Republic of Turkey Presidency of Strategy and Budget. "Decision on the approval of the 11th Development Plan (2019-2023)," 2019. https://www.sbb.gov.tr/wp-content/uploads/2021/12/Eleventh_Development_Plan_2019-2023.pdf
- [4] H. G Onder, "Renewable energy consumption policy in Turkey: An energy extended input-output analysis," Renewable Energy, Vol. 175, pp.783–796, 2021. [CrossRef]
- [5] X. Wang, J. Yun, P. Shi, Z. Li, P. Li, and Y. Xing, "Root growth, fruit yield and water use efficiency of greenhouse grown tomato under different irrigation regimes and nitrogen levels," Journal of Plant Growth Regulation, Vol. 38(2), 400-415, 2019. [CrossRef]
- [6] W. Wang, "Effects of different soil moistures on the yield, water use efficiency of solar greenhouse tomatoes in liaoning, China," IOP Conference Series: Earth and Environmental Science, Vol. 208(1), Article 012075, 2018. [CrossRef]
- [7] W. Xiukang, and X. Yingying. "Evaluation of the effect of irrigation and fertilization by drip fertigation

- on tomato yield and water use efficiency in greenhouse,” *International Journal of Agronomy*, Vol. 1, Article 3961903, 2016. [[CrossRef](#)]
- [8] A. Hoekstra, A. Chapagain, M. M. Aldaya, M. M. Mekonnen, “Water Footprint Manual” Spinal Cord, 2009.
- [9] A. F. Abou-Hadid, M. Z. El-Shinawy, I. El-Oksh, H. Gomaa, and A. S. El Beltagy. “Studies on water consumption of sweet pepper plant under plastic houses,” *Acta Horticulturae*, Vol. 366, pp. 365–372, 1994. [[CrossRef](#)]
- [10] A. Tari, M. Sapmaz, “The effect of different irrigation levels on the yield and quality of tomatoes in greenhouse,” *Toprak Su Dergisi*, Vol. 6, pp. 11–17, 2017. [Turkish] [[CrossRef](#)]
- [11] C. von Zabeltitz, “Integrated greenhouse systems for mild climates: Climate conditions, design, construction, maintenance, climate control,” Springer Heidelberg Dordrecht, 2011. [[CrossRef](#)]
- [12] E. Gonen, Y. Bozkurt, A. Yazar, C. Tanriverdi, and S. Sesveren, “Bitkiye dayalı ölçümler kullanılarak gün içerisinde en uygun sulama zamanının belirlenmesi,” *Ziraat Fakültesi Dergisi 1. Uluslararası Tarımsal Yapılar ve Sulama Kongresi Özel Sayısı*, pp. 281-289, 2018. [Turkish]
- [13] M. Ashraf, and P. J. C. Haris, “Potential biochemical indicators of salinity tolerance in plants,” *Plant Science*, Vol. 166, pp. 3–16, 2004. [[CrossRef](#)]
- [14] T. Oweis, D. Prinz A. Hachum, “Water harvesting: Indigenous knowledge for the future of the drier environments,” *International Center for Agricultural Research in the Dry Areas*, pp. 40, 2001.
- [15] C. von Zabeltitz, “Gewächshäuser,” *Handbuch der Erwerbsgärtner*, Verlag Eugen-Ulmer, 1986. [Deutsch]